WAVE TRANSFORMATION BY BATHYMETRIC ANOMALIES WITH GRADUAL TRANSITIONS IN DEPTH AND RESULTING SHORELINE RESPONSE

By

CHRISTOPHER J. BENDER

A DISSERTATION PRESENTED TO THE GRADUATE SCHOOL
OF THE UNIVERSITY OF FLORIDA IN PARTIAL FULFILLMENT
OF THE REQUIREMENTS FOR THE DEGREE OF
DOCTOR OF PHILOSOPHY

UNIVERSITY OF FLORIDA

2003

ACKNOWLEDGMENTS

I am truly blessed to have my wife and best friend, Kathryn, in my life. This completion of this work was made possible by her support, encouragement, and love. I am fortunate beyond measure to have her next to me as I walk life's journey.

Many individuals at the University of Florida have made the completion of this work possible. Dr. Robert G. Dean has not only been my major advisor but also my mentor and friend during my studies at the University of Florida. I have gained many valuable lessons from his work ethic, his character, and his tireless quest for understanding the coastal environment. I am grateful to the other members of my committee (Dr. Daniel M. Hanes, Dr. Andrew Kennedy, Dr. Ulrich H. Kurzweg, Dr. Robert J. Thieke) for their instruction and involvement during the course of my doctoral studies.

I wish to thank my family (especially Mom and Dad B, Mom and Dad Z, Caryn, John, and Kristin) and friends for their support in all my endeavors. Each of them has contributed to who I am today.

An Alumni Fellowship granted by the University of Florida sponsored this study with partial support from the Bureau of Beaches and Wetland Resources of the State of Florida.

TABLE OF CONTENTS

page

ACKNOWLEDGMENTS ii

LIST OF TABLES vi

LIST OF FIGURES vii

ABSTRACT xix

CHAPTER

1 INTRODUCTION AND MOTIVATION 1

1.1 Motivation 2
1.2 Models Developed and Applications 4

2 LITERATURE REVIEW 7

2.1 Case Studies 8
2.1.1 Grand Isle, Louisiana (1984) 8
2.1.2 Anna Maria Key, Florida (1993) 11
2.1.3 Martin County, Florida (1996) 15
2.2 Field Experiments 16
2.2.1 Price et al. (1978) 17
2.2.2 Kojima et al. (1986) 17
2.3 Laboratory Experiments 19
2.3.1 Horikawa et al. (1977) 19
2.3.2 Williams (2002) 20
2.4 Wave Transformation 23
2.4.1 Analytic Methods 23
2.4.1.1 2-Dimensional methods 24
2.4.1.2 3-Dimensional methods 34
2.4.2 Numerical Methods 40
2.5 Shoreline Response 46
2.5.1 Longshore Transport Considerations 46
2.5.2 Refraction Models 47
2.5.2.1 Motyka and Willis (1974) 47
2.5.2.2 Horikawa et al. (1977) 49
2.5.3 Refraction and Diffraction Models 51
2.5.3.1 Gravens and Rosati (1994) 51

2.5.3.2 Tang (2002) 54
2.5.4 Refraction, Diffraction, and Reflection Models 54
2.5.4.1 Bender (2001) 54

3 2-DIMENSIONAL MODEL THEORY AND FORMULATION 59

3.1 Introduction 59
3.2 Step Method: Formulation and Solution 60
3.2.1 Abrupt Transition 63
3.2.2 Gradual Transition 65
3.3 Slope Method: Formulation and Solution 67
3.3.1 Single Transition 69
3.3.2 Trench or Shoal 72
3.4 Numerical Method: Formulation and Solution 74

4 3-DIMENSIONAL MODEL THE0RY AND FORMULATION 77

4.1 Introduction 77
4.2 Step Method: Formulation and Solution 77
4.2.1 Abrupt Transition 81
4.2.2 Gradual Transition 85
4.3 Exact Shallow Water Solution Method: Formulation and Solution 88

5 2-DIMENSIONAL MODEL RESULTS AND COMPARISONS 92

5.1 Introduction 92
5.2 Matching Condition Evaluation 92
5.3 Wave Transformation 95
5.3.1 Comparison of 2-D Step Model to Numerical Model FUNWAVE 1.0. 97
5.4 Energy Reflection 99
5.4.1 Comparison to Previous Results 99
5.4.2 Arbitrary Water Depth 101
5.4.3 Long Waves 116

6 3-DIMENSIONAL MODEL RESULTS AND COMPARISONS 125

6.1 Introduction 125
6.2 Matching Condition Evaluation 126
6.3 Wave Height Modification 127
6.3.1 Comparison of 3-D Step Model and Analytic Shallow Water Exact Model 141
6.4 Wave Angle Modification 144
6.5 Comparison of 3-D Step Model to Numerical Models 147
6.5.1 3-D Step Model Versus REF/DIF-1 148
6.5.2 3-D Step Model Versus 2-D Fully Nonlinear Boussinesq Model 154
6.6 Comparison to Laboratory Data of Chawla and Kirby (1996) 156
6.7 Direction Averaged Wave Field Modification 161

6.8 Energy Reflection 166
6.8.1 Comparison to Prior Results 166
6.8.2 Effect of Transition Slope on Reflection 167
6.9 Analytic Nearshore Shoaling and Refraction Method 171
6.9.1 Comparison of Analytic Method to REF/DIF-1 176
6.9.2 Wave Averaged Results 183
6.10 Shoreline Evolution Model 185
6.10.1 Shoreline Change Estimates Shoreward of Bathymetric Anomalies . 186
6.10.2 Effect of Nearshore Form on Shoreline Change 197
6.10.3 Investigation of Boundary Conditions 200
6.10.4 Investigation of Transition Slope on Shoreline Evolution 202

7 CONCLUSIONS AND DIRECTIONS FOR FUTURE STUDY 208

7.1 Conclusions 208
7.2 Future Work 211

APPENDIX

A ANALYTIC WAVE ANGLE CALCULATION 213

B ANALYTIC FAR-FIELD APPROXIMATION OF ENERGY REFLECTION 215

C ANALYTIC NEARSHORE SHOALING AND REFRACTION METHOD 218

D ANALYTIC SHORELINE CHANGE THEORY AND CALCULATION 222

REFERENCES 228

BIOGRAPHICAL SKETCH 236

LIST OF TABLES

Table page

2-1 Capabilities of selected nearshore wave models.....42

4-1 Specifications for two bathymetries for exact solution method.....91

LIST OF FIGURES

Figure page

2-1 Aerial photograph showing salients shoreward of borrow area looking East to West along Grand Isle, Louisiana, in August, 1985. 9

2-2 Aerial photograph showing salients shoreward of borrow area along Grand Isle, Louisiana, in 1998. 10

2-3 Bathymetry off Anna Maria Key, Florida, showing location of borrow pit following beach nourishment project. 13

2-4 Beach profile through borrow area at R-26 in Anna Maria Key, Florida 14

2-5 Shoreline position for Anna Maria Key Project for different periods relative to August, 1993 14

2-6 Project area for Martin County beach nourishment project. 15

2-7 Four-year shoreline change for Martin County beach nourishment project: predicted versus survey data. 16

2-8 Setup for laboratory experiment. 19

2-9 Results from laboratory experiment showing plan shape after two hours. 20

2-10 Experiment sequence timeline for Williams laboratory experiments. 21

2-11 Volume change per unit length for first experiment 22

2-12 Shifted even component of shoreline change for first experiment. 23

2-13 Reflection and transmission coefficients for linearly varying depth $[h_I/h_{III}]$ and linearly varying breadth $[b_I^2/b_{III}^2]$. 26

2-14 Approximate reflection and transmission coefficients for the rectangular parallelepiped of length $8.86h_0$ in infinitely deep water. 27

2-15 Reflection coefficient for a submerged obstacle. 28

2-16 Transmission coefficient as a function of relative wavelength (h=10.1 cm, d=67.3 cm, trench width =161.6 cm) 30

2-17 Transmission coefficient as a function of relative wavelength for trapezoidal trench; setup shown in inset diagram 31

2-18 Reflection coefficient for asymmetric trench and normally incident waves as a function of Kh_1: $h_2/h_1=2$, $h_3/h_1=0.5$, $L/h_1=5$; L = trench width. 32

2-19 Transmission coefficient for symmetric trench, two angles of incidence: $L/h_1=10$, $h_2/h_1=2$; L = trench width. 32

2-20 Transmission coefficient as a function of relative trench depth; normal incidence: $k_1h_1= 0.2$: (a) $L/h_1=2$; (b) $L/h_1=8$, L = trench width. 33

2-21 Total scattering cross section of vertical circular cylinder on bottom 35

2-22 Contour plot of relative amplitude in and around pit for normal incidence; $k_1/d = \pi/10$, $k_2/h=\pi/10\sqrt{2}$, h/d=0.5, b/a =1, a/d=2, a = cross-shore pit length, b = longshore pit length, h = water depth outside pit, d = depth inside pit, L_2 = wavelength outside pit. 37

2-23 Contour plot of diffraction coefficient in and around pit for normal incidence; a/L=1, b/L=0.5, d/h =3, kh=0.167. 39

2-24 Contour plot of diffraction coefficient around surface-piercing breakwater for normal incidence; a/L=1, b/L=0.5, kh=0.167. 39

2-25 Maximum and minimum relative amplitudes for different k_oa, for normal incidence, a/b=6, a/d=π, and d/h=2 40

2-26 Comparison of wave height profiles for selected models along transect parallel to shore located 9 m shoreward of shoal apex[•=experimental data] 44

2-27 Comparison of wave height profiles for selected models along transect perpendicular to shore and through shoal apex [•=experimental data]. 44

2-28 Calculated beach planform due to refraction after two years of prototype waves for two pit depths. 48

2-29 Calculated beach planform due to refraction over dredged hole after two years of prototype waves. 50

2-30 Comparison of changes in beach plan shape for laboratory experiment and numerical model after two years of prototype waves. 51

2-31 Nearshore wave height transformation coefficients near borrow pit from RCPWAVE study. 53

2-32 Nearshore wave angles near borrow pit from RCPWAVE study; wave angles are relative to shore normal and are positive for westerly transport....53

2-33 Reflection coefficients versus dimensionless pit diameter divided by wavelength inside and outside the pit; water depth = 2 m, pit depth = 4 m. 55

2-34 Shoreline evolution resulting from each transport term individually for transect located 80 m shoreward of a pit with a radius = 6 m, last time step indicated with [+]....57

2-35 Shoreline evolution using full transport equation and analytic solution model for transect located 80 m shoreward of a pit with a radius = 6 m, last time step indicated with [+]. 58

3-1 Definition sketch for trench with vertical transitions. 63

3-2 Definition sketch for trench with stepped transitions. 66

3-3 Definition sketch for linear transition....70

3-4 Definition sketch for trench with sloped transitions....73

4-1 Definition sketch for circular pit with abrupt depth transitions....78

4-2 Definition sketch for boundary of abrupt depth transition. 82

4-3 Definition sketch for boundaries of gradual depth transitions. 85

4-4 Definition sketch for boundaries of exact shallow water solution method. 90

5-1 Matching conditions with depth for magnitude of the horizontal velocity and velocity potential for trench with abrupt transitions and 16 evanescent modes. 94

5-2 Matching conditions with depth for phase of the horizontal velocity and velocity potential for trench with abrupt transitions and 16 evanescent modes. 94

5-3 Relative amplitude for cross-trench transect for $k_1h_1 = 0.13$; trench bathymetry included with slope = 0.1....95

5-4 Relative amplitude for cross-shoal transect for $k_1h_1 = 0.22$; shoal bathymetry included with slope = 0.05....96

5-5 Relative amplitude along cross-trench transect for Analytic Model and FUNWAVE 1-D for $k_1h_1 = 0.24$; trench bathymetry included with slope = 0.1 98

5-6 Relative amplitude along cross-shoal transect for Analytic Model and FUNWAVE 1-D for $k_1h_1 = 0.24$; shoal bathymetry included with upwave slope of 0.2 and downwave slope of 0.05. 99

5-7 Comparison of reflection coefficients from step method and Kirby and Dalrymple (1983a Table 1) for symmetric trench with abrupt transitions and normal wave incidence: $h_3 = h_1$, $h_2/h_1 = 3$, $W/h_1 = 10$. 100

5-8 Comparison of transmission coefficients from step method and Kirby and Dalrymple (1983a Table 1) for symmetric trench with abrupt transition and normal wave incidence: $h_3 = h_1$, $h_2/h_1 = 3$, $W/h_1 = 10$. 101

5-9 Setup for symmetric trenches with same depth and different bottom widths and transition slopes. 102

5-10 Reflection coefficients versus k_1h_1 for trenches with same depth and different bottom widths and transition slopes. Only one-half of the symmetric trench cross-section is shown with slopes of 5000, 1, 0.2 and 0.1. ...103

5-11 Transmission coefficients versus k_1h_1 for trenches with same depth and different bottom widths and transition slopes. Only one-half of the symmetric trench cross-section is shown with slopes of 5000, 1, 0.2 and 0.1. ...104

5-12 Reflection coefficient versus the number of evanescent modes used for trenches with same depth and transition slopes of 5000, 1, and 0.1. 105

5-13 Reflection coefficient versus the number of steps for trenches with same depth and transition slopes of 5000, 1, and 0.1. 106

5-14 Reflection coefficients versus k_1h_1 for trenches with same bottom width and different depths and transition slopes. Only one-half of the symmetric trench cross-section is shown with slopes of 5000, 1, 0.2 and 0.05. 107

5-15 Reflection coefficients versus k_1h_1 for trenches with same top width and different depths and transition slopes. Only one-half of the symmetric trench cross-section is shown with slopes of 5000, 5, 2, and 1. 108

5-16 Reflection coefficients versus k_1h_1 for trenches with same depth and bottom width and different transition slopes. Only one-half of the symmetric trench cross-section is shown with slopes of 5000, 0.2, 0.1, and 0.05. 109

5-17 Reflection coefficients versus k_1h_1 for shoals with same depth and different top widths and transition slopes. Only one-half of the symmetric shoal cross-section is shown with slopes of 5000, 0.5, 0.2 and 0.05. 110

5-18 Reflection coefficients versus k_1h_1 for Gaussian trench with $C_1 = 2$ m and $C_2 = 12$ m and $h_o = 2$ m. Only one-half of the symmetric trench cross-section is shown with 43 steps approximating the non-planar slope. 111

5-19 Reflection coefficients versus k_1h_1 for Gaussian shoal with $C_1 = 1$ m and $C_2 = 8$ m and $h_o = 2$ m. Only one-half of the symmetric shoal cross-section is shown with 23 steps approximating the non-planar slope. 112

5-20 Reflection coefficients versus k_1h_1 for a symmetric abrupt transition trench, an asymmetric trench with $s_1 = 1$ and $s_2 = 0.1$ and a mirror image of the asymmetric trench. 113

5-21 Reflection coefficients versus k_1h_1 for an asymmetric abrupt transition trench ($h_1 \neq h_5$), an asymmetric trench with gradual depth transitions ($h_1 \neq h_5$ and $s_1 = s_2 = 0.2$) and a mirror image of the asymmetric trench with $s_1 = s_2$. 114

5-22 Reflection coefficients versus k_1h_1 for an asymmetric abrupt transition trench ($h_1 \neq h_5$), an asymmetric trench with gradual depth transitions ($h_1 \neq h_5$ and $s_1 = 1$ and $s_2 = 0.2$) and a mirror image of the asymmetric trench with $s_1 \neq s_2$. 115

5-23 Reflection coefficient versus the space step, dx, for trenches with same depth and different bottom width and transition slopes. Only one-half of the symmetric trench cross-section is shown with slopes of 5000, 1 and 0.1. 117

5-24 Reflection coefficients versus k_3h_3 for three solution methods for the same depth trench case with transition slope equal to 5000. Only one-half of the symmetric trench cross-section is shown.....118

5-25 Reflection coefficients versus k_3h_3 for three solution methods for same depth trench case with transition slope equal to 1. Only one-half of the symmetric trench cross-section is shown.....119

5-26 Reflection coefficients versus k_3h_3 for three solution methods for same depth trench case with transition slope equal to 0.1. Only one-half of the symmetric trench cross-section is shown.....119

5-27 Conservation of energy parameter versus k_3h_3 for three solution methods for same depth trench case with transition slope equal to 1. Only one-half of the symmetric trench cross-section is shown. 120

5-28 Reflection coefficients versus k_1h_1 for step and numerical methods for Gaussian shoal ($h_o = 2$ m, $C_1 = 1$ m, $C_2 = 8$ m). Only one-half of the

symmetric shoal cross-section is shown with 23 steps approximating the non-planar slope....121

5-29 Reflection coefficients versus k_3h_3 for step and numerical methods for Gaussian trench in shallow water (h_o = 0.25 m, C_1 = 0.2 m, C_2 = 3 m). Only one-half of the symmetric trench cross-section is shown with 23 steps approximating the non-planar slope....122

5-30 Reflection coefficients versus k_3h_3 for three solution methods for same depth trench case with symmetric abrupt transition trench and asymmetric trench with unequal transition slopes equal to 1 and 0.1....123

5-31 Reflection coefficients versus k_3h_3 for three solution methods for same depth trench case with asymmetric abrupt transition trench and asymmetric trench with unequal transition slopes equal to 1 and 0.2....124

6-1 Matching conditions with depth for magnitude of the horizontal velocity and velocity potential for pit with abrupt transitions and 10 evanescent modes....127

6-2 Matching conditions with depth for phase of the horizontal velocity and velocity potential for pit with abrupt transitions and 10 evanescent modes....128

6-3 Contour plot of relative amplitude with k_1h_1 = 0.24 for pit with transition slope = 0.1; cross-section of pit bathymetry through centerline included....129

6-4 Relative amplitude for cross-shore transect at Y = 0 with k_1h_1 = 0.24 for pit with transition slope = 0.1; cross-section of pit bathymetry through centerline included. Note small reflection....130

6-5 Relative amplitude for longshore transect at X = 300 m with k_1h_1 = 0.24 for pit with transition slope = 0.1; cross-section of pit bathymetry through centerline included....130

6-6 Relative amplitude versus number of evanescent modes included for different Bessel function summations at two locations directly shoreward of a pit with abrupt transitions in depth....132

6-7 Relative amplitude versus number of steps approximating slope for different Bessel function summations for two pits with gradual transitions in depth....133

6-8 Contour plot of relative amplitude for shoal with k_1h_1 = 0.29 and transition slope = 0.1; cross-section of shoal bathymetry through centerline included....134

6-9 Relative amplitude for cross-shore transect at Y = 0 for same depth pits for k_1h_1 = 0.15; cross-section of pit bathymetries through centerline included with slopes of abrupt, 1, 0.2 and 0.07....135

6-10 Relative amplitude for cross-shore transect at Y = 0 for same depth pits for $k_1h_1 = 0.3$; cross-section of pit bathymetries through centerline included with slopes of abrupt, 1, 0.2 and 0.07. 136

6-11 Relative amplitude for alongshore transect at X = 200 m for same depth pits for $k_1h_1 = 0.15$; cross-section of pit bathymetries through centerline included with slopes of abrupt, 1, 0.2 and 0.07. 137

6-12 Relative amplitude for alongshore transect at X = 200 m for same depth pits for $k_1h_1 = 0.3$; cross-section of pit bathymetries through centerline included with slopes of abrupt, 1, 0.2 and 0.07. 138

6-13 Relative amplitude for cross-shore transect located at Y = 0 for same depth shoals with $k_1h_1 = 0.15$; cross-section of shoal bathymetries through centerline included with slopes abrupt, 1, 0.2 and 0.05. 139

6-14 Relative amplitude for alongshore transect located at X = 300 m for same depth shoals with $k_1h_1 = 0.15$; cross-section of shoal bathymetries through centerline included abrupt, 1, 0.2 and 0.05. 140

6-15 Relative amplitude for cross-shore transect at Y = 0 for pit with Gaussian transition slope for $k_1h_1 = 0.24$; cross-section of pit bathymetry through centerline included. 141

6-16 Relative amplitude for cross-shore transect at Y = 0 for pit with for h = C/r in region of transition slope; cross-section of pit bathymetry through centerline included. 142

6-17 Relative amplitude for longshore transect at X = 100 m for pit with for h = C/r in region of transition slope; cross-section of pit bathymetry through centerline included. 143

6-18 Relative amplitude for cross-shore transect at Y = 0 for shoal with for h = C*r in region of transition slope; cross-section of shoal bathymetry through centerline included. 143

6-19 Relative amplitude for longshore transect at X = 100 m for shoal with for h = C*r in region of transition slope; cross-section of shoal bathymetry through centerline included. 144

6-20 Contour plot of wave angles in degrees for pit with $k_1h_1 = 0.24$ and transition slope = 0.1; cross-section of pit bathymetry through centerline included. 145

6-21 Contour plot of wave angles for Gaussian shoal with $C_1 = 1$ and $C_2 = 10$ for $k_1h_1 = 0.22$; cross-section of shoal bathymetry through centerline included with 23 steps approximating slope. 146

6-22 Wave angle for alongshore transect at X = 300 m for same depth pits for $k_1h_1 = 0.15$; cross-section of pit bathymetries through centerline included with slopes of abrupt, 1, 0.2 and 0.07. Negative angles indicate divergence of wave rays. 147

6-23 Relative amplitude using 3-D Step Model and REF/DIF-1 for cross-shore transect at Y = 0 for Gaussian pit with $k_1h_1 = 0.24$; cross-section of pit bathymetry through centerline included. 149

6-24 Relative amplitude using 3-D Step Model and REF/DIF-1 for longshore transect at X = 100 m for Gaussian pit with $k_1h_1 = 0.24$; cross-section of pit bathymetry through centerline included. 150

6-25 Relative amplitude using 3-D Step Model and REF/DIF-1 for longshore transect at X = 400 m for Gaussian pit with $k_1h_1 = 0.24$; cross-section of pit bathymetry through centerline included. 151

6-26 Wave angle using 3-D Step Model and REF/DIF-1 for longshore transect at X = 100 m for Gaussian pit with $k_1h_1 = 0.24$; cross-section of pit bathymetry through centerline included. 152

6-27 Relative amplitude using 3-D Step Model and REF/DIF-1 for cross-shore transect at Y = 0 for pit with linear transitions in depth with $k_1h_1 = 0.24$; cross-section of pit bathymetry through centerline included with slope = 0.1 153

6-28 Relative amplitude using 3-D Step Model and REF/DIF-1 for longshore transect at X = 350 m for pit with linear transitions in depth with $k_1h_1 = 0.24$; cross-section of pit bathymetry through centerline included with slope = 0.1. 154

6-29 Relative amplitude using 3-D Step Model and 2-D fully nonlinear Boussinesq model for cross-shore transect at Y = 0 for shoal with $k_1h_1 = 0.32$; cross-section of pit bathymetry through centerline included. 155

6-30 Experimental setup of Chawla and Kirby (1986) for shoal centered at (0,0) with data transects used in comparison shown. 157

6-31 Relative amplitude using 3-D Step Model, FUNWAVE 2-D and data from Chawla and Kirby (1996) for cross-shore transect A-A with $k_1h_1 = 1.89$; cross-section of shoal bathymetry through centerline included. 158

6-32 Relative amplitude using 3-D Step Model, FUNWAVE 2-D and data from Chawla and Kirby (1996) for longshore transect E-E with $k_1h_1 = 1.89$; cross-section of shoal bathymetry through centerline included. 159

6-33 Relative amplitude using 3-D Step Model, FUNWAVE 2-D and data from Chawla and Kirby (1996) for longshore transect D-D with $k_1h_1 = 1.89$; cross-section of shoal bathymetry through centerline included.....160

6-34 Relative amplitude using 3-D Step Model, FUNWAVE 2-D and data from Chawla and Kirby (1996) for longshore transect B-B with $k_1h_1 = 1.89$; cross-section of shoal bathymetry through centerline included.....161

6-35 Relative amplitude averaged over incident direction (centered at 0 deg) for alongshore transect at X = 300 m for pit with $k_1h_1 = 0.24$; cross-section of pit bathymetries through centerline included with slope = 0.1.....162

6-36 Wave angle averaged over incident direction (centered at 0 deg) for alongshore transect at X = 300 m for pit with $k_1h_1 = 0.24$ with bathymetry indicated in inset diagram of previous figure. 163

6-37 Relative amplitude averaged over incident direction (centered at 20 deg) for alongshore transect at X = 300 m for pit with $k_1h_1 = 0.24$; cross-section of pit bathymetries through centerline included with slope = 0.1.....165

6-38 Wave angle averaged over incident direction (centered at 20 deg) for alongshore transect at X = 300 m for pit with $k_1h_1 = 0.24$ with bathymetry indicated in inset diagram of previous figure. 165

6-39 Reflection coefficient versus non-dimensional diameter; comparison between shallow water transect method and far-field approximation method. ...167

6-40 Reflection coefficient versus k_1h_1 based on far-field approximation and constant volume and depth pits; cross-section of pit bathymetries through centerline included with slopes of abrupt, 1, 0.2 and 0.07.....168

6-41 Reflection coefficient versus k_1h_1 based on far-field approximation and constant volume bottom width pits; cross-section of pit bathymetries through centerline included with slopes of abrupt, 1, 0.2 and 0.05. 169

6-42 Reflection coefficient versus k_1h_1 based on far-field approximation and constant volume and depth shoals; cross-section of shoal bathymetry through centerline included with slopes of abrupt, 1, 0.2 and 0.07. 170

6-43 Bathymetry for two nearshore regions used in analytic shoaling and refraction model: Pit 1; linear transition slopes with linear nearshore slope and Pit 2; Gaussian transition slopes with Equilibrium Beach form for nearshore slope.....172

6-44 Wave height and wave angle values at start of nearshore region and at breaking for longshore transect with bathymetry with H = 1 m and T = 12 s for Pit 1. 173

6-45 Contour plot of wave height for Pit 1 in nearshore region with breaking location indicated with H = 1 m and T = 12 s.....174

6-46 Wave height and wave angle values at start of nearshore region and at breaking for longshore transect with bathymetry with H = 1 m and T = 12 s for Pit 2 bathymetry. 175

6-47 Contour plot of wave height for Pit 2 in nearshore region with breaking location indicated with H = 1 m and T = 12 s.....176

6-48 Wave height and wave angle values at start of nearshore region from 3-D Step Model and REF/DIF-1 (linear) with H = 1 m and T = 12 s for Pit 1.....177

6-49 Wave height and wave angle values at h = 1.68 m (X = 616 m) from 3-D Step Model and REF/DIF-1 (linear) with H = 1 m and T = 12 s for Pit 1.....178

6-50 Wave height and wave angle values at h = 1.44 m (X = 628 m) from 3-D Step Model and REF/DIF-1 (linear) with H = 1 m and T = 12 s for Pit 1.....179

6-51 Wave height and wave angle values at start of nearshore region from 3-D Step Model and REF/DIF-1 (linear) with H = 1 m and T = 12 s for Pit 2.....180

6-52 Wave height and wave angle values at h = 2.04 m (X = 672 m) from 3-D Step Model and REF/DIF-1 (linear) with H = 1 m and T = 12 s for Pit 2.....181

6-53 Wave height and wave angle values at h = 1.6 m (X = 704 m) from 3-D Step Model and REF/DIF-1 (linear) with H = 1 m and T = 12 s for Pit 2.....182

6-54 Weighted wave averaged values of wave height and wave angle at start of nearshore region and at breaking for longshore transect with H = 1 m and T = 12 s and bathymetry for Pit 1.....184

6-55 Weighted wave averaged values of wave height and wave angle at start of nearshore region and at breaking for longshore transect with H = 1 m and T = 12 s and bathymetry for Pit 2.....184

6-56 Shoreline evolution for case Pit 1 with $K_1 = 0.77$ and $K_2 = 0.4$ for incident wave height of 1 m, wave period of 12 s, and time step of 50 s with shoreline advancement in the negative X direction; Pit 1 bathymetry along cross-shore transect included. 187

6-57 Parameters for shoreline change after 1st time step showing shoreline position, and longshore transport terms for case Pit 1 with $K_1 = 0.77$ and $K_2 = 0$. 188

6-58 Final shoreline planform for case Pit 1 with $K_1 = 0.77$ and $K_2 = 0$, 0.2, 0.4, and 0.77 for incident wave height of 1 m and T = 12 s, with shoreline

advancement in the negative X direction; Pit 1 bathymetry along cross-shore transect included. 189

6-59 Change in shoreline position with modeling time at 4 longshore locations (Yp = 0, 100, 200, 300 m) for case Pit 1 with $K_1 = 0.77$ and $K_2 = 0.4$ with shoreline advancement in the negative X direction; Pit 1 bathymetry along cross-shore transect included. 191

6-60 Comparison of wave height and wave angle values at 600 m and 600 m +/- 20 m for case of Pit 1 for T = 12 s with bathymetry and transect locations indicated in bottom plot. 192

6-61 Final shoreline planform for case Pit 2 with $K_1 = 0.77$ and $K_2 = 0$, 0.2, 0.4, and 0.77 for incident wave height of 1 m, wave period of 12 s, and time step of 50 s with shoreline advancement in the negative X direction; Pit 2 bathymetry along cross-shore transect included. 193

6-62 Shoreline evolution for case Pit 2 with $K_1 = 0.77$ and $K_2 = 0$ for incident wave height of 1 m, wave period of 12 s, and time step of 50 s with shoreline advancement in the negative X direction; Pit 2 bathymetry along cross-shore transect included. 194

6-63 Change in shoreline position with modeling time at 4 longshore locations (Yp = 0, 100, 200, 300 m) for case Pit 2 with $K_1 = 0.77$ and $K_2 = 0$ with shoreline advancement in the negative X direction; Pit 2 bathymetry along cross-shore transect included. 195

6-64 Final shoreline planform for case Shoal 1 with $K_1 = 0.77$ and $K_2 = 0$, 0.2, 0.4, and 0.77 for incident wave height of 1 m, wave period of 12 s, and time step of 50 s with shoreline advancement in the negative X direction; Shoal 1 bathymetry along cross-shore transect included. 196

6-65 Shoreline evolution for case Shoal 1 with $K_1 = 0.77$ and $K_2 = 0.2$ for incident wave height of 1 m, wave period of 12 s, and time step of 50 s with shoreline advancement in the negative X direction; Shoal 1 bathymetry along cross-shore transect included. 197

6-66 Final shoreline planform for case Pit 1 with linear nearshore slope and EBP form for T = 12 s and with $K_1 = 0.77$ and $K_2 = 0$ and 0.77 with shoreline advancement in the negative X direction; Pit 1 and Pit 1b bathymetry along cross-shore transect included. 198

6-67 Final shoreline planform for case Shoal 1 (linear nearshore slope) and Shoal 1b (Equilibrium Beach Profile) for T = 12 s and with $K_1 = 0.77$ and $K_2 = 0$ and 0.77 with shoreline advancement in the negative X direction; Shoal 1 and Shoal 1b bathymetry along cross-shore transect included. 199

6-68 Final shoreline planform for case Pit 1 for T = 12 s and with K_1 = 0.77 and K_2 = 0.4 for two boundary conditions with shoreline advancement in the negative X direction; Pit 1 bathymetry along cross-shore transect included.....201

6-69 Final shoreline planform for case Shoal 1 for T = 12 s and with K_1 = 0.77 and K_2 = 0.77 for two boundary conditions with shoreline advancement in the negative X direction; Shoal 1 bathymetry along cross-shore transect included.....202

6-70 Final shoreline planform for constant volume pits for T = 12 s and with K_1 = 0.77 and K_2 = 0 with shoreline advancement in the negative X direction; cross-section of pit bathymetries through centerline included with slopes of abrupt, 1, 0.2, 0.07. 203

6-71 Final shoreline planform for constant volume pits for T = 12 s and with K_1 = 0.77 and K_2 = 0 and 0.4 with shoreline advancement in the negative X direction; cross-section of pit bathymetries through centerline included with slopes of abrupt, 1, 0.2, 0.07. 205

6-72 Final shoreline planform for 5 periods for constant volume pits with K_1 = 0.77 and K_2 = 0 with shoreline advancement in the negative X direction; cross-section of pit bathymetry through centerline included with slope 0.2. 205

6-73 Maximum shoreline advancement and retreat versus period for constant volume pits with K_1 = 0.77 and K_2 = 0; cross-section of pit bathymetries through centerline included with slopes of abrupt, 1, 0.2, 0.07. 206

6-74 Maximum shoreline advancement and retreat versus period for constant volume pits with K_1 = 0.77 and K_2 = 0.4; cross-section of pit bathymetries through centerline included with slopes of abrupt, 1, 0.2, 0.07. 207

C-1 Setup for analytic nearshore shoaling and refraction method.....218

D-1 Definition sketch for analytic shoreline change method showing shoreline and contours for initial location and after shoreline change. 223

Abstract of Dissertation Presented to the Graduate School
of the University of Florida in Partial Fulfillment of the
Requirements for the Degree of Doctor of Philosophy

WAVE TRANSFORMATION BY BATHYMETRIC ANOMALIES WITH GRADUAL TRANSITIONS IN DEPTH AND RESULTING SHORELINE RESPONSE

By

Christopher J. Bender

May 2003

Chair: Robert G. Dean
Major Department: Civil and Coastal Engineering

Analytic models for the propagation of linear water waves over a trench or shoal of finite width and infinite length (2-D Step Model) and over an axisymmetric bathymetric anomaly (3-D Step Model) are developed. The models are valid in a region of uniform depth containing a bathymetric anomaly of uniform depth with gradual transitions in depth allowed as a series of uniform depth steps approximating linear or non-linear slopes. The velocity potential obtained determines the wave field in the domain.

The 2-D Step Model provides the complete wave field and, therefore, the reflection and transmission characteristics for depth anomalies of infinite length that are either symmetric or asymmetric. The 3-D Step Model determines the wave transformation caused by the processes of wave refraction, diffraction and reflection. Using the known velocity potential an energy flux approach is used to calculate the wave angle and reflected energy at large distances from the anomaly. The 3-D Step Model is

joined with an analytic shoaling and refraction model (Analytic S/R Model) to extend the solution into the nearshore region. The Analytic S/R Model is employed to propagate the wave field up to the point of depth limited breaking. The breaking wave conditions are used to drive the longshore sediment transport and associated shoreline change using the Shoreline Change Model, which provides estimates of the equilibrium shoreline planform located landward of a bathymetric anomaly.

Comparisons of the 2-D Step Model to shallow water models developed in the study, previous studies, and a numerical model are made with good agreement demonstrated. The reflection coefficients found for symmetric and asymmetric trenches and shoals indicate multiple and no instances of complete transmission, respectively, with the solution independent of the incident wave direction for both cases.

Comparisons to a shallow water model, numerical models, and experimental data verify the results of the 3-D Step Model for several bathymetries, with the Analytic S/R Model verified by a numerical model for breaking wave conditions. Modeled equilibrium planforms landward of bathymetric anomalies indicate the importance of the longshore transport coefficients with either erosion or shoreline advancement possible for several cases presented.

CHAPTER 1
INTRODUCTION AND MOTIVATION

Irregular and unexpected shoreline planforms adjacent to nearshore borrow areas have increased awareness of the wave field modification caused by bathymetric anomalies such as borrow pits or shoals. When a wave field in a region of generally uniform depth encounters a bathymetric anomaly the wave field is modified through wave refraction, wave diffraction, wave reflection and wave dissipation, with the first three known collectively as scattering. These four wave transformation processes result in a modified wave field that propagates towards, and eventually impacts, the shoreline. The modified wave field will alter the longshore transport leading to a shoreline planform that is held to an artificial equilibrium.

Case studies such as the beach nourishment projects at Grand Isle, Louisiana, and Anna Maria Key, Florida, have shown the possible effects of a nearshore borrow area on the adjacent shoreline planform. The ability to predict, and possibly design for, the equilibrium planform in the vicinity of a bathymetric anomaly requires a better understanding of both the wave and sediment processes near the anomaly. The focus of this report is to better understand the wave field modifications caused by bathymetric anomalies, of both two-dimensional and three-dimensional forms, with results providing the foundation for study on the sediment transport processes and shoreline changes induced.

Several studies including field and laboratory scales have been conducted to investigate this issue. These studies examined the wave transformation over a bathymetric anomaly with the shoreline changes caused by the altered wave field. Earlier, dating back to the early 1900's, the focus was on the modification of a wave train encountering a change in bathymetry, which was solved using analytic methods. This early research included development of analytical solutions for bathymetric changes in the form of a step, or a pit, first of infinite length (in one horizontal dimension; 2-D models), and, more recently, of finite dimensions (in two horizontal dimensions; 3-D models). The complexity of the 3-D models has advanced from a pit/shoal with vertical sidewalls and uniform depth surrounded by water of uniform depth, which can be solved analytically, to domains with arbitrary bathymetry that are solved using complex numerical schemes. Some models combine the calculation of the wave transformation and resulting shoreline change, whereas others perform the wave calculations separately and rely on a different program for shoreline evolution.

1.1 Motivation

Changes in offshore bathymetry modify the local wave field, thus causing an equilibrium planform that may be altered significantly from the previous, relatively straight shoreline. Not only can a bathymetric change cause wave transformation, but also may change the sediment transport dynamics by drawing sediment into it from the nearshore or by intercepting the onshore movement of sediment. Knowledge of wave field modifications and the resulting effects on sediment transport and shoreline evolution is essential in the design of beach nourishment projects and other engineering activities that alter offshore bathymetry.

Beach nourishment has become the preferred technique to address shoreline erosion. In most beach nourishment projects, the fill placed on the eroded beach is obtained from borrow areas located offshore of the nourishment site. The removal of large quantities of fill needed for most projects can result in substantial changes to the offshore bathymetry through the creation of borrow pits or by modifying existing shoals. The effect of the modified bathymetry in the borrow area on the wave field and the influence of the modified wave field on the shoreline can depend on the incident wave conditions, the nourishment sediment characteristics and some features of the borrow area including the location, size, shape and orientation.

The large quantities of sediment used in beach nourishment projects combined with the increase in the number of projects constructed, and an increased industrial need for quality sediment have, in many areas, led to a shortage of quality offshore fill material located relatively near to the shore. This shortage has increased interest in the mining of sediment deposits located in Federal waters, which fall under the jurisdiction of the Minerals Management Service (MMS). Questions have been raised by the MMS regarding the potential effects on the shoreline of removing large quantities of sediment from borrow pits lying in Federal waters (Minerals Management Service, 2003).

A better understanding of the effects of altering the offshore bathymetry is currently needed. The scattering processes of wave refraction, diffraction, and reflection modify the wave field in a complex manner dependent on the local wave and nearshore conditions. A more complete understanding and predictive capability of the effect of bathymetric changes to the wave field and the resulting shoreline modification leading to less impactive design of dredge pit geometries should be the goal of current research.

1.2 Models Developed and Applications

A better understanding of the wave field near bathymetric anomalies can be obtained through models that more accurately represent their shapes and the local wave transformation processes. The models developed in this study extend previous analytic methods to better approximate the natural domain and extend the problem from the offshore region to the shoreline. By meshing a model constrained by a uniform depth requirement outside of the bathymetric anomaly to a nearshore model with a sloped bottom, linear waves can be propagated from the offshore over the anomaly and into the nearshore where shoaling and refraction lead to wave breaking and sediment transport. A longshore sediment transport model can then predict the shoreline changes resulting from the wave field modified by the bathymetric anomaly.

Previous analytic 3-D models and all of the previous 2-D models, with the exception of Dean (1964) and Lee et al. (1981), have domains that contain abrupt transitions in depth (vertical sidewalls) for the bathymetric anomaly. A more realistic representation of natural bathymetric anomalies should allow for gradual transitions (sloped sidewalls). The focus of the present study is the propagation of water waves over a 2-D (trench or shoal) or 3-D (pit or shoal) bathymetric anomaly of more realistic geometry and the wave transformation they induce.

Three solution methods are developed for a 2-D domain with linear water waves and normal wave incidence: (1) the 2-D step method, (2) the slope method and (3) a numerical method. The 2-D step method is valid in arbitrary water depth while the slope method and the numerical method are valid only for shallow water conditions. The step method is an extension of the Takano (1960) solution as modified by Kirby and Dalrymple (1983a) that allows for a trench or shoal with "stepped" transitions that

approximate a specific slope or shape. The slope method is an extension of the Dean (1964) solution that allows for linear transitions between the changes in bathymetry for a trench or shoal creating regular or irregular trapezoids. The numerical method employs a backward space-stepping procedure for arbitrary (but shallow water) bathymetry with the transmitted wave specified. The 2-D models are compared against each other, with the results of Kirby and Dalrymple (1983a) and with the numerical model FUNWAVE 1.0 [1-D] (Kirby et al., 1998).

For a 3-D domain, an analytic solution to the wave field modification caused by bathymetric anomalies with sloped transitions in depth is developed. This solution is an extension of previous work for anomalies with abrupt depth transitions in regions of otherwise uniform depth that employs steps to approximate a gradual transition in depth. A shallow water analytic solution is also developed, which is valid for specific sidewall slope and pit size combinations. The 3-D models are validated with the laboratory data of Chawla and Kirby (1996), the numerical models REF/DIF-1 (Kirby and Dalrymple, 1994) and FUNWAVE 1.0 [2-D] (Kirby et al., 1998), and the numerical model of Kennedy et al. (2000) and through direct comparisons.

The application of the different models to real-world problems depends on the situation of interest. The study of 2-D models can demonstrate the reflection caused by long trenches or shoals of finite width such as navigation channels and underwater breakwaters, respectively. The 3-D models can be employed to study problems with variation in the longshore and non-oblique incidence. Wave related quantities such as energy flux and wave direction are calculated and indicate the influence of the bathymetric anomaly. The wave heights and directions for transects located shoreward of

the anomaly are combined with an analytic shoaling and refraction method to determine the wave propagation in a nearshore zone of arbitrary slope. The longshore transport and shoreline evolution are also calculated for the nearshore (shoaled and refracted) wave field that occurs shoreward of the anomaly. Through the methods developed in this study the wave transformation, energy reflection, longshore transport, and shoreline evolution induced by a 3-D bathymetric anomaly with gradual transitions in depth can be investigated.

CHAPTER 2
LITERATURE REVIEW

Several methods have been employed to quantify the impact on the shoreline caused by changes in the offshore bathymetry including case studies, field experiments, analytical developments, numerical models, and laboratory studies. The intriguing behavior of the shoreline following beach nourishment projects at Grand Isle, Louisiana, Anna Maria Key, Florida, and Martin County, Florida, have led to questions and investigations regarding the impact of the significant offshore borrow areas present in each case.

Field studies have been used to investigate the impact of offshore dredging in relatively deeper water to attempt to define a depth at which bathymetric changes will not induce significant wave transformation. Laboratory experiments have documented wave transformations caused by changes in the bathymetry and the resulting effects on the shoreline in controlled settings possible only in the laboratory.

Solutions for wave transformation by changes in the bathymetry are outlined primarily in chronological order following the development from analytical solutions for long waves in one horizontal dimension (2-D) through numerical models for arbitrary bathymetry that include many wave-related nearshore processes in 3 dimensions. Modeling of shoreline responses due to wave field modification from changes in offshore bathymetry is examined with models that include both wave field and shoreline changes and by coupling models that evaluate these processes independently. The wave

transformation processes included in nearshore models are important factors in the capability to predict a salient leeward of a pit, the shoreline responses observed in the limited laboratory experiments and at Grand Isle, Louisiana.

2.1 Case Studies

2.1.1 Grand Isle, Louisiana (1984)

The beach nourishment project at Grand Isle, Louisiana, provides one of the most interesting, and well publicized examples of an irregular planform resulting from the effects of a large borrow area lying directly offshore. One year after the nourishment project was completed, two large salients, flanked by areas of increased erosion, developed immediately shoreward of the offshore borrow area. Combe and Soileau (1987) provide a detailed account of the shoreline maintenance history at Grand Isle, Louisiana, specifications of the beach nourishment project that was completed in 1984, and details of the shoreline evolution in the two years following completion.

The project required 2.1×10^6 m^3 of sediment with approximately twice this amount dredged from an area lying 800 m from the shore (Combe and Soileau, 1987) in 4.6 m of water (Gravens and Rosati, 1994). The dredging resulted in a borrow pit that was "dumbbell" shaped in the planform with two outer lobes dredged to a depth of 6.1 m below the bed, connected by a channel of approximate 1,370 m length dredged to 3.1 m below the bed (Combe and Soileau, 1987). The salients seen in Figure 2-1 started to form during storm events that occurred during the winter and spring of 1984/85 (Combe and Soileau, 1987).

By August 1985 the salients and associated areas of increased erosion were prominent features on the shoreline. An aerial survey of the area that was completed by the New Orleans District of the Army Corps of Engineers and the Coastal Engineering

Research Center concluded that the size and location of the borrow area were such that its presence could affect the local wave climate (Combe and Soileau, 1987). Oblique aerial photography identified the diffraction of the wave field as a result of the borrow area (Combe and Soileau, 1987). The area of increased erosion near the salients was found to "affect 25% of the project length and amounted to about 8% of the neat project volume" (Combe and Soileau, 1987, pg. 1236).

Figure 2-1: Aerial photograph showing salients shoreward of borrow area looking East to West along Grand Isle, Louisiana, in August, 1985 (Combe and Solieau, 1987).

Three major hurricanes impacted the project area in the hurricane season following the project's completion, the first time that three hurricanes struck the Louisiana coastline in the same season (Combe and Soileau, 1987). While these storms did tremendous damage to the newly formed berm and caused large sediment losses, the location and size of the salients remained relatively unchanged. The salients have remained on the Grand Isle shoreline as shown by an aerial photograph from 1998

(Figure 2-2). It appears that the eastern salient has decreased in size while the western salient has remained the same size or even become larger.

Figure 2-2: Aerial photograph showing salients shoreward of borrow area along Grand Isle, Louisiana, in 1998 (modified from Louisiana Oil Spill Coordinator's Office (LOSCO), 1999).

A series of detached offshore breakwaters was constructed along the eastern part of Grand Isle in the 1990's, which terminate at the eastern salient and may have affected its shape.

Bathymetric surveys taken through the borrow area in February 1985 and August 1986 revealed that the outer lobes had filled to about half their original depth and the channel connecting the lobes had reached the sea bed elevation (Combe and Soileau, 1987). Currently, the borrow area is reported to be completely filled by fine material

(Combe, personal correspondence) which would have required the same approximate volume of sediment that was dredged for the initial placement. Although the origin of the sediment that has refilled the borrow pit is not known, it is reported to be finer than the sediment dredged for the nourishment project, indicating that the material did not originate from the project. While no longer a bathymetric anomaly, the borrow areas are reported to continue to modify the wave field as local shrimpers use the waters shoreward of the pit as a harbor to weather storms. The reason for the sheltering effect of the filled pit may be due to the energy-dissipating characteristic of the finer material that has filled the pit.

2.1.2 Anna Maria Key, Florida (1993)

The 1993 beach nourishment project at Anna Maria Key, Florida, is another example of a project with a large borrow area lying offshore in relatively shallow water. The project placed 1.6×10^6 m^3 of sediment along a 6.8 km segment (DNR Monuments R-12 to R-35*) of the 11.6 km long barrier island (Dean et al., 1999). The borrow area for the project was approximately 3,050 m long and ranged from 490 to 790 m offshore in approximately 6 m of water (Dean et al., 1999). A planview of the bathymetry near the project including the borrow area is shown in Figure 2-3. A transect through the borrow area, indicated in the previous figure at Monument R-26, is shown in Figure 2-4 and shows dredging to a depth of 3.1 m below the local seabed. This figure shows one pre-project transect, a transect immediately following completion, and two post-nourishment transects. The post-nourishment transects indicate minimal infilling of the borrow pit.

* The "DNR Monuments" are permanent markers spaced at approximately 300 m along the Florida sandy beaches for surveying purposes

The shoreline planform was found to show the greatest losses shoreward of the borrow area. Figure 2-5 shows the shoreline position relative to the August, 1993, data for seven different periods. A large area of negative shoreline change indicating erosion is found from DNR Monument numbers 25 to 34 for the July, 1997, and February, 1998, data. This area lies directly shoreward of the borrow area shown in Figure 2-3. The behavior of the shoreline directly leeward of the borrow area is seen to be the opposite of the Grand Isle, Louisiana, response where shoreline advancement occurred.

Volume changes determined from profiles in the project area did not show large negative values near the southern end of the project. The difference between the shoreline and volume changes at the southern end of the project implies that the constructed profiles may have been steeper near the southern end of the project as compared to those near the northern end (Wang and Dean, 2001).

The proximity of the borrow area to the shoreline is one possible contribution to the local erosion. Although the reason for the increased erosion in this area is not clear, it is interesting that the anomalous shoreline recession did not occur until the passage of Hurricanes Erin and Opal in August and October, 1995, respectively. Hurricane Opal was a category 4 hurricane with sustained winds of 67 m/s when it passed 600 km west of Manatee County (Liotta, 1999). A reported storm surge of 0.3 to 1.0 m, combined with the increased wind and wave action, resulted in overtopping of the beach berm, flooding of the back area of the project and transport of sediment to the back beach or offshore (Liotta, 1999). The average shoreline retreat for the project area was approximately 9.1 to 15.2 m, based on observations (Liotta, 1999).

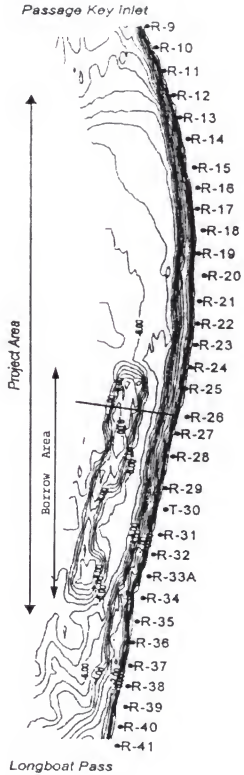

Figure 2-3: Bathymetry off Anna Maria Key, Florida, showing location of borrow pit following beach nourishment project (modified from Dean et al., 1999).

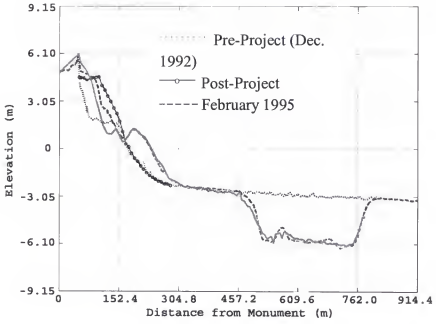

Figure 2-4: Beach profile through borrow area at R-26 in Anna Maria Key, Florida (modified from Wang and Dean, 2001).

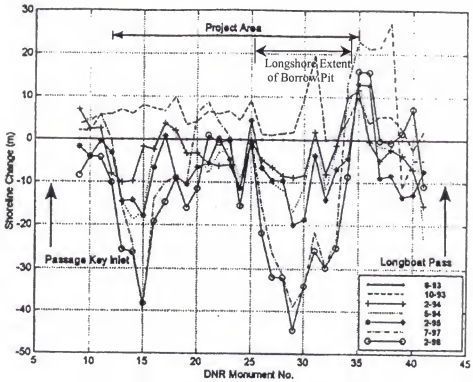

Figure 2-5: Shoreline position for Anna Maria Key Project for different periods relative to August, 1993 (modified from Dean et al. 1999).

2.1.3 Martin County, Florida (1996)

The Hutchinson Island beach nourishment project in Martin County, Florida was constructed in 1996 with the placement of approximately 1.1×10^6 m^3 of sediment along 6.4 km of shoreline, between DNR Monuments R-1 and R-25 (Sumerell, 2000). The borrow area for this project was a shoal rising 4.9 m above the adjacent bed and lying 910 m offshore in 12.8 m of water (Sumerell, 2000). Figure 2-6 shows the borrow area location offshore of the southern end of the project area. An average of 3 m of sediment was dredged from the central portion of the shoal.

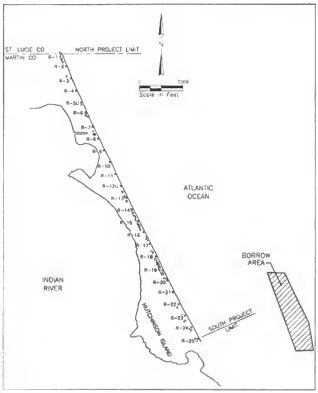

Figure 2-6: Project area for Martin County beach nourishment project (Applied Technology and Management, 1998).

The 3-year and 4-year post-nourishment shoreline surveys show reasonable agreement with modeling conducted for the project, except at the southern end, near the borrow area (Sumerell, 2002). Figure 2-7 shows the predicted shoreline and the survey

data for the 4-year shoreline change. This case differs from the previous two as the borrow area did not create a pit but reduced the height of an offshore shoal. By lowering the height of the shoal the shoreline leeward of the borrow area was exposed to greater wave action, which is the opposite of the sheltering (through reflection) effect of an offshore pit. The borrow area, with its large extent and proximity to the project, is a possible reason for the higher than expected erosion at the southern end of the project.

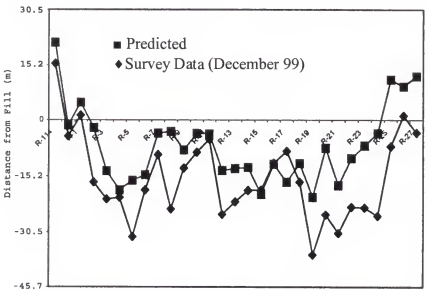

Figure 2-7: Four-year shoreline change for Martin County beach nourishment project: predicted versus survey data (modified from Sumerell, 2000).

2.2 Field Experiments

Field studies have been conducted to examine the effects of offshore dredging on the coastal environment. The purposes of the these studies have varied and include the tendency of a dredged pit to induce sediment flows into it from the nearshore, the interception of sediment transport, and wave transformation effects of a newly dredged pit on the shoreline.

2.2.1 Price et al. (1978)

Price et al. (1978) investigated the effect of offshore dredging on the coastline of England. The tendency of a dredge pit to cause a drawdown of sediment and to prevent the onshore movement of sediment was investigated. The study by Inman and Rusnak (1956) on the onshore-offshore interchange of sand off La Jolla, California, was cited. This three-year study found vertical bed elevation changes of only +/- 0.03 m at depths greater than 9 m. Based on the consideration that the wave conditions off the southern coast of England would be less energetic than off La Jolla, California, Price et al. (1978) concluded that beach drawdown at a depth greater than 10 m would not occur.

A radioactive tracer experiment off Worthing, on the south coast of England, was performed to investigate the mobility of sediment at depths of 9, 12, 15, and 18 m. The 20-month study found that at the 9 and 12 m contours there was a slight onshore movement of sediment and it was concluded that the movement of sediment beyond a depth contour of 18 m on the south coast of England would be negligible. Therefore, at these locations and in instances when the onshore movement of sediment seaward of the dredge area is a concern, dredging in water beyond 18 m depth below low water level was considered acceptable (Price et al., 1978).

A numerical model of the shoreline change due to wave refraction over dredged holes was also employed in the study, the details of which will be examined later in Section 2.5.2.1. The model found that minimal wave refraction occurred for pits in depths greater than 14 m for wave conditions typical off the coast of England.

2.2.2 Kojima et al. (1986)

The impact of dredging on the coastline of Japan was studied by Kojima et al. (1986). The wave climate as well as human activities (dredging, construction of

structures) for areas with significant beach erosion and/or accretion was studied in an attempt to determine a link between offshore dredging and beach erosion. The study area was located offshore of the northern part of Kyushu Island. The wave climate study correlated yearly fluctuations in the beach erosion with the occurrence of both storm winds and severe waves and found that years with high frequencies of storm winds were likely to have high erosion rates. A second study component compared annual variations in offshore dredging with annual beach erosion rates and found strong correlation at some locations between erosion and the initiation of dredging although no consistent correlation was identified.

Hydrographic surveys documented profile changes of dredged holes over a four-year period. At depths less than 30 m, significant infilling of the holes was found, mainly from the shoreward side, indicating a possible interruption in the longshore and offshore sediment transport. This active zone extends to a much larger depth than found by Price et al. (1978) and by Inman and Rusnak (1956). The explanation by Kojima et al. is that although the active onshore/offshore region does not extend to 30 m, sediment from the ambient bed will fill the pit causing a change in the supply to the upper portion of the beach and an increase in the beach slope. Changes in the beach profiles at depths of 35 and 40 m were small, and the holes were not filled significantly.

Another component of the study involved tracers and seabed level measurements to determine the depths at which sediment movement ceases. Underwater photographs and seabed elevation changes at fixed rods were taken at 5 m depth intervals over a period of 3 months during the winter season for two sites. The results demonstrated that sediment movement at depths up to 35 m could be significant. This depth was found to

be slightly less than the average depth (maximum 49 m, minimum 20 m) for five proposed depth of closure equations using wave inputs with the highest energy (H = 4.58 m, T = 9.20 s) for the 3-month study period.

2.3 Laboratory Experiments

2.3.1 Horikawa et al. (1977)

Laboratory studies have been carried out to quantify wave field and nearshore modifications due to the presence of offshore pits. Horikawa et al. (1977) performed wave basin tests with a model of fixed offshore bathymetry and uniform depth containing a rectangular pit of uniform depth and a nearshore region composed of moveable lightweight sediments. The experimental arrangement is shown in Figure 2-8. The incident wave period and height were 0.41 s and 1.3 cm, respectively. With the pit covered, waves were run for 5.5 hours to obtain an equilibrium planform followed by wave exposure for three hours with the pit present. Shoreline measurements were conducted at 1 hour intervals to determine the pit induced changes.

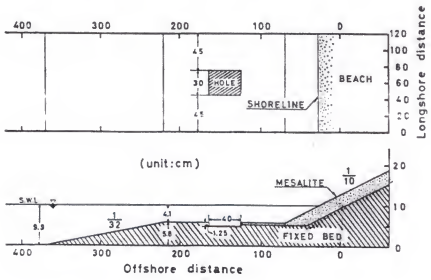

Figure 2-8: Setup for laboratory experiment (Horikawa et al., 1977).

The results of the experiment are presented in Figure 2-9. Almost all of the shoreline changes with the pit present occurred in the first two hours. At the still water level, a salient formed shoreward of the pit, flanked by two areas of erosion that generally extend to the sidewalls of the experiment; however, the depth contour at a water depth, h = 0.85 cm, also shown in Figure 2-9, shows only a slightly seaward displacement at the pit centerline.

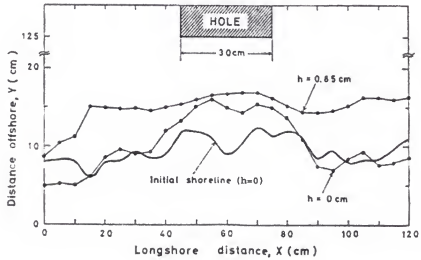

Figure 2-9: Results from laboratory experiment showing plan shape after two hours (Horikawa et al., 1977).

2.3.2 Williams (2002)

Williams (2002) performed wave basin experiments similar to those of Horikawa et al. (1977). The experimental setup of a fixed bed model containing a pit with a moveable sand shoreline was constructed for similar trials by Bender (2001) and was a larger scale version of the Horikawa et al. (1977) arrangement. The Williams experimental procedure consisted of shoreline, bathymetric, and profile measurements after specified time intervals that comprised a complete experiment. Figure 2-10 shows the experiment progression sequence that was used. For analysis, the shoreline and

volume measurements were made relative to the last measurements of the previous 6-hour phase. The conditions for the experiments were 6 cm waves with 1.35 s period and a depth of 15 cm in the constant depth region surrounding the pit. The pit was 80 cm long in the cross-shore direction, 60 cm in the longshore direction and 12 cm deep relative to the adjacent bottom.

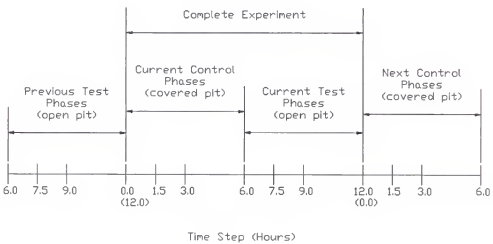

Figure 2-10: Experiment sequence timeline for Williams laboratory experiments (Williams, 2002)

Shoreline and volume change results were obtained for three experiments. Figure 2-11 shows the volume change per unit length versus longshore distance for results with pit covered (control phase) and uncovered (test phase). The dashed line represents volume changes for a covered pit relative to the time step zero which concluded 6 hours of waves with the pit uncovered. The solid line shows the change with the pit uncovered relative to time step six when six hours of wave exposure with the pit covered ended. The volume change results show the model beach landward of the pit lost volume at almost every survey location during the period with the pit covered and experienced a gain in volume with the pit uncovered.

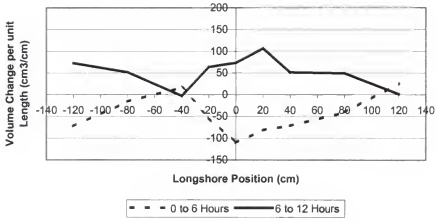

(pit covered) (pit present)

Figure 2-11: Volume change per unit length for first experiment (Williams, 2002).

The net volume change for the first complete experiment (control and test phase) was approximately 2500 cm^3. Different net volume changes were found for the three experiments. However, similar volume change per unit length results were found in all three experiments indicating a positive volumetric relationship between the presence of the pit and the landward beach.

The shoreline change results showed shoreline retreat, relative to Time Step 0.0, in the lee of the borrow pit during the control phase (pit covered) for all three experiments with the greatest retreat at or near the centerline of the borrow pit. All three experiments showed shoreline advancement in the lee of the borrow pit with the pit uncovered (test phase). With the magnitude of the largest advancement being almost equal to the largest retreat in each experiment, it was concluded that, under the conditions tested, the presence of the borrow pit resulted in shoreline advancement for the area shoreward of the borrow pit (Williams, 2002).

An even-odd analysis was applied to the shoreline and volume change results in an attempt to isolate the effect of the borrow pit. The even function was assumed to represent the changes due solely to the presence of the borrow pit. The even components

were adjusted to obtain equal positive and negative areas, which were not obtained using the laboratory data. For each experiment, the shifted even results shoreward of the pit showed positive values during the test phase for both the shoreline and volume changes with negative values during the control phase. The shifted even component of shoreline change for the first experiment is shown in Figure 2-12. These results further verify the earlier findings concerning the effect of the pit.

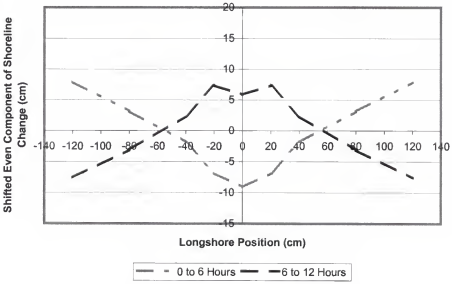

Figure 2-12: Shifted even component of shoreline change for first experiment (Williams, 2002).

2.4 Wave Transformation

2.4.1 Analytic Methods

There is a long history of the application of analytic methods to determine wave field modifications by bathymetric changes. Early research centered on the effect on normally incident long waves of an infinite step, trench or shoal of uniform depth in an otherwise uniform depth domain. More complex models were later developed to remove the long wave restriction, add oblique incident waves and allow for the presence of a

current. More recently, many different techniques have been developed to obtain solutions for domains containing pits or shoals of finite extent. Some of these models focused solely on the wave field modifications, while others of varying complexity examined both the wave field modifications and the resulting shoreline impact.

2.4.1.1 2-Dimensional methods

By matching surface displacement and mass flux normal to the change in bathymetry Lamb (1932) was one of the first to develop a long wave approximation for the reflection and transmission of a normally incident wave at a finite step. Bartholomeauz (1958) performed a more thorough analysis of the finite depth step problem and found that the Lamb solution gave correct results for the reflection and transmission coefficients for lowest order (kh) where k is the wave number and h is the water depth prior to the step. Sretenskii (1950) investigated oblique waves over a step between finite and infinite water depths assuming the wavelength to be large compared to the finite depth. An extensive survey of early theoretical work on surface waves including obstacle problems is found in Wehausen and Laitone (1960).

Kreisel (1949) developed a method that conformally mapped a domain containing certain obstacles of finite dimensions into a rectangular strip. The reflection from obstacles at the surface and on the bottom were considered. Kreisel (1949) presents a proof demonstrating that the reflection coefficient is independent of the incident wave direction for a symmetric (upwave and downwave depth equal) or asymmetric obstacle (trench or shoal) in arbitrary water depth.

Jolas (1960) studied the reflection and transmission of water waves of arbitrary relative depth over a long submerged rectangular parallelepiped (sill) and performed an experiment to document the wave transformation. To solve the case of normal wave

incidence and arbitrary relative depth over a sill or a fixed obstacle at the surface Takano (1960) used an eigenfunction expansion of the velocity potentials in each constant depth region and matched them at the region boundaries. The set of linear integral equations was solved for a truncated series. A laboratory experiment was also conducted in this study.

Dean (1964) investigated long wave modification by linear transitions. The linear transitions included both horizontal and vertical changes. The formulation allowed for many domains including a step, either up or down, and converging or diverging linear transitions with a sloped wall. A proposed solution was defined with plane-waves of unknown amplitude and phase for the incident and reflected waves with the transmitted wave specified. Wave forms, both transmitted and reflected, were represented by Bessel functions in the region of linear variation in depth and/or width. The unknown coefficients were obtained through matching the values and gradients of the water surfaces at the ends of the transitions. Analytic expressions were found for the reflection and transmission coefficients. The results indicate that the reflection and transmission coefficients depend on the relative depth and/or width and a dimensionless parameter containing the transition slope, the wavelength and the depth or width (Figure 2-13). In Figure 2-13 the parameter $Z_I = \frac{4\pi h_I}{L_I S_v}$ for the case of linearly varying depth and $Z_I = \frac{\pi b_I}{L S_H}$ for linearly varying breadth where I indicates the region upwave of the transition, S_V is equal to the depth gradient, and S_H is equal to one-half the breadth gradient. These solutions were shown to converge to those of Lamb (1932) for the case of an abrupt transition (Z_I=0).

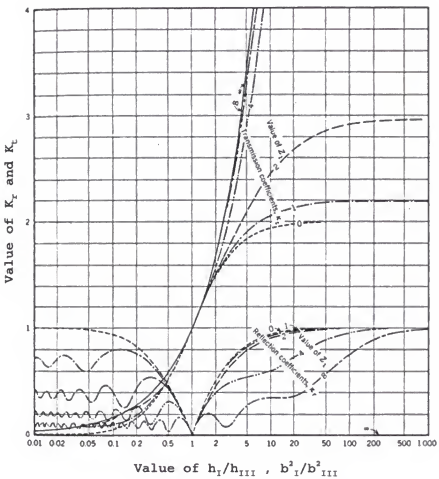

Figure 2-13: Reflection and transmission coefficients for linearly varying depth [h_I/h_{III}] and linearly varying breadth [b_I^2/b_{III}^2] (modified from Dean, 1964).

Newman (1965a) studied wave transformation due to normally incident waves on a single step between regions of finite and infinite water depth with an integral-equation approach. This problem was also examined by Miles (1967) who developed a plane-wave solution for unrestricted kh values using a variational approach (Schwinger & Saxon 1968), which for this case essentially solves a single equation instead of a series of equations (up to 80 in Newman's solution) as in the integral equation approach. The difference between the results for the two solution methods was within 5 percent for all kh values (Miles, 1967).

Newman (1965b) examined the propagation of water waves past long obstacles. The problem was solved by constructing a domain with two steps placed "back to back" and applying the solutions of Newman (1965a). Complete transmission was found for certain water depth and pit length combinations; a result proved by Kriesel (1949). Figure 2-14 shows the reflection coefficient, K_r, and the transmission coefficient, K_t, versus $K_\infty h_0$ where K_∞ is the wave number in the infinitely deep portion before the obstacle and h_0 is the depth over the obstacle. The experimental results of Takano (1960) are included for comparison. It is evident that the Takano experimental data included energy losses.

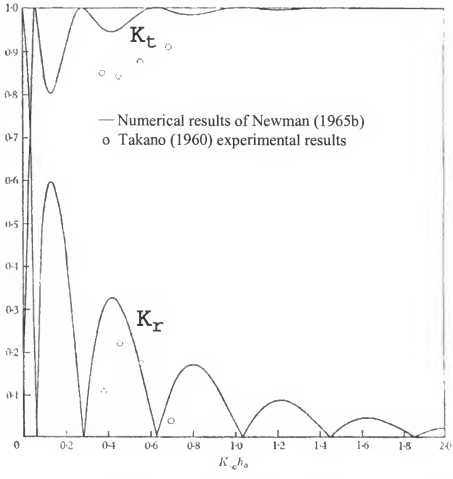

Figure 2-14: Approximate reflection and transmission coefficients for the rectangular parallelepiped of length $8.86h_0$ in infinitely deep water (Newman, 1965b).

The variational approach was applied by Mei and Black (1969) to investigate the scattering of surface waves by rectangular obstacles. For a submerged obstacle, complete transmission was found for certain kh_o values where h_o is the depth over the obstacle. A comparison of the results of Mei and Black (1969) and those of Newman (1965b) is shown in Figure 2-15, which presents the reflection coefficient versus kh_o for a submerged obstacle. Data from the Jolas (1960) experiment are also included on the plot and compared to the results of Mei and Black (1969) for a specific ℓ / h_o, where ℓ is the half-length of the obstacle.

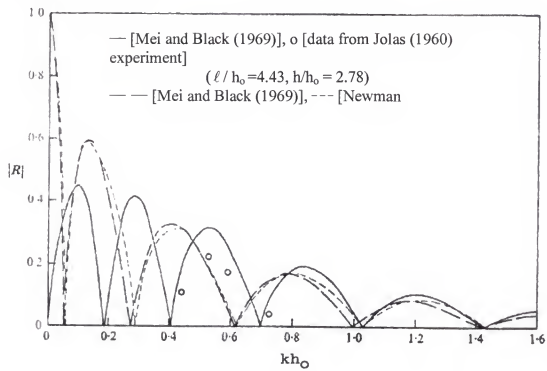

Figure 2-15: Reflection coefficient for a submerged obstacle (Mei and Black, 1969).

Black and Mei (1970) applied the variational approach to examine the radiation caused by oscillating bodies and the disturbance caused by an object in a wave field. Two domains were used for both submerged and semi-immersed (surface) bodies: the first domain was in Cartesian coordinates, with one vertical and one horizontal

dimension, for horizontal cylinders of rectangular cross section and the second domain was in cylindrical coordinates, for vertical cylinders of circular section. The second domain allowed for objects with two horizontal dimensions to be studied for the first time (see Section 2.4.1.2.). Black et al. (1971) used the variational formulation to study the radiation due to the oscillation of small bodies and the scattering induced by fixed bodies. Black et al. demonstrated the scattering caused by a fixed object in a single figure; see Black and Mei (1970) for further results.

Lassiter (1972) used complementary variational integrals to solve the problem of normally incident waves on an infinite trench where the depth on the two sides of the trench may be different (the asymmetric case). The symmetric infinite trench problem was studied by Lee and Ayer (1981), who employed a transform method. The fluid domain was divided into two regions, one an infinite uniform depth domain and the other a rectangular region representing the trench below the uniform seabed level. The transmission coefficient for the trench is shown in Figure 2-16 with the theoretical results plotted along with data from a laboratory experiment conducted as part of the study. Results from a boundary integral method used to compare with the theoretical results are also plotted. The results show six of an infinite number of relative wavelengths where complete transmission (K_t=1) will occur, a result that had been found in prior studies (Newman (1965b), Mei and Black (1969)). The laboratory data show the general trend of the theoretical results, with some variation due to energy losses and reflections from the tank walls and ends.

Lee et al. (1981) proposed a boundary integral method for the propagation of waves over a prismatic trench of arbitrary shape, which was used for comparison to

selected results in Lee and Ayer (1981). The solution was found by matching the unknown normal derivative of the potential at the boundary of the two regions. A comparison to previous results for trenches with vertical sidewalls was conducted with good agreement. A case with bathymetry containing gradual transitions in depth was shown in a plot of the transmission coefficient for a trapezoidal trench (Figure 2-17). Note that the complete dimensions of the trapezoidal trench are not specified in the inset diagram, making direct comparison to the results impossible.

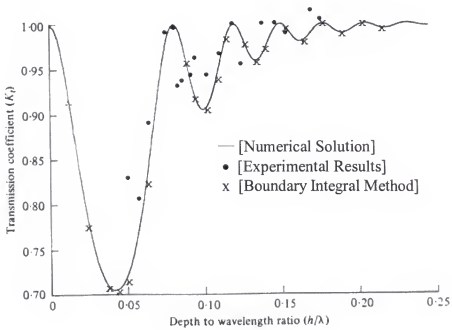

Figure 2-16: Transmission coefficient as a function of relative wavelength (h=10.4 cm, d=67.3 cm, trench width =161.6 cm) (modified from Lee and Ayer, 1981).

Miles (1982) solved for the diffraction by an infinite trench for obliquely incident long waves. The solution method for normally incident waves used a procedure developed by Kreisel (1949) that conformally mapped a domain containing certain obstacles of finite dimensions into a rectangular strip. To add the capability of solving

for obliquely incident waves, Miles used the variational formulation of Mei and Black (1969).

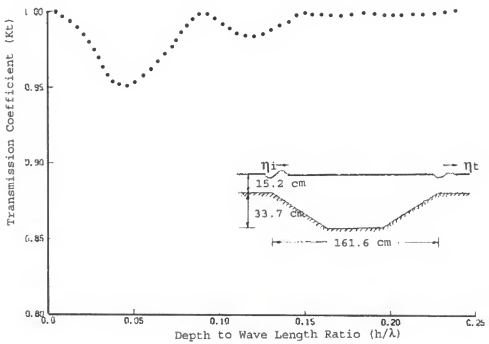

Figure 2-17: Transmission coefficient as a function of relative wavelength for trapezoidal trench; setup shown in inset diagram (modified from Lee et al., 1981).

The problem of obliquely incident waves over an asymmetric trench was solved by Kirby and Dalrymple (1983a) using a modified form of Takano's (1960) method. Figure 2-18 compares the reflection coefficient for the numerical solution for normally incident waves and the results of Lassiter (1972). The results from a boundary integral method used to provide verification are included. Differences in the results of Kirby and Dalrymple and those of Lassiter are evident. Lee and Ayer (1981,[see their Figure 2]) also demonstrated differences in their results and those of Lassiter (1972). The effect of oblique incidence is shown in Figure 2-19 where the reflection and transmission coefficients for two angles of incidence are plotted.

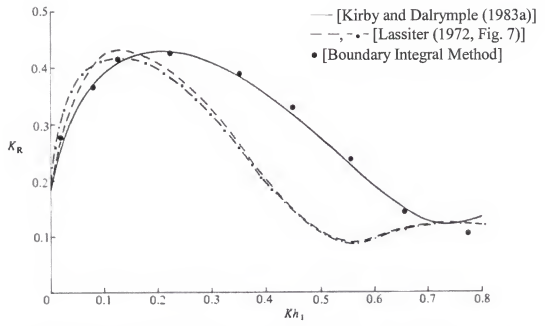

Figure 2-18: Reflection coefficient for asymmetric trench and normally incident waves as a function of Kh_1: $h_2/h_1=2$, $h_3/h_1=0.5$, $L/h_1=5$; L = trench width (Kirby and Dalrymple, 1983a).

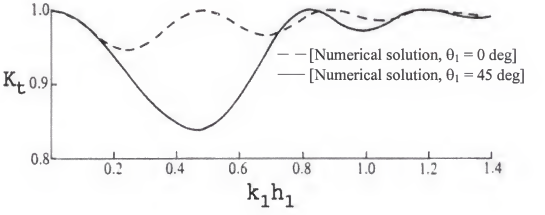

Figure 2-19: Transmission coefficient for symmetric trench, two angles of incidence: $L/h_1=10$, $h_2/h_1=2$; L = trench width (modified from Kirby and Dalrymple, 1983a).

This study also investigated the plane-wave approximation and the long-wave limit, which allowed for comparison to Miles (1982). Figure 2-20 shows transmission coefficients with the results of the numerical solution, the long wave solution, and values from the Miles (1982) solution, which is only valid for small kh values in each region. For the first case, with a small relative trench width, the numerical results from Kirby and

Dalrymple compare well with the results using the Miles (1982) method and the plane-wave solution is seen to deviate from these. For the case of a relative trench length equal to eight, the numerical results differ from the plane-wave solution, which diverge from the values using Miles (1982) for this case where the assumptions are violated.

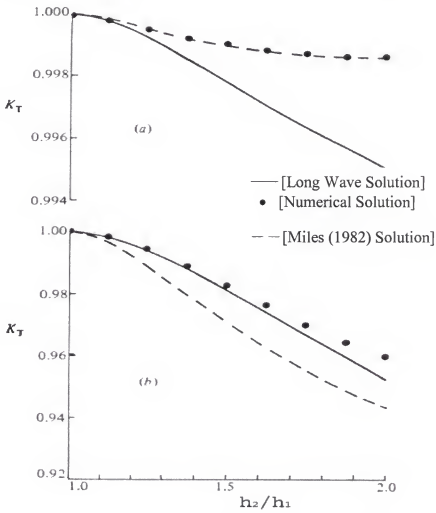

Figure 2-20: Transmission coefficient as a function of relative trench depth; normal incidence: $k_1h_1 = 0.2$: (a) $L/h_1=2$; (b) $L/h_1=8$, L = trench width. (Kirby and Dalrymple, 1983a).

The difference in scales between the two plots is noted. An extension of this study is found in Kirby et al. (1987) where the effects of currents flowing along the trench are included. The presence of an ambient current was found to significantly alter

the reflection and transmission coefficients for waves over a trench compared to the no current case. Adverse currents and following currents made a trench less reflective and more reflective, respectively (Kirby et al., 1987).

2.4.1.2 3-Dimensional methods

Extending the infinite trench and step solutions (one horizontal dimension) to a domain with variation in the longshore (two-horizontal dimensions) is a natural progression allowing for the more realistic case of wave transformation by a finite object or depth anomaly to be studied. Changes in bathymetry can cause changes in wave height and direction through the four wave transformation processes noted earlier. Some of the two-dimensional models study only the wave transformation, while others use the modified wave field to determine the impact of a pit or shoal on the shoreline. Several models use only a few equations or matching conditions on the boundary of the pit or shoal to determine the wave field and in some cases the impact on the shoreline in a simple domain containing a pit or shoal. Other, much more complex and complete models and program packages have been developed to solve numerically for the wave field over a complex bathymetry, which may contain pits and/or shoals. Both types of models can provide insight into the effect of a pit or shoal on the local wave field and the resulting impact on the shoreline.

The wave transformation in a three-dimensional domain was investigated in a study by Black and Mei (1970), which solved for the radially symmetric case of a submerged or floating circular cylinder in cylindrical coordinates. A series of Bessel functions was used for the incident and reflected waves, as well as for the solution over the shoal with modified Bessel functions representing the evanescent modes. As mentioned previously in the 2-D section, a variational approach was used and both the

radiation by oscillating bodies and the disturbance caused by a fixed body were studied. The focus of the fixed body component of the study was the total scattering cross section, Q, which is equal to the width between two wave rays within which the normally incident wave energy flux would be equal to that scattered by the obstacle and the differential scattering cross-section, which shows the angular distribution of the scattered energy (Black and Mei, 1970). Figure 2-21 shows the total scattering cross section for a circular cylinder at the seabed for three ratios of cylinder radius (a) to depth over the cylinder (h).

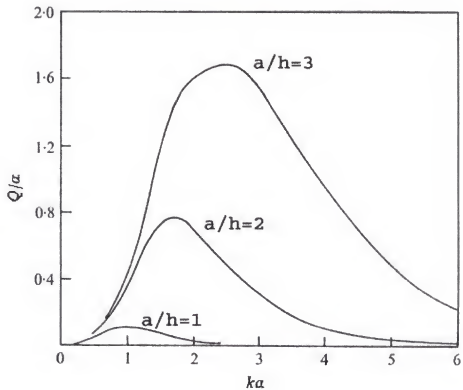

Figure 2-21: Total scattering cross section of vertical circular cylinder on bottom (modified from Black et al., 1971).

Williams (1990) developed a numerical solution for the modification of long waves by a rectangular pit using Green's second identity and appropriate Green's functions in each region that comprise the domain. This formulation accounts for the diffraction, refraction and reflection caused by the pit. The domain for this method

consists of a uniform depth region containing a rectangular pit of uniform depth with vertical sides. The solution requires discretizing the pit boundary into a finite number of points at which the velocity potential and the derivative of the velocity potential normal to the boundary must be determined. Applying matching conditions for the pressure and mass flux across the boundary results in a system of equations amenable to matrix solution techniques. Knowledge of the potential and derivative of the potential at each point on the pit boundary allows determination of the velocity potential solution anywhere in the fluid domain. The effect of a pit on the wave field is shown in a contour plot of the relative amplitude in Figure 2-22. A partial standing wave pattern of increased and decreased relative amplitude is seen seaward of the pit with a shadow zone of decreased wave amplitude landward of the pit flanked by two areas of increased relative amplitude.

McDougal et al. (1996) applied the method of Williams (1990) to the case of a domain with multiple pits. The first part of the study reinvestigated the influence of a single pit on the wave field for various pit geometries. A comparison of the wave field in the presence of a pit versus a surface piercing structure is presented in Figures 2-23 and 2-24, which present contour plots of the transformation coefficient, K, (equal to relative amplitude) that contain the characteristics discussed in the last paragraph. For this case with the pit depth equal to 3 times the water depth a greater sheltering effect is found (K = 0.4) landward of the pit than for the case of the full depth breakwater.

An analysis of the effect of various pit characteristics on the minimum value of K found in the domain was also performed. The dimensionless pit width, a/L, (a = cross-shore dimension, L = wave length outside pit) was found to increase the distance to the

region where $K < 0.5$ behind the pit and the value of K was found to decrease and then become approximately constant as a/L increases. The minimum values of the transformation coefficient for a wide pit are much lower than those values found in Lee and Ayer (1981) and Kirby and Dalrymple (1983a), which may be explained by the refraction divergence that occurs behind the pit in the 2-D case (McDougal et al., 1996).

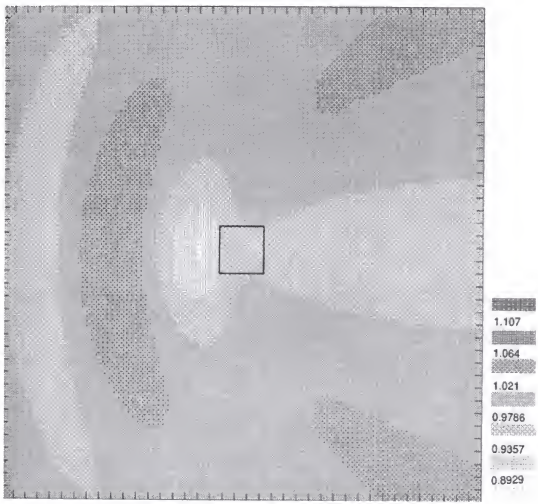

Figure 2-22: Contour plot of relative amplitude in and around pit for normal incidence; $k_1/d = \pi/10$, $k_2/h = \pi/10\sqrt{2}$, h/d=0.5, b/a =1, a/d=2, a = cross-shore pit length, b = longshore pit length, h = water depth outside pit, d = depth inside pit, L_2 = wavelength outside pit. (Williams, 1990).

The effect of the dimensionless pit length, b/L, indicates that K decreases as b/L increases to 1 with a change in the trend, and an increase in K, from b/L = 0.55 to b/L = 0.65. Increasing the dimensionless pit depth, d/L, was found to decrease the minimum value of K with a decreasing rate. The incident wave angle was not found to significantly alter the magnitude or the location of the minimum K value, although the width of the shadow zone changes with incident angle. For the case of multiple pits, it was found that placement of one pit in the shadow zone of a more seaward pit was most effective in reducing the wave height. However, adding a third pit did not produce significant wave height reduction as compared to the two-pit results.

Williams and Vazquez (1991) removed the long wave restriction of Williams (1990) and applied the Green's function solution method outside of the pit. This solution was matched to a Fourier expansion solution inside the pit with matching conditions at the pit boundary. Once again the pit boundary must be discretized into a finite number of points and a matrix solution for the resulting series of equations was used. Removing the shallow water restriction allowed for many new cases to be studied, as the wave conditions approach deep water, the influence of the pit diminishes. A plot of the minimum and maximum relative amplitude found in the domain versus the dimensionless pit length (the wave number outside of the pit times the cross-shore pit dimension, $k_o a$) is shown in Figure 2-25. The maximum and minimum relative amplitudes in Figure 2-25 are seen to occur near $k_o a = 2\pi$ or when L = a and then approach unity as the dimensionless pit length increases. The reason that the extreme values do not occur exactly at $k_o a = 2\pi$ is explained by Williams and Vazquez (1991) as due to diffraction effects near the pit modifying the wave characteristics.

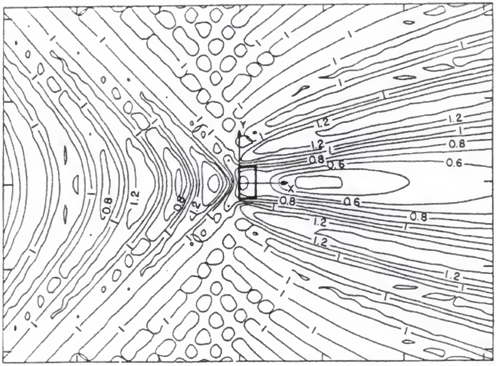

Figure 2-23: Contour plot of diffraction coefficient in and around pit for normal incidence; a/L=1, b/L=0.5, d/h =3, kh=0.167 (McDougal et al., 1996).

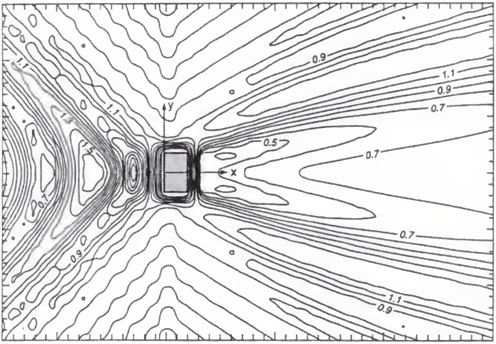

Figure 2-24: Contour plot of diffraction coefficient around surface-piercing breakwater for normal incidence; a/L=1, b/L=0.5, kh=0.167 (McDougal et al., 1996).

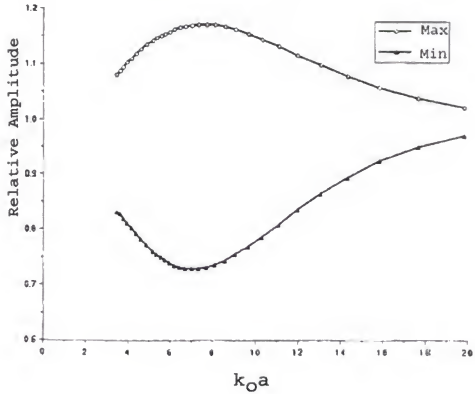

Figure 2-25: Maximum and minimum relative amplitudes for different $k_o a$, for normal incidence, a/b=6, a/d=π, and d/h=2. (modified from Williams and Vasquez, 1991).

2.4.2 Numerical Methods

The previous three-dimensional solutions, while accounting for most of the wave transformation processes caused by a pit, are simple in their representation of the bathymetry and their neglect of many wave-related processes including energy dissipation. Berkhoff (1972) developed a formulation for the 3-dimensional propagation of waves over an arbitrary bottom in a vertically integrated form that reduced the problem to two-dimensions. This solution is known as the mild slope equation and different forms of the solution have been developed into parabolic (Radder, 1979), hyperbolic, and elliptic (Berkhoff et al., 1982) models of wave propagation, which vary in their approximations and solution techniques. Numerical methods allow solution for wave propagation over an arbitrary bathymetry. Some examples of the parabolic and elliptic

models are RCPWAVE (Ebersole et al., 1986), REF/DIF-1 (Kirby and Dalrymple, 1994), and MIKE 21's EMS Module (Danish Hydraulics Institute, 1998). Other models such as SWAN (Holthuijsen et al., 2000) and STWAVE (Smith et al., 2001) model wave transformation in the nearshore zone using the wave-action balance equation. These models provide the capability to model wave transformation over complicated bathymetries and may include processes such as bottom friction, nonlinear interaction, breaking, wave-current interaction, wind-wave growth, and white capping to better simulate the nearshore zone. An extensive review of any of the models is beyond the scope of this paper; however, a brief outline of the capabilities of some of the models is presented in Table 1.

Maa et al. (2000) provides a comparison of six numerical models. Two parabolic models are examined: RCPWAVE and REF/DIF-1. RCPWAVE employs a parabolic approximation of the elliptic mild slope equation and assumes irrotationality of the wave phase gradient. REF/DIF-1 extends the mild slope equation by including nonlinearity and wave-current interaction (Kirby and Dalrymple, 1983b; Kirby, 1986). Of the four other models included, two are defined by Maa et al. (2000) as based on the transient mild slope equation (Copeland, 1985; Madsen and Larson, 1987) and two are classified as elliptic mild slope equations (Berkhoff et al., 1982) models.

The transient mild slope equation models presented are Mike 21's EMS Module and the PMH Model (Hsu and Wen, in review). The elliptic mild slope equation models use different solution techniques with the RDE Model (Maa and Hwung, 1997; Maa et al. 1998a) applying a special Gaussian elimination method and the PBCG Model employing a Preconditioned Bi-conjugate Gradient method (Maa et al., 1998b).

Table 2-1: Capabilities of selected nearshore wave models.

	RCPWAVE	REF/DIF-1	Mike 21 ~ EMS	STWAVE	SWAN ~ 3rd Gen.
Solution Method	Parabolic Mild Slope Equation	Parabolic Mild Slope Equation	Elliptic Mild Slope Equation (Berkhoff et al. (1972)	Conservation of Wave Action	Conservation of Wave Action
Phase	Averaged	Resolved	Resolved	Averaged	Averaged
Spectral	No	No Use REF/DIF-S	No Use NSW unit	Yes	Yes
Shoaling	Yes	Yes	Yes	Yes	Yes
Refraction	Yes	Yes	Yes	Yes	Yes
Diffraction	Yes (Small-Angle)	Yes (Wide-Angle)	Yes (Total)	No (Smoothing)	No
Reflection	No	Yes (Forward only)	Yes (Total)	No	Yes (Specular)
Breaking	Stable Energy Flux: Dally et al. (1985)	Stable Energy Flux: Dally et al. (1985)	Bore Model: Battjes & Janssen (1978)	Depth limited: Miche (1951) criterion	Bore Model: Battjes & Janssen (1978)
White-capping	No	No	No	Resio (1987)	Komen et al. (1984), Janssen (1991), Komen et al. (1994)
Bottom Friction	No	Dalrymple et al. (1984) both laminar and turbulent BBL	Quadratic Friction Law, Dingemans (1983)	No	Hasselmann et al. (1973), Collins (1972), Madsen et al. (1988)
Currents	No	Yes	No	Yes	Yes
Wind	No	No	No	Resio (1988)	Cavaleri & Malanotte-Rizzoli (1981), Snyder et al., (1981), Janssen et al. (1989, 1991)
Availability	Commercial	Free	Commercial	Free	Free

A table in Maa et al. (2000) provides a comparison of the capabilities of the six models. A second table summarizes the computation time, memory required and, where required, the number of iterations for a test case of monochromatic waves over a shoal on an incline; the Berkhoff et al. (1982) shoal. The parabolic approximation solutions of REF/DIF and RCPWAVE required significantly less memory (up to 10 times less) and computation time (up to 70 times less) than the elliptic models, which is expected due to the solution techniques and approximations contained in the parabolic models. The required computation times and memory requirements for the transient mild slope equation models were found to be intermediate to the other two methods.

Wave height and direction were calculated in the test case domain for each model. The models based on the transient mild slope equation and the elliptic mild slope equation were found to produce almost equivalent values of the wave height and direction. The parabolic approximation models were found to have different values, with RCPWAVE showing different wave heights and directions behind the shoal and REF/DIF showing good wave height agreement with the other methods, but no change in the wave direction behind the shoal. Plots of the computed wave heights for the six models and experimental data along one transect taken perpendicular to the shoreline and one transect parallel to the shoreline are shown in Figures 2-26 and 2-27. Only four results are plotted because the RDE model, the PMH model and PBCG model produced almost identical results.

The wave directions found with REF/DIF-1 in Maa et al. (2000) were found to be in error by Grassa and Flores (2001), who demonstrated that a second order parabolic

model, equivalent to REF/DIF-1 was able to reproduce the wave direction field behind a shoal such as in the Berkhoff et al. (1982) experiment.

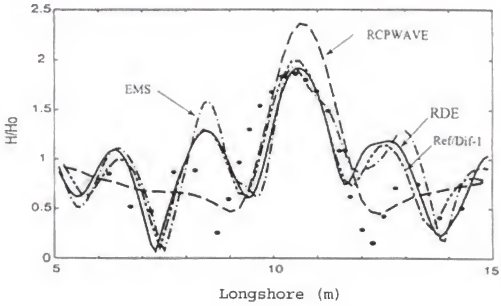

Figure 2-26: Comparison of wave height profiles for selected models along transect parallel to shore located 9 m shoreward of shoal apex[•=experimental data] (Maa et al., 2000).

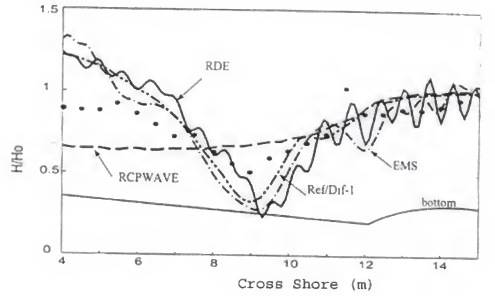

Figure 2-27: Comparison of wave height profiles for selected models along transect perpendicular to shore and through shoal apex [•=experimental data] (Maa et al., 2000).

Application of numerical models to the problem of potential impact on the shoreline caused by changes to the offshore bathymetry was conducted by Maa and Hobbs (1998) and Maa et al. (2001). In Maa and Hobbs (1998) the impact on the coast due to the dredging of an offshore shoal near Sandbridge, Virginia was investigated using RCPWAVE. National Data Buoy Center (NDBC) data from an offshore station and bathymetric data for the area were used to examine several cases with different wave events and directions. The resulting wave heights, directions, and sediment transport at the shoreline were compared. The sediment transport was calculated using the formulation of Gourlay (1982), which contains two terms, one driven by the breaking wave angle and one driven by the gradient in the breaking wave height in the longshore direction. Section 2.5.4 provides a more detailed examination of the longshore transport equation with two terms. The study found that the proposed dredging would have little impact on the shoreline for the cases investigated.

Later, Maa et al. (2001) revisited the problem of dredging at the Sandbridge Shoal by examining the impact on the shoreline caused by three different borrow pit configurations. RCPWAVE was used to model the wave transformation over the shoal and in the nearshore zone. The focus was on the breaking wave height; wave direction at breaking was not considered. The changes in the breaking wave height modulation (BHM) along the shore after three dredging phases were compared to the results found for the original bathymetry and favorable or unfavorable assessments were provided for ensuing impact on the shoreline. The study concluded that there could be significant differences in the wave conditions, revealed by variations in the BHM along the shoreline depending on the location and extent of the offshore dredging.

Regions outside the inner surf zone have also been studied through application of nearshore wave models. Jachec and Bosma (2001) used the numerical model REF/DIF-S (a spectral version of REF/DIF-1) to study borrow pit recovery time for seven borrow areas located on the inner continental shelf off New Jersey. The input wave conditions were obtained from Wave Information Study (WIS) data with nearshore bathymetry for the existing conditions and also different dredging scenarios. Changes in the wave-induced bottom velocity were obtained from the wave height and direction changes determined by REF/DIF-S. The wave-induced bottom velocities were coupled with ambient near-bottom currents to determine the sediment transport and then recovery times of the borrow areas. The recovery times from the numerical modeling were the same order of magnitude as recovery times estimated from two independent data sets of seafloor change rates offshore of New Jersey.

2.5 Shoreline Response

2.5.1 Longshore Transport Considerations

The previous discussion on one and two-dimensional models focused first on simple and complex methods of determining the wave transformation caused by changes in the offshore bathymetry and then applications that determined the changes to the wave height, direction and even longshore transport at the shoreline. However, none of the applications were intended to determine the change in shoreline planforms due to an anomaly or a change in the offshore bathymetry. With wave heights and directions specified along the shoreline, sediment transport can be calculated and, based on the gradients in longshore transport, the changes in shoreline position can be determined.

The longshore transport can be driven by two terms as was discussed previously in the review of Maa and Hobbs (1998). In most situations where the offshore

bathymetry is somewhat uniform, the magnitude and direction of the longshore transport will depend mostly on the wave height and angle at breaking as the longshore gradient in the breaking wave height will be small. In areas with irregular bathymetry or in the presence of structures, the transformation of the wave field can lead to areas of wave focusing and defocusing resulting in considerable longshore gradients in the wave height. Longshore transport equations containing a transport term driven by the breaking wave angle and another driven by the longshore gradient in the wave height can be found in Bakker (1971), Ozasa and Brampton (1980), who cite the formulation of Bakker (1971), Gourlay (1982), Kraus and Harikai(1983), and Kraus (1983). While the value of the coefficient for the transport term driven by the gradient in the wave height is not well established, the potential contribution of this term is significant. It is shown later that under steady conditions the diffusive nature of the angle-driven transport term is required to modify the wave height gradient transport term in order to generate an equilibrium planform when the two terms are both active.

2.5.2 Refraction Models

2.5.2.1 Motyka and Willis (1974)

Motyka and Willis (1974) were one of the first to apply a numerical model to predict shoreline changes due to altered offshore bathymetry. The model only included the effect of refraction caused by offshore pits for idealized sand beaches representative of those found on the English Channel or North Sea coast of England. A simplified version of the Abernethy and Gilbert (1975) wave refraction model was used to determine the transformation of uniform deep water waves over the nearshore bathymetry. The breaking wave height and direction were calculated and used to determine the sediment transport and combined with the continuity equation to predict

shoreline change. The longshore transport was calculated using the Scripps Equation as modified by Komar (1969):

$$Q = \frac{0.045}{\gamma_s} \rho g H_b^2 C_g \sin(2\alpha_b) \tag{2-1}$$

where Q is the volume rate of longshore transport, γ_s is the submerged unit weight of the beach material, ρ is the density of the fluid, H_b is the breaking wave height, C_g is the group velocity at breaking, and α_b is the angle of the breaking wave relative to the shoreline. This form of the Scripps Equation combines the transport and porosity coefficients into one term; the values used for either parameter was not stated. This process was repeated to account for shoreline evolution with time.

Figure 2-28 shows a comparison of the predicted shorelines for the equivalent of two years of waves over 1 m and 4 m deep pits with a longshore extent of 880 m and a cross-shore extent of 305 m. The detailed pit geometries were not specified.

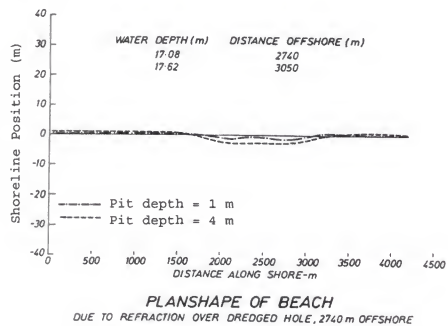

Figure 2-28: Calculated beach planform due to refraction after two years of prototype waves for two pit depths (modified from Motyka and Willis, 1974).

The model determined that erosion occurs shoreward of a pit, with adjacent areas of accretion. For the wave conditions used, stability was found after an equivalent period of two years. During the runs, "storm" waves (short period and large wave height) were found to cause larger shoreline changes than the "normal" waves with longer periods and smaller heights, which actually reduced the erosion caused by the storm waves. The erosion shoreward of the pits is shown in Figure 2-28 with more erosion occurring for the deeper pit.

2.5.2.2 Horikawa et al. (1977)

Horikawa et al. (1977) developed a mathematical model for shoreline changes due to offshore pits. The model applies a refraction program and the following equation for the longshore sediment transport:

$$Q = \frac{0.77\rho g}{16(\rho_s - \rho)(1-\lambda)} H_b^2 C_g \sin(2\alpha_b) \qquad (2\text{-}2)$$

where λ is the porosity of the sediment. Equation 2-2 is identified as the Scripps Equation in Horikawa et al. (1977); however, to match the Scripps Equation and for a dimensionally correct expression, the g term in the numerator should be removed. A model by Sasaki (1975) for diffraction behind breakwaters was modified to account for refraction only. The model computes successive points along the wave ray paths. Interpolation for the depth and slope is used along the ray path with an iteration procedure to calculate each successive point. The wave conditions were selected to be typical of the Eastern Japan coast facing the Pacific Ocean. Several pit dimensions and pit locations were used with the longshore dimension of the pit ranging from 2 km to 4 km, a cross-shore length of 2 km, pit depth of 3 m and water depths at the pit from 20 m to 50 m.

For the configurations modeled, accretion was found directly shoreward of the pit, flanked by areas of erosion. The magnitude of the accretion behind the pit and the erosion in the adjacent areas were found to increase with increasing longshore pit length and for pits located closer to shore. The shoreline planform for a model after the equivalent of 2 years of waves is shown in Figure 2-29 with a salient directly shoreward of the pit.

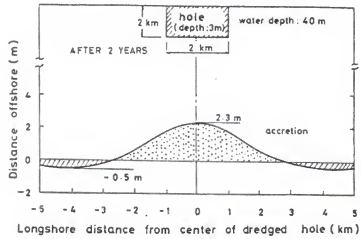

Figure 2-29: Calculated beach planform due to refraction over dredged hole after two years of prototype waves (Horikawa et al., 1977).

Although Horikawa et al. state that good qualitative agreement was found with Motyka and Willis (1974), the results were the opposite with Horikawa et al. and Motyka and Willis (1974) predicting accretion and erosion shoreward of a pit, respectively. The proposed reason for the accretion given in Horikawa et al. was that sand accumulates behind the pit due to the quiet water caused by the decrease in wave action behind the pit. However, a model that considers only refraction caused by a pit and only includes a transport term dependent on the breaking wave angle would have wave rays that diverge over the pit and cause sand to be transported away from the area behind the pit, resulting

in erosion. The two models used different refraction programs and basically the same transport equation with Horikawa et al. having a pit that was 2 or 3 times as large, lying in deeper water and with longer period incoming waves. The refraction grid was 250 m square in the Horikawa et al. model and 176 m square in Motyka and Willis.

Regardless of the differing results from Motyka and Willis, the mathematical model results of Horikawa et al. follow the trend of the lab results contained in that study showing accretion behind a pit (Figure 2-30); however, the aforementioned anomalous prediction of accretion considering only wave refraction remains.

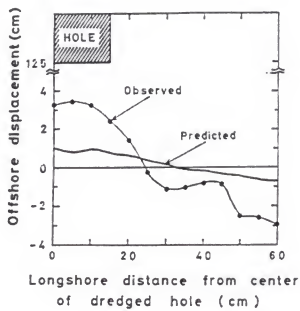

Figure 2-30: Comparison of changes in beach plan shape for laboratory experiment and numerical model after two years of prototype waves (Horikawa et al., 1977).

2.5.3 Refraction and Diffraction Models

2.5.3.1 Gravens and Rosati (1994)

Gravens and Rosati (1994) performed a numerical study of the salients and a set of offshore breakwaters at Grand Isle, Louisiana (Figures 2-1 and 2-2). Of particular interest is the analysis and interpretation of the impact on the wave field and the resulting

influence on the shoreline, of the "dumbbell" shaped planform borrow area located close to shore. The report employs two numerical models to determine the change in the shoreline caused by the presence of the offshore pits: a wave transformation numerical model (RCPWAVE) and a shoreline change model (GENESIS (Hanson, 1987, Hanson, 1989)) using the wave heights from the wave transformation model. RCPWAVE was used to calculate the wave heights and directions from the nominal 12.8 m contour to the nominal 4.3 m contour along the entire length of the island for 3 different input conditions. Figures 2-31 and 2-32 show the wave height transformation coefficients and wave angles near the pit (centered about alongshore coordinate 130). Significant changes in the wave height and direction are found near the offshore borrow area. The shadow zone centered at Cell 130 suggests the presence of one large offshore pit as opposed to the "dumbbell" shaped borrow pit for the project described in Combe and Soileau (1987).

The shoreline changes were calculated using a longshore transport equation with two terms; one driven by the breaking wave angle, and one driven by the longshore gradient in the breaking wave height. Each of these terms includes a dimensionless transport coefficient. In order for GENESIS to produce a salient leeward of the borrow pit, an unrealistically large value for the transport coefficient associated with the gradient in the breaking wave height ($K_2 = 2.4$) was needed, whereas 0.77 is the normal upper limit. While a single salient was modeled after applying the large K_2 value, the development of two salients leeward of the borrow pit, as shown in Figures 2-1 and 2-2, did not occur. The nearshore bathymetric data used in the modeling was from surveys taken in 1990 and 1992. Significant infilling of the borrow pit occurred prior to the

surveys in 1990 and 1992; however, details of how the pit filled over this time period are not known.

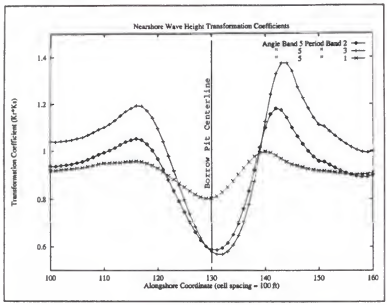

Figure 2-31: Nearshore wave height transformation coefficients near borrow pit from RCPWAVE study (modified from Gravens and Rosati, 1994).

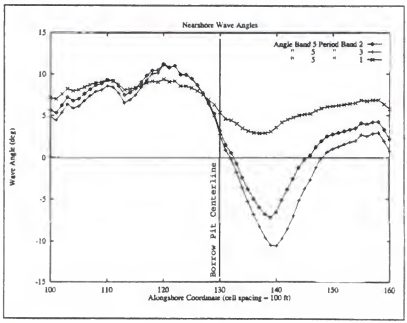

Figure 2-32: Nearshore wave angles near borrow pit from RCPWAVE study; wave angles are relative to shore normal and are positive for westerly transport (modified from Gravens and Rosati, 1994).

The authors proposed that the salient was formed by the refractive divergence of the wave field created by the borrow pit that resulted in a region of low energy directly shoreward of the borrow area and regions of increased energy bordering the area. The gradient in the wave energy will result in a circulation pattern where sediment mobilized in the high-energy zone is carried into the low energy zone. For GENESIS to recreate this circulation pattern K_2 must be large enough to allow the second transport term to dominate over the first transport term.

2.5.3.2 Tang (2002)

Tang (2002) employed RCPWAVE and a shoreline modeling program to evaluate the shoreline evolution leeward of an offshore pit. The modeling was only able to generate embayments in the lee of the offshore pits using accepted values for the transport coefficients. This indicates that wave reflection and/or dissipation are important wave transformation processes that must be included when modeling shoreline evolution in areas with bathymetric anomalies.

2.5.4 Refraction, Diffraction, and Reflection Models

2.5.4.1 Bender (2001)

A study by Bender (2001) extended the numerical solution of Williams (1990) for the transformation of long waves by a pit to determine the energy reflection and shoreline changes caused by offshore pits and shoals. An analytic solution was also developed for the radially symmetric case of a pit following the form of Black and Mei (1970). The processes of wave refraction, wave diffraction, and wave reflection are included in the model formulations, however, wave dissipation is not. Both the numerical and analytic solutions provide values of the complex velocity potential at any point, which allows determination of quantities such as velocity and pressure.

The amount of reflected energy was calculated by comparing the energy flux through a transect perpendicular to the incident wave field extending to the pit center to the energy flux through the same transect with no pit present (Figure 2-33). The amount of energy reflected was found to be significant and dependent on the dimensionless pit diameter and other parameters. Subsequently a new method has been developed which allows the reflected energy to be calculated using a far-field approximation with good agreement between the two methods.

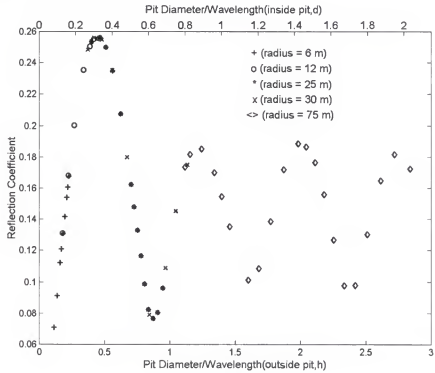

Figure 2-33: Reflection coefficients versus dimensionless pit diameter divided by wavelength inside and outside the pit; water depth = 2 m, pit depth = 4 m (Bender, 2001).

The shoreline changes caused by the pit were calculated using a simple model that considers continuity principles and the longshore transport equation with values of the wave height and direction determined along a transect representing the shoreline. A nearshore slope and no nearshore refraction were assumed. The impact on the shoreline

was modeled by determining the wave heights and directions along an initially straight shoreline, then calculating the transport and resulting shoreline changes. After updating the shoreline positions, the transport, resulting shoreline changes, and updated shoreline positions were recalculated for a set number of iterations after which the wave transformation was recalculated with the new bathymetry and values of the wave height and direction were updated at the modified breaker line.

The impact on the shoreline was found to be highly dependent on the transport coefficients. Considering transport driven only by the breaking wave angle and wave height, erosion was found to occur directly leeward of the pit flanked by two areas of accretion as in Motyka and Willis (1974). Following an initial advancement directly shoreward of the pit, erosion occurs and an equilibrium shape was reached. Examining only the effect of the second transport term (driven by the longshore gradient in the wave height) accretion was found directly shoreward of the pit, with no equilibrium planform achieved. Figure 2-34 shows the shoreline evolution for each transport term. Including both transport terms with the same transport coefficients resulted in a shoreline with accretion directly shoreward of the pit that was able to reach an equilibrium state (Figure 2-35). The two-term transport equation used to determine the shoreline in Figure 2-35 is

$$Q = \frac{K_1 H_b^{2.5} \sqrt{g/\kappa} \sin(\theta - \alpha_b)\cos(\theta - \alpha_b)}{8(s-1)(1-p)} - \frac{K_2 H_b^{2.5} \sqrt{g/\kappa} \cos(\theta - \alpha_b)}{8(s-1)(1-p)\tan(m)} \frac{dH}{dy} \quad (2\text{-}3)$$

where H_b is the breaking wave height, g is gravity, κ is the breaking index, θ is the shoreline orientation, α is the breaking wave angle, m is the beach slope, s and p are the specific gravity and porosity of the sediment, respectively, and K_1 and K_2 are sediment

transport coefficients, which were set equal to 0.77 for the results presented here. A review of the development of Eq. 2-3 is contained in Appendix D.

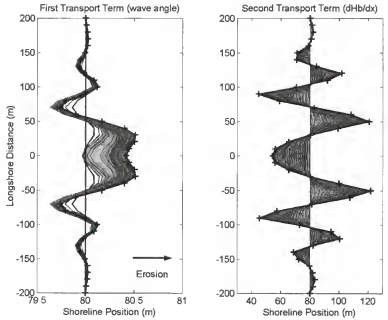

Figure 2-34: Shoreline evolution resulting from each transport term individually for transect located 80 m shoreward of a pit with a radius = 6 m, last time step indicated with [+] (modified from Bender and Dean, 2001).

In application the wave height and angle calculations were limited to a uniform depth region; therefore no nearshore shoaling and refraction was performed to resolve the depth limited breaking values. The wave height and angle values at the transect location representing the shoreline were assumed to be the values at breaking; this limitation is removed in the model developed in Section 6.10.

In these figures the water depth and pit depth were 2 m and 4 m, respectively, the period was 10 s, the incident wave height was 1 m, and averaging over 5 wave directions was used to smooth out the longshore variation in the wave height at large distances from the pit. The time step was 120 s and 10 iterations of shoreline change were calculated between wave height and direction updates for a total modeling time of 48 hours. The

diffusive nature of the angle-driven transport term is seen to modify the much larger wave height gradient transport term in order to generate an equilibrium planform when the two terms are used together. Comparison of these results with those described earlier establishes the significance of wave reflection and the second transport term on the equilibrium planform.

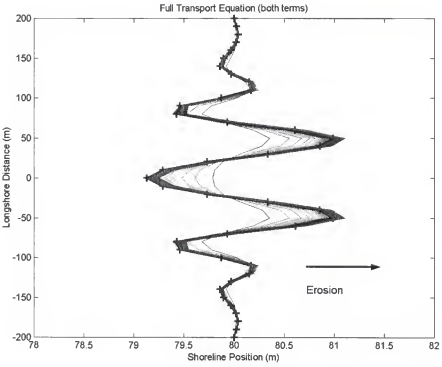

Figure 2-35: Shoreline evolution using full transport equation and analytic solution model for transect located 80 m shoreward of a pit with a radius = 6 m, last time step indicated with [+] (modified from Bender and Dean, 2001).

CHAPTER 3
2-DIMENSIONAL MODEL THEORY AND FORMULATION

3.1 Introduction

The reflection and transmission of normally incident waves by two-dimensional trenches and shoals of finite width with sloped transitions between the depth changes are studied. Prior two-dimensional studies, outlined in Chapter 2, have all investigated the interaction of water waves with changes in bathymetry that have featured domains with an abrupt transition, with the exception of Dean (1964) and Lee et al. (1981). A more realistic representation of natural trenches and shoals should allow for gradual transitions (sloped sidewalls).

The focus of the 2-dimensional study is the propagation of water waves over a 2-D trench or shoal of more realistic geometry. This will extend the study of Dean (1964) that investigated long wave modification by a sloped step and Lee et al. (1981), which did not directly address the effect of the transition slope on the reflection and transmission coefficients. Three solution methods are developed for linear water waves: (1) the step method, (2) the slope method and (3) a numerical method. The step method is valid in arbitrary water depth while the slope method and the numerical method are valid only for shallow water conditions. The step method is an extension of the Takano (1960) eigenfunction expansion solution as modified by Kirby and Dalrymple (1983a) that allows for a trench or shoal in arbitrary depth with "stepped" transitions that approximate a specific slope or shape. The slope method extends the long wave solution

of Dean (1964) that allows for linear transitions between the changes in bathymetry for a trench or shoal creating regular or irregular trapezoids. The numerical method employs a backward space-stepping procedure for arbitrary (but shallow water) bathymetry with the transmitted wave specified.

3.2 Step Method: Formulation and Solution

The two-dimensional motion of monochromatic, small-amplitude water waves in an inviscid and irrotational fluid of arbitrary depth is investigated. The waves are normally incident and propagate in an infinitely long channel containing a two-dimensional obstacle (trench or shoal) of finite width. Details of the fluid domain and the formulation of the solution vary depending on the case studied: abrupt transition or gradual transition with the slope approximated by the step method.

The step method is an extension of the Takano (1960) formulation for the propagation of waves over a rectangular sill. The eigenfunction expansion method of Takano (1960) was extended in Kirby and Dalrymple (1983a) to allow for oblique wave incidence and again in 1987 by Kirby et al. to include the effects of currents along the trench. In the present formulation the method of Takano, as formulated in Kirby and Dalrymple (1983a), was generally followed for normal wave incidence.

The solution starts with the definition of a velocity potential:

$$\tilde{\phi}_j(x,z,t) = \phi_j(x,z)e^{i\sigma t} \qquad (j = 1 \rightarrow J) \tag{3-1}$$

where j indicates the region, J is the total number of regions (3 for the case of a trench or sill with an abrupt transition), and σ is the angular frequency. The velocity potential must satisfy the Laplace Equation:

$$\left(\frac{\partial^2}{\partial x^2}+\frac{\partial^2}{\partial z^2}\right)\phi(x,z)=0 \tag{3-2}$$

the free-surface boundary condition:

$$\frac{\partial\phi(x,z)}{\partial z}+\frac{\sigma^2}{g}\phi=0 \tag{3-3}$$

and the condition of no flow normal to any solid boundary:

$$\frac{\partial\phi(x,z)}{\partial n}=0 \tag{3-4}$$

The velocity potential must also satisfy radiation conditions at large |x|.

The boundary value problem defined by Eq. 3-2, the boundary conditions of Eqs. 3-3 and 3-4, and the radiation condition can be solved with a solution in each region of the form

$$\phi_j(x,z)=A_j^{\pm}\frac{\cosh\left[k_j\left(h_j+z\right)\right]}{\cosh\left[k_j h_j\right]}e^{\pm ik_j(x)}+\sum_{n=1}^{\infty}B_{j,n}^{\pm}\cos\left[\kappa_{j,n}\left(h_j+z\right)\right]e^{\pm\kappa_{j,n}\left(x-x_j\right)}$$

$$\left(j=1\rightarrow J\right),\ \left(n=1\rightarrow\infty\right) \tag{3-5}$$

In the previous equation A_1^+ is the incident wave amplitude coefficient, A_1^- is the reflected wave amplitude coefficient and A_J^+ is the transmitted wave amplitude coefficient. The coefficient B is an amplitude function for the evanescent modes $\left(n=1\rightarrow\infty\right)$ at the boundaries, which are standing waves that decay exponentially with distance from the boundary. The values of the wave numbers of the propagating modes, k_j, are determined from the dispersion relation:

$$\sigma^2=gk_j\tanh(k_j h_j) \qquad \left(j=1\rightarrow J\right) \tag{3-6}$$

and the wave numbers for the evanescent modes, $\kappa_{j,n}$ are found from

$$\sigma^2 = -g\kappa_{j,n}\tan(\kappa_{j,n}h_j) \qquad (j=1\rightarrow J),\ (n=1\rightarrow\infty) \tag{3-7}$$

In each region a complete set of orthogonal equations over the depth is formed by Eqs. 3-5 to 3-7.

To gain the full solution, matching conditions are applied at each boundary between adjacent regions. The matching conditions ensure continuity of pressure:

$$\phi_j = \phi_{j+1} \qquad (x=x_j),\ (j=1\rightarrow J-1) \tag{3-8}$$

and continuity of horizontal velocity normal to the vertical boundaries:

$$\frac{\partial\phi_j}{\partial x} = \frac{\partial\phi_{j+1}}{\partial x} \qquad (x=x_j),\ (j=1\rightarrow J-1) \tag{3-9}$$

The matching conditions are applied over the vertical plane between the two regions: $(-h_j \le z \le 0)$ if $h_j < h_{j+1}$ or $(-h_{j+1} \le z \le 0)$ if $h_j > h_{j+1}$.

In order to form a solution, one wave form in the domain must be specified, usually the incident or the transmitted wave. Knowing the value of the incident, reflected and transmitted wave amplitudes, the reflection and transmission coefficients can be calculated from

$$K_R = \frac{a_R}{a_I} \tag{3-10}$$

$$K_T = \frac{a_T}{a_I}\frac{\cosh(k_j h_j)}{\cosh(k_1 h_1)} \tag{3-11}$$

where the cosh terms account for the change in depth at the upwave and downwave ends of the trench/shoal for the asymmetric case. A convenient check of the solution is to apply conservation of energy considerations:

$$K_R^2 + \left(\frac{a_T}{a_I}\right)^2\left[\frac{n_j k_1}{n_1 k_j}\right] = 1 \tag{3-12}$$

where n_j is the ratio of the group velocity to the wave celerity:

$$n_j = \frac{1}{2}\left(1 + \frac{2k_j h_j}{\sinh(2k_j h_j)}\right) \tag{3-13}$$

3.2.1 Abrupt Transition

The solution of Takano (1960) for an elevated sill and that of Kirby and Dalrymple (1983a) for a trench are valid for abrupt transitions (vertical walls) between the regions of different depth. For these cases the domain is divided into three regions (J = 3) and the matching conditions are applied over the two boundaries between the regions. The definition sketch for the case of a trench with vertical transitions is shown in Figure 3-1 where W is the width of the trench.

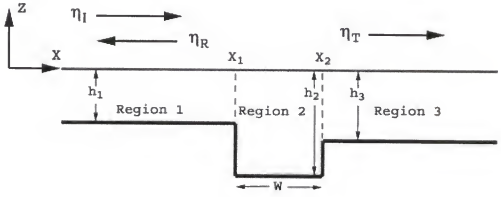

Figure 3-1: Definition sketch for trench with vertical transitions.

Takano constructed a solution to the elevated sill problem by applying the matching conditions [Eqs. 3-8 and 3-9] for a truncated series $(n = 1 \rightarrow N)$ of eigenfunction expansions of the form in Eq. 3-5. Applying the matching conditions results in a truncated set of independent integral equations each of which is multiplied by the appropriate eigenfunction; $\cosh[k_j(h_j+z)]$ or $\cos[\kappa_{j,n}(h_j+z)]$. The proper eigenfunction to use depends on whether the boundary results in a "step down" or a "step up"; thereby

making the form of the solution for an elevated sill different than that of a trench. With one wave form specified, the orthogonal properties of the eigenfunctions result in 4N+4 unknown coefficients and a closed problem.

By applying the matching conditions at the boundary between Regions 1 and 2 ($x = x_1$), 2N+2 integral equations are constructed. For the case of a trench with vertical transitions (Figure 3-1) the resulting equations are of the form

$$\int_{-h_1}^{0} \phi_1(x_1,z)\cosh\left[k_1(h_1+z)\right]dz = \int_{-h_1}^{0} \phi_2(x_1,z)\cosh\left[k_1(h_1+z)\right]dz \tag{3-14}$$

$$\int_{-h_1}^{0} \phi_1(x_1,z)\cos\left[\kappa_{1,n}(h_1+z)\right]dz = \int_{-h_1}^{0} \phi_2(x_1,z)\cos\left[\kappa_{1,n}(h_1+z)\right]dz \quad (n=1\rightarrow N) \tag{3-15}$$

$$\begin{aligned}\int_{-h_1}^{0} \frac{\partial\phi_1}{\partial x}(x_1,z)\cosh\left[k_2(h_2+z)\right]dz &= \int_{-h_1}^{0} \frac{\partial\phi_2}{\partial x}(x_1,z)\cosh\left[k_2(h_2+z)\right]dz \\ &= \int_{-h_2}^{0} \frac{\partial\phi_2}{\partial x}(x_1,z)\cosh\left[k_2(h_2+z)\right]dz\end{aligned} \tag{3-16}$$

$$\begin{aligned}\int_{-h_1}^{0} \frac{\partial\phi_1}{\partial x}(x_1,z)\cos\left[\kappa_{2,n}(h_2+z)\right]dz &= \int_{-h_1}^{0} \frac{\partial\phi_2}{\partial x}(x_1,z)\cos\left[\kappa_{2,n}(h_2+z)\right]dz \\ &= \int_{-h_2}^{0} \frac{\partial\phi_2}{\partial x}(x_1,z)\cos\left[\kappa_{2,n}(h_2+z)\right]dz\end{aligned} \quad (n=1\rightarrow N) \tag{3-17}$$

The limits of integration for the right hand side in Eqs. 3-16 and 3-17 are shifted from $-h_1$ to $-h_2$ as there is no contribution to the horizontal velocity for $(-h_2 \le z < -h_1)$ at $x = x_1$ and $(-h_2 \le z < -h_3)$ at $x = x_2$, for this case. In Eqs. 3-14 and 3-15 the limits of integration for the pressure considerations are $(-h_1 \le z < 0)$ at $x = x_1$ and $(-h_3 \le z < 0)$ at $x = x_2$.

At the boundary between Regions 2 and 3 the remaining 2N+2 equations are developed. For the case of a trench the downwave boundary is a "step up", which

requires different eigenfunctions to be used and changes the limits of integrations from the case of the "step down" at the upwave boundary [Eqs. 3-14 to 3-17].

$$\int_{-h_3}^{0}\phi_2(x_2,z)\cosh\left[k_3(h_3+z)\right]dz = \int_{-h_3}^{0}\phi_3(x_2,z)\cosh\left[k_3(h_3+z)\right]dz \tag{3-18}$$

$$\int_{-h_3}^{0}\phi_2(x_2,z)\cos\left[\kappa_{3,n}(h_3+z)\right]dz = \int_{-h_3}^{0}\phi_3(x_2,z)\cos\left[\kappa_{3,n}(h_3+z)\right]dz \quad (n=1\rightarrow N) \tag{3-19}$$

$$\int_{-h_2}^{0}\frac{\partial\phi_2}{\partial x}(x_2,z)\cosh\left[k_2(h_2+z)\right]dz = \int_{-h_3}^{0}\frac{\partial\phi_3}{\partial x}(x_2,z)\cosh\left[k_2(h_2+z)\right]dz \tag{3-20}$$

$$\int_{-h_2}^{0}\frac{\partial\phi_2}{\partial x}(x_2,z)\cos\left[\kappa_{2,n}(h_2+z)\right]dz = \int_{-h_3}^{0}\frac{\partial\phi_3}{\partial x}(x_2,z)\cos\left[\kappa_{2,n}(h_2+z)\right]dz \quad (n=1\rightarrow N) \tag{3-21}$$

At each boundary the appropriate evanescent mode contributions from the other boundary must be included in the matching conditions. The resulting set of simultaneous equations may be solved as a linear matrix equation. The value of N (number of non-propagating modes) must be large enough to ensure convergence of the solution. Kirby and Dalrymple (1983a) found that N = 16 provided adequate convergence for most values of k_1h_1.

3.2.2 Gradual Transition

The step method is an extension of the work by Takano (1960) and Kirby and Dalrymple (1983a) that allows for a domain with a trench or sill with gradual transitions (sloped sidewalls) between regions. Instead of having a "step down" and then "step up" as in the Kirby and Dalrymple solution for a trench or the reverse for Takano's solution for an elevated sill, in the step method a series of steps either up or down are connected by a constant depth region followed by a series of steps in the other direction. A sketch

of a domain with a stepped trench is shown in Figure 3-2. In this method, as in the case of a trench or a sill, a domain with J regions will contain J-1 steps and boundaries.

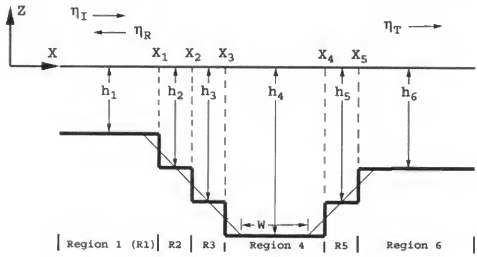

Figure 3-2: Definition sketch for trench with stepped transitions.

Each region will have a specified depth and each boundary between regions will have a specified x location where the matching conditions must be applied.

At each boundary the matching conditions are applied and depend on whether the boundary is a "step up" or a "step down." With the incident wave specified, a set of equations with 2(J-1)N+2(J-1) unknown coefficients is formed.

The resulting integral equations are of the form: for $(j = 1 \rightarrow J-1)$ if $(-h_j > -h_{j+1})$ at x = x_j then the boundary is a "step down";

$$\int_{-h_j}^{0} \phi_j(x_j,z)\cosh\left[k_j(h_j+z)\right]dz = \int_{-h_j}^{0} \phi_{j+1}(x_j,z)\cosh\left[k_j(h_j+z)\right]dz \qquad (3\text{-}22)$$

$$\int_{-h_j}^{0} \phi_j(x_j,z)\cos\left[\kappa_{j,n}(h_j+z)\right]dz = \int_{-h_j}^{0} \phi_{j+1}(x_j,z)\cos\left[\kappa_{j,n}(h_j+z)\right]dz \ (n = 1 \rightarrow N) \qquad (3\text{-}23)$$

$$\int_{-h_j}^{0} \frac{\partial \phi_j}{\partial x}(x_j,z)\cosh\left[k_{j+1}(h_{j+1}+z)\right]dz = \int_{-h_{j+1}}^{0} \frac{\partial \phi_{j+1}}{\partial x}(x_j,z)\cosh\left[k_{j+1}(h_{j+1}+z)\right]dz \qquad (3\text{-}24)$$

$$\int_{-h_j}^{0} \frac{\partial \phi_j}{\partial x}(x_j, z)\cos\left[\kappa_{j+1,n}\left(h_{j+1}+z\right)\right]dz = \int_{-h_{j+1}}^{0} \frac{\phi_{j+1}}{\partial x}(x_j, z)\cos\left[\kappa_{j+1,n}\left(h_{j+1}+z\right)\right]dz$$

$$\left(n = 1 \rightarrow N\right) \quad (3\text{-}25)$$

if $\left(-h_j < -h_{j+1}\right)$ at x = x_j then the boundary is a "step up";

$$\int_{-h_{j+1}}^{0} \phi_j(x_j, z)\cosh\left[k_{j+1}\left(h_{j+1}+z\right)\right]dz = \int_{-h_{j+1}}^{0} \phi_{j+1}(x_j, z)\cosh\left[k_{j+1}\left(h_{j+1}+z\right)\right]dz \quad (3\text{-}26)$$

$$\int_{-h_{j+1}}^{0} \phi_j(x_j, z)\cos\left[\kappa_{j+1,n}\left(h_{j+1}+z\right)\right]dz = \int_{-h_{j+1}}^{0} \phi_{j+1}(x_j, z)\cos\left[\kappa_{j+1,n}\left(h_{j+1}+z\right)\right]dz$$

$$\left(n = 1 \rightarrow N\right) \quad (3\text{-}27)$$

$$\int_{-h_j}^{0} \frac{\partial \phi_j}{\partial x}(x_j, z)\cosh\left[k_j\left(h_j+z\right)\right]dz = \int_{-h_{j+1}}^{0} \frac{\partial \phi_{j+1}}{\partial x}(x_j, z)\cosh\left[k_j\left(h_j+z\right)\right]dz \quad (3\text{-}28)$$

$$\int_{-h_j}^{0} \frac{\partial \phi_j}{\partial x}(x_j, z)\cos\left[\kappa_{j,n}\left(h_j+z\right)\right]dz = \int_{-h_{j+1}}^{0} \frac{\partial \phi_{j+1}}{\partial x}(x_j, z)\cos\left[\kappa_{j,n}\left(h_j+z\right)\right]dz$$

$$\left(n = 1 \rightarrow N\right) \quad (3\text{-}29)$$

At each boundary (x_j) the appropriate evanescent mode contributions from the adjacent boundaries (x_{j-1}, x_{j+1}) must be included in the matching conditions. The resulting set of simultaneous equations is solved as a linear matrix equation with the value of N large enough to ensure convergence of the solution.

3.3 Slope Method: Formulation and Solution

The slope method is an extension of the analytic solution by Dean (1964) for long wave modification by linear transitions. Linear transitions in the channel width, depth, and both width and depth were studied. The solution of Dean (1964) is valid for one linear transition in depth and/or width, which in the case of a change in depth allowed for

an infinite step, either up or down, to be studied. In the slope method a domain with two linear transitions allows the study of obstacles of finite width with sloped transitions.

The long wave formulation of Dean (1964) for a linear transition in depth was followed. By combining the equations of continuity and motion the governing equation of the water surface for long wave motion in a channel of variable cross-section can be developed. The continuity equation is a conservation of mass statement requiring that the net influx of fluid into a region during a time, Δt, must be equal to a related rise in the water surface, η. For a channel of uniform width, b, this can be expressed as

$$[Q(x) - Q(x + \Delta x)]\Delta t = b\Delta x[\eta(t + \Delta t) - \eta(t)] \tag{3-30}$$

where Q(x) and Q(x+Δx) are the volume rates of flow into and out of the control volume, respectively. The volume flow rate for the uniform channel can be expressed as the product of the cross sectional width, A, and the horizontal velocity, u, in the channel:

$$Q = Au \tag{3-31}$$

By substituting Eq. 3-31 into Eq. 3-30 and expanding the appropriate terms in their Taylor series while neglecting higher order terms, Eq. 3-30 can be rewritten as

$$-\frac{\partial}{\partial x}(Au) = b\frac{\partial \eta}{\partial t} \tag{3-32}$$

The hydrostatic pressure equation is combined with the linearized form of Euler's equation of motion to develop the equation of motion for small amplitude, long waves. The pressure field, p(x,y,t), for the hydrostatic conditions under long waves is

$$p(x,z,t) = \rho g[\eta(x,t) - z] \tag{3-33}$$

Euler's equation of motion in the x direction for no body forces and linearized motion is

$$-\frac{1}{\rho}\frac{\partial p}{\partial x} = \frac{\partial u}{\partial t} \tag{3-34}$$

The equation of motion for small amplitude, long waves follows from combining Eqs. 3-33 and 3-34:

$$-g\frac{\partial \eta}{\partial x}=\frac{\partial u}{\partial t} \tag{3-35}$$

The governing equation is developed by differentiating the continuity equation [Eq. 3-32] with respect to t:

$$\frac{\partial}{\partial t}\left[-\frac{\partial}{\partial x}(Au)=b\frac{\partial \eta}{\partial t}\right]\rightarrow -\frac{\partial}{\partial x}\left[A\frac{\partial u}{\partial t}\right]=b\frac{\partial^2 \eta}{\partial t^2} \tag{3-36}$$

and inserting the equation of motion [Eq. 3-35] into the resulting equation, Eq. 3-36 yields the result

$$g\frac{\partial}{\partial x}\left[A\frac{\partial \eta}{\partial x}\right]=b\frac{\partial^2 \eta}{\partial t^2} \tag{3-37}$$

Eq. 3-37 is valid for any small amplitude, long wave form and expresses η as a function of distance and time. Eq. 3-37 can be further simplified under the assumption of simple harmonic motion:

$$\eta(x,t)=\eta_1(x)e^{i(\sigma t+\alpha)} \tag{3-38}$$

where α is the phase angle. Eq. 3-37 can now be written as

$$\frac{g}{b}\frac{\partial}{\partial x}\left[bh\frac{\partial \eta}{\partial x}\right]+\sigma^2\eta=0 \tag{3-39}$$

where the subscript $\eta_1(x)$ has been dropped and the substitution, A = bh, was made.

3.3.1 Single Transition

The case of a channel of uniform width with an infinitely long step either up or down was a specific case solved in Dean (1964). The definition sketch for a "step down" is shown in Figure 3-3. The three regions in Figure 3-3 have the following depths:

Region 1, $x < x_1$; $h = h_1$ (3-40)

Region 2, $x_1 < x < x_2$; $h = h_3 \frac{x}{x_2}$ (3-41)

Region 3, $x > x_2$; $h = h_3$ (3-42)

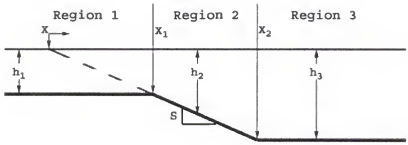

Figure 3-3: Definition sketch for linear transition.

For the regions of uniform depth, Eq. 3-39 simplifies to

$$gh\frac{\partial^2 \eta}{\partial x^2} + \sigma^2 \eta = 0 \tag{3-43}$$

which has the solution for η of cos(kx) and sin(kx) where $k = \frac{2\pi}{\lambda}$ and λ is the wave length. The most general solution of η(x,t) from Eq. 3-43 is

$$\eta(x,t) = B_1 \cos(kx - \sigma t + \alpha_1) + B_2 \cos(kx + \sigma t + \alpha_2) \tag{3-44}$$

The wave form of Eq. 3-44 consists of two progressive waves of unknown amplitude and phase: an incident wave traveling in the positive x direction and a reflected wave traveling in the negative x direction.

For the region of linearly varying depth, Eq. 3-41 is inserted in Eq. 3-39 resulting in a Bessel equation of zero order:

$$x\frac{\partial^2\eta}{\partial x^2}+\frac{\partial\eta}{\partial x}+\beta\eta=0 \tag{3-45}$$

where

$$\beta=\frac{\sigma^2 x_2}{gh_3} \tag{3-46}$$

The solutions of $\eta(x)$ for Eq. 3-45 are

$$\eta(x)=J_0(2\beta^{1/2}x^{1/2}) \quad and \quad Y_0(2\beta^{1/2}x^{1/2}) \tag{3-47}$$

where J_0 and Y_0 are zero-order Bessel functions of the first and second kind, respectively. From Eq. 3-47 the solutions for $\eta(x,t)$ in Region 2 follow

$$\begin{aligned}\eta(x,t)=&B_3J_0(2\beta^{1/2}x^{1/2})\cos(\sigma t+\alpha_3)+B_3Y_0(2\beta^{1/2}x^{1/2})\sin(\sigma t+\alpha_3)\\&+B_4J_0(2\beta^{1/2}x^{1/2})\cos(\sigma t+\alpha_4)-B_4Y_0(2\beta^{1/2}x^{1/2})\sin(\sigma t+\alpha_4)\end{aligned} \tag{3-48}$$

The wave system of Eq. 3-48 consists of two waves of unknown amplitude and phase; one wave propagating in the positive x direction (B_3) and the other in the negative x direction (B_4).

The problem described by Figure 3-3 and Eqs. 3-44 and 3-48 contains eight unknowns: $B_{1\to4}$ and $\alpha_{1\to4}$. Solution to the problem is obtained by applying matching conditions at the two boundaries between the three regions. The conditions match the water surface and the gradient of the water surface:

$$\eta_j=\eta_{j+1} \quad at\ x=x_j \quad (j=1,2) \tag{3-49}$$

$$\frac{\partial\eta_j}{\partial x}=\frac{\partial\eta_{j+1}}{\partial x} \quad at\ x=x_j \quad (j=1,2) \tag{3-50}$$

Eqs. 3-49 and 3-50 result in eight equations (four complex equations), four from setting $\sigma t = 0$ and four from setting $\sigma t = \frac{\pi}{2}$, which can be solved for the eight unknowns as a linear matrix equation.

3.3.2 Trench or Shoal

The slope method is an extension of the Dean (1964) solution that allows for a domain with a trench or a sill with sloped transitions. Two linear transitions are connected by a constant depth region by placing two solutions from Dean (1964) "back to back." A trench/sill with sloped side walls can be formed by placing a "step down" upwave/downwave of a "step up." The definition sketch for the case of a trench is shown in Figure 3-4.

In the slope method the depths are defined as follows

$$\text{Region 1, } x < x_1; \quad h = h_1 \tag{3-51}$$

$$\text{Region 2, } x_1 < x < x_2; \quad h = h_1 + s_1(x - x_1) \tag{3-52}$$

$$\text{Region 3, } x_2 < x < x_3; \quad h = h_3 \tag{3-53}$$

$$\text{Region 4, } x_3 < x < x_4; \quad h = h_3 - s_2(x - x_3) \tag{3-54}$$

$$\text{Region 5, } x > x_4; \quad h = h_5 \tag{3-55}$$

where h_1, h_3, h_5, s_1, s_2, and W are specified. With the new definition for the depth in regions 2 and 4, the definition of the coefficient β in Eq. 3-45 changes to $\beta = \frac{\sigma^2}{g s_1}$ and $\beta = \frac{\sigma^2}{g s_2}$ in regions 2 and 4, respectively.

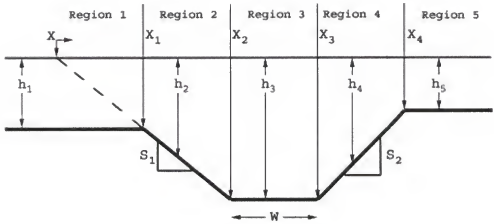

Figure 3-4: Definition sketch for trench with sloped transitions.

The matching conditions of Eqs. 3-49 and 3-50 are applied at the four boundaries between the regions. With the transmitted wave specified and by setting $\sigma t = 0$ and $\sigma t = \frac{\pi}{2}$ for each matching condition a set of 16 independent equations is developed. Using standard matrix techniques the eight unknown amplitudes and eight unknown phases can then be determined.

The reflection and transmission coefficients can be determined from

$$K_R = \frac{a_R}{a_I} \text{ and } K_T = \frac{a_T}{a_I} \qquad \text{(3-56), (3-57)}$$

Conservation of energy arguments in the shallow water region require

$$K_R^2 + K_T^2 \left[\frac{\sqrt{h_5}}{\sqrt{h_1}} \right] = 1 \qquad \text{(3-58)}$$

This method can be extended to the representation of long wave interaction with any depth transition form represented by a series of line segments.

3.4 Numerical Method: Formulation and Solution

A numerical method was developed to determine the long wave transformation caused by a trench or shoal of arbitrary, but shallow water bathymetry. A transmitted wave form in a region of constant depth downwave of the depth anomaly is the specified input to the problem. Numerical methods are used to space step the wave form backwards over the trench or shoal and then into a region of constant depth upwave of the depth anomaly where two wave forms exist; an incident wave and a reflected wave.

As in the long wave solution of Section 3, the continuity equation and the equation of motion are employed to develop the governing equation for the problem. The continuity equation and the equation of motion in the x direction are written in a slightly different form than in Eqs. 3-32 and 3-35 of Section 3.3:

$$\frac{\partial \eta}{\partial t} = -\frac{\partial q_x}{\partial x} \tag{3-59}$$

$$gh\frac{\partial \eta}{\partial x} = -\frac{\partial q_x}{\partial t} \tag{3-60}$$

Taking the derivative of Eq. 3-59 with respect to t and the derivative of Eq. 3-60 with respect to x results in the governing equation for this method:

$$\frac{\partial^2 \eta}{\partial t^2} - gh\frac{\partial^2 \eta}{\partial x^2} - g\frac{dh}{dx}\frac{\partial \eta}{\partial x} = 0 \tag{3-61}$$

where the depth, h, is a function of x and η may be written as a function of x and t:

$$\eta = \eta(x)e^{i\sigma t} \tag{3-62}$$

Inserting the form of η in Eq. 3-62 into the governing equation of Eq. 3-61 casts the equation in a different form (equivalent to Eq. 3-39)

$$\eta(x) + \frac{gh}{\sigma^2}\frac{\partial^2 \eta(x)}{\partial x^2} + \frac{g}{\sigma^2}\frac{dh}{dx}\frac{\partial \eta(x)}{\partial x} = 0 \tag{3-63}$$

Central differences are used to perform the backward space stepping of the numerical method.

$$F''(x) = \frac{F(x+\Delta x) - 2F(x) + F(x-\Delta x)}{\Delta x^2} \tag{3-64}$$

$$F'(x) = \frac{F(x+\Delta x) - F(x-\Delta x)}{2\Delta x} \tag{3-65}$$

Inserting the forms of the central differences into Eq. 3-63 for η results in

$$\eta(x) + \frac{gh}{\sigma^2}\left[\frac{\eta(x+\Delta x) - 2\eta(x) + \eta(x-\Delta x)}{\Delta x^2}\right] + \frac{g}{\sigma^2}\frac{dh}{dx}\left[\frac{\eta(x+\Delta x) - \eta(x-\Delta x)}{2\Delta x}\right] = 0 \tag{3-66}$$

For the backward space stepping calculation, Eq. 3-66 can be rearranged

$$\eta(x-\Delta x) = \frac{-\eta(x+\Delta x)\left[\frac{gh}{\sigma^2\Delta x^2} + \frac{g}{\sigma^2}\frac{dh}{dx}\frac{1}{2\Delta x}\right] - \eta(x)\left[1 - \frac{2gh}{\sigma^2\Delta x^2}\right]}{\left[\frac{gh}{\sigma^2\Delta x^2} - \frac{g}{\sigma^2}\frac{dh}{dx}\frac{1}{2\Delta x}\right]} \tag{3-67}$$

To initiate the calculation, values of η(x) and η(x+Δx) must be specified in the constant depth region downwave from the depth anomaly. If the starting point of the calculation is taken as x = 0 then the initial values may be written as

$$\eta(0) = \frac{H}{2} \tag{3-68}$$

$$\eta(\Delta x) = \frac{H}{2}\left[\cos(k\Delta x) - i\sin(k\Delta x)\right] \tag{3-69}$$

The solution upwave of the depth anomaly comprises of an incident and reflected wave. The form of the incident and reflected waves are specified as

$$\eta_I = \frac{H_I}{2}\cos(kx - \sigma t - \varepsilon_I) \tag{3-70}$$

$$\eta_R = \frac{H_R}{2}\cos(kx + \sigma t - \varepsilon_R) \tag{3-71}$$

where the ε's are arbitrary phases. At each location upwave of the depth anomaly the total water surface elevation will be the sum of the two individual components:

$$\eta_T = \eta_I + \eta_R = \frac{H_I}{2}\cos(kx-\varepsilon_I)\cos(\sigma t) + \sin(kx-\varepsilon_I)\sin(\sigma t) + \frac{H_R}{2}\cos(kx-\varepsilon_R)\cos(\sigma t) - \sin(kx-\varepsilon_R)\sin(\sigma t)$$

$$= \cos(\sigma t)\underbrace{\left[\frac{H_I}{2}\cos(kx-\varepsilon_I)+\frac{H_r}{2}\cos(kx-\varepsilon_R)\right]}_{I} + \sin(\sigma t)\underbrace{\left[\frac{H_I}{2}\sin(kx-\varepsilon_I)-\frac{H_r}{2}\sin(kx-\varepsilon_R)\right]}_{II}$$

$$= \sqrt{I^2+II^2}\,\cos\left(\sigma t-\varepsilon^*\right) \qquad \varepsilon^* = \tan^{-1}\left(\frac{II}{I}\right) \tag{3-72}$$

Using several trigonometric identities, Eq. 3-72 can be reduced further to the form

$$\eta_T = \frac{1}{2}\sqrt{H_I^2+H_R^2+2H_IH_R\cos(2kx-\varepsilon_I-\varepsilon_R)}\cos\left(\sigma t-\varepsilon^*\right) \tag{3-73}$$

which is found to have maximum and minimum values of

$$\eta_{T\max} = \frac{1}{2}\left(H_I+H_R\right) \tag{3-74}$$

$$\eta_{T\min} = \frac{1}{2}\left(H_I-H_R\right) \tag{3-75}$$

Eqs. 3-74 and 3-75 are used to determine the values of H_I and H_R upwave of the trench/shoal, and allow calculation of the reflection and transmission coefficients.

CHAPTER 4
3-DIMENSIONAL MODEL THE0RY AND FORMULATION

4.1 Introduction

The three-dimensional motion of monochromatic, small-amplitude water waves in an inviscid and irrotational fluid of arbitrary depth is investigated. The waves propagate in an infinitely long, uniform depth domain containing a three-dimensional axisymmetric anomaly (pit or shoal) of finite extent. The addition of the second horizontal dimension provides many new, and more practical, possibilities for study compared to the 2-D model domains, which excluded longshore variation.

Two different models are developed for the 3-D domains that contain linear transitions in depth. The analytic step method is an extension of Bender (2001) that determines the wave transformation in arbitrary water depth for domains with gradual transitions in depth that are approximated by a series of steps of uniform depth. The exact analytic model solves the wave transformation in shallow water for specific bathymetries that reduce the governing equations to known forms.

4.2 Step Method: Formulation and Solution

The step method for a three-dimensional domain is an extension of the Bender (2001) formulation for the propagation of waves past a circular anomaly with abrupt transitions. This method allowed oblique wave incidence, but was limited to the shallow water region. Following Bender (2001) with significant changes in notation the governing equations for the three-dimensional models are developed.

Details of the fluid domain and the formulation of the solution vary depending on the case studied: abrupt transition in depth between regions or gradual transition with the slope approximated by the step method. The definition sketch for the case of a circular pit with an abrupt depth transition is shown in Figure 4-1.

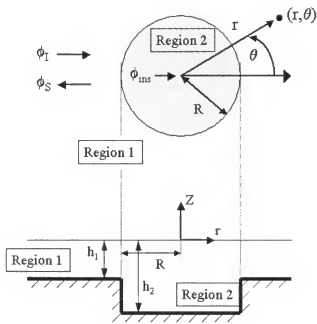

Figure 4-1: Definition sketch for circular pit with abrupt depth transitions.

The domain is divided into regions with the bathymetric anomaly and its projection comprising Regions 2→Ns+1 where Ns is the number of steps approximating the depth transition slope and the rest of the domain, of depth h_1, in Region 1. For the case of an abrupt transition in depth the bathymetric anomaly occurs in Region 2 of uniform depth h_2, where abrupt is defined as one step either down or up. For the case of a gradual depth transition the bathymetric anomaly will be divided into subregions with the depth in each subregion equal to h_j for each step $j = 2 \rightarrow N_s + 1$.

The solution starts with the definition of a velocity potential in cylindrical coordinates that is valid in each Region j:

$$\Phi_j = \mathrm{Re}(\phi_j(r,\theta,z)e^{-i\omega t}) \qquad (j = 1 \rightarrow N_s) \tag{4-1}$$

where ω is the wave frequency.

Linear wave theory is employed and Laplace's solution in cylindrical coordinates is valid:

$$\nabla^2\phi = \frac{\partial^2\phi}{\partial r^2} + \frac{1}{r}\frac{\partial\phi}{\partial r} + \frac{\partial^2\phi}{r^2\partial\theta^2} + \frac{\partial^2\phi}{\partial z^2} = 0 \tag{4-2}$$

where the free surface boundary condition is

$$\frac{\partial\phi}{\partial z} - \frac{\sigma^2}{g}\phi = 0 \tag{4-3}$$

and the bottom boundary condition is taken as

$$\frac{\partial\phi}{\partial z} = 0 \tag{4-4}$$

at $z = -h_1$ in Region 1 or $z = -h_j$ in Region 2.

Separation of variables is used to solve the equations with the velocity potential given the form

$$\phi(r,\theta,z) = R(r)\Theta(\theta)Z(z) \tag{4-5}$$

A valid solution for the dependency with depth is

$$Z(z) = \cosh(k_j(h_j+z)) \tag{4-6}$$

where k_j is the wave number in the appropriate region and h_j is constant within each region. Inserting Eqs. 4-5 and 4-6 into the Laplace equation gives

$$R''\Theta + \frac{1}{r}R'\Theta + \frac{1}{r^2}\Theta''R + R\Theta k^2 = 0 \tag{4-7}$$

If the form of the dependence with θ is assumed to be

$$\Theta(\theta) = \cos(m\theta) \tag{4-8}$$

then Eq. 4-7 may be reduced to

$$r^2 R'' + rR' + R\left(k^2 r^2 - m^2\right) = 0 \tag{4-9}$$

which is a standard Bessel equation with solutions $J_m(kr)$, $Y_m(kr)$, and $H_m(kr)$. The dependency of the solution on θ cancels out of Eq. 4-9; a result of the separation of variables approach. The wave number is determined from the dispersion relation:

$$\sigma^2 = gk_j \tanh(k_j h_j) \tag{4-10}$$

The standard Bessel solutions and the wave numbers of Eq. 4-10 represent the plane progressive wave component of the solution.

Another solution is found when the dependence with depth is defined as

$$Z(z) = \cos(\kappa_j(h_j+z)) \tag{4-11}$$

Inserting Eqs. 4-5, 4-8 and 4-11 into the Laplace Equation gives

$$r^2 R'' + rR' - R\left(\kappa^2 r^2 + m^2\right) = 0 \tag{4-12}$$

which is a modified Bessel equation with solutions $K_m(\kappa r)$ and $I_m(\kappa r)$ where κ is the wave number for the evanescent modes obtained using

$$\sigma^2 = -g\kappa_{j,n} \tan(\kappa_{j,n} h_j) \qquad \left(n = 1 \rightarrow \infty\right) \tag{4-13}$$

where n indicates the number of the evanescent mode. The modified Bessel solutions and the wave numbers of Eq. 4-13 represent the evanescent mode solutions, which decay with distance from each interface between regions. The evanescent terms are included to account for the distortion of the plane wave near the interface (Black and Mei, 1970) and to extend the range of the solution into the arbitrary depth region.

At each interface between changes in depth, matching conditions must be applied to ensure continuity of pressure:

$$\phi_j = \phi_{j+1} \qquad (r = r_j),\ (j = 1 \rightarrow N_s) \tag{4-14}$$

and continuity of horizontal velocity normal to the vertical boundaries:

$$\frac{\partial \phi_j}{\partial r_j} = \frac{\partial \phi_{j+1}}{\partial r_j} \qquad (r = r_j),\ (j = 1 \rightarrow N_s) \tag{4-15}$$

The matching conditions are applied over the vertical plane between the two regions: $(-h_j \le z \le 0)$ if $h_j < h_{j+1}$ or $(-h_{j+1} \le z \le 0)$ if $h_j > h_{j+1}$. The solution must also meet the radiation condition for large r:

$$\lim r_{\to\infty} \sqrt{r}\left(\frac{\partial}{\partial r} - ik_1\right)(\phi_1 - \phi_1^I) \tag{4-16}$$

where ϕ_1^I is the specified incident velocity potential.

4.2.1 Abrupt Transition

The solution method for an abrupt transition ($N_s = 1$) will be shown first to illustrate the simplest case for the three-dimensional step method. The definition sketch for the case of an abrupt transition is shown in Figure 4-2.

The solution starts with the definition of an incident velocity potential in the form of a plane progressive wave:

$$\phi_I(r,\theta,z,t) = M_I\left[\sum_{m=0}^{\infty} \gamma_m \cos(m\theta) J_m(k_1 r)\right] \frac{\cosh\left[k_1(h_1 + z)\right]}{\cosh(k_1 h_1)} e^{-i\omega t} \tag{4-17}$$

where $\gamma_m = 1$ for m = 0 and $2i^m$ otherwise, $M_I = \dfrac{-igH}{2\omega}$, r is the radial distance from the center of the bathymetric anomaly to the point in the fluid domain and θ is the angle to the point measured counter-clockwise from the θ origin as shown in Figure 4-1.

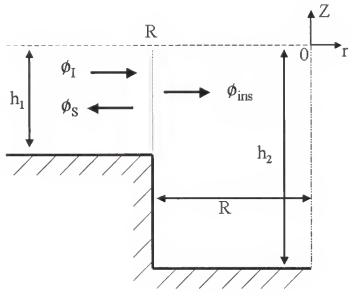

Figure 4-2: Definition sketch for boundary of abrupt depth transition.

The scattered velocity potential consists of reflected modes that persist with substantial distance from the pit and evanescent modes, which decay rapidly with distance from the pit:

$$\phi_S(r,\theta,z,t) = \left[\sum_{m=0}^{\infty} A_m \cos(m\theta) H_{1,m}(k_1 r)\right] \frac{\cosh\left[k_1(h_1+z)\right]}{\cosh(k_1 h_1)} e^{-i\omega t}$$
$$+ \left\{\sum_{m=1}^{\infty}\left[\sum_{n=1}^{\infty} \alpha_{m,n} K_m(\kappa_{1,n} r) \frac{\cos\left[\kappa_{1,n}(h_1+z)\right]}{\cos(\kappa_{1,n} h_1)}\right]\cos(m\theta)\right\} e^{-i\omega t} \qquad (4\text{-}18)$$

where $H_{1,m}$ indicates the Hankel function of the first kind and m^{th} order. Inside the pit the velocity potential is given the form

$$\phi_{ins}(r,\theta,z,t) = \left[\sum_{m=0}^{\infty} B_m \cos(m\theta) J_m(k_2 r)\right] \frac{\cosh\left[k_2(h_2+z)\right]}{\cosh(k_2 h_2)} e^{-i\omega t}$$
$$+ \left\{\sum_{m=1}^{\infty}\left[\sum_{n=1}^{\infty} \beta_{m,n} I_m(\kappa_{2,n} r) \frac{\cos\left[\kappa_{2,n}(h_2+z)\right]}{\cos(\kappa_{2,n} h_2)}\right]\cos(m\theta)\right\} e^{-i\omega t} \qquad (4\text{-}19)$$

A_m, $\alpha_{m,n}$, B_m and $\beta_{m,n}$ are unknown amplitude coefficients that must be determined for each Bessel function mode included in the solution.

The solution is obtained by applying the matching conditions of Eq. 4-14 and 4-15 at the single interface (r = R) between Regions 1 and 2 for two truncated series: $(m = 1 \rightarrow M)$ and $(n = 1 \rightarrow N_e)$. The velocity potential in Region 1 is the sum of the incident potential, Eq. 4-17, and scattered potential, Eq. 4-18.

Applying the matching conditions results in a truncated set of independent integral equations each of which is multiplied by the appropriate eigenfunction; $\cosh[k_j(h_j+z)]$ or $\cos[\kappa_{j,n}(h_j+z)]$. The proper eigenfunction to use depends on whether the boundary results in a "step down" or a "step up" as r approaches zero; thereby making the form of the solution for a pit different than that of a shoal. With the incident wave form specified, the orthogonal properties of the eigenfunctions result in $2M(N_e+1)$ complex unknown coefficients and a closed problem where M and N_e are the number of Bessel modes and evanescent modes, respectively, taken in the solution.

Applying the matching conditions at the interface between Regions 1 and 2 the necessary $2M(N_e+1)$ equations are developed. For the case of a pit ("step down") the resulting equations are of the form

$$\int_{-h_1}^{0} \phi_1(R,z)\cosh[k_1(h_1+z)]\,dz = \int_{-h_1}^{0} \phi_2(R,z)\cosh[k_1(h_1+z)]\,dz \qquad (4\text{-}20)$$

$$\int_{-h_1}^{0} \phi_1(R,z)\cos[\kappa_{1,n}(h_1+z)]\,dz = \int_{-h_1}^{0} \phi_2(R,z)\cos[\kappa_{1,n}(h_1+z)]\,dz \quad (n = 1 \rightarrow N_e) \qquad (4\text{-}21)$$

$$\int_{-h_1}^{0} \frac{\partial \phi_1}{\partial r}(R,z)\cosh\left[k_2(h_2+z)\right]dz = \int_{-h_1}^{0} \frac{\partial \phi_2}{\partial r}(R,z)\cosh\left[k_2(h_2+z)\right]dz$$
$$= \int_{-h_2}^{0} \frac{\partial \phi_2}{\partial r}(R,z)\cosh\left[k_2(h_2+z)\right]dz \qquad (4\text{-}22)$$

$$\int_{-h_1}^{0} \frac{\partial \phi_1}{\partial r}(R,z)\cos\left[\kappa_{2,n}(h_2+z)\right]dz = \int_{-h_1}^{0} \frac{\partial \phi_2}{\partial r}(R,z)\cos\left[\kappa_{2,n}(h_2+z)\right]dz$$
$$= \int_{-h_2}^{0} \frac{\partial \phi_2}{\partial r}(R,z)\cos\left[\kappa_{2,n}(h_2+z)\right]dz \qquad (n=1\rightarrow N_e)\ (4\text{-}23)$$

The limits of integration for the right hand side in Eqs. 4-22 and 4-23 are shifted from $-h_1$ to $-h_2$ as there is no contribution to the horizontal velocity for $(-h_2 \le z < -h_1)$ at the interface for a pit. In Eqs. 4-20 and 4-21 the limits of integration for the pressure considerations are $(-h_1 \le z < 0)$ at r = R.

For the case of a shoal ("step up") the resulting equations are of the form

$$\int_{-h_2}^{0} \phi_1(R,z)\cosh\left[k_2(h_2+z)\right]dz = \int_{-h_2}^{0} \phi_2(R,z)\cosh\left[k_2(h_2+z)\right]dz \qquad (4\text{-}24)$$

$$\int_{-h_2}^{0} \phi_1(R,z)\cos\left[\kappa_{2,n}(h_2+z)\right]dz = \int_{-h_2}^{0} \phi_2(R,z)\cos\left[\kappa_{2,n}(h_2+z)\right]dz \quad (n=1\rightarrow N_e) \quad (4\text{-}25)$$

$$\int_{-h_1}^{0} \frac{\partial \phi_1}{\partial r}(R,z)\cosh\left[k_1(h_1+z)\right]dz = \int_{-h_2}^{0} \frac{\partial \phi_2}{\partial r}(R,z)\cosh\left[k_1(h_1+z)\right]dz \qquad (4\text{-}26)$$

$$\int_{-h_1}^{0} \frac{\partial \phi_1}{\partial r}(R,z)\cos\left[\kappa_{1,n}(h_1+z)\right]dz = \int_{-h_2}^{0} \frac{\partial \phi_2}{\partial r}(R,z)\cos\left[\kappa_{1,n}(h_1+z)\right]dz$$

$$(n=1\rightarrow N_e) \quad (4\text{-}27)$$

The limits of integration for the left hand side in Eqs. 4-26 and 4-27 are shifted from $-h_2$ to $-h_1$ as there is no contribution to the horizontal velocity for $(-h_1 \le z < -h_2)$ at

the interface for a shoal. In Eqs. 4-24 and 4-25 the limits of integration for the pressure considerations are $(-h_2 \le z < 0)$ at r = R.

The resulting set of simultaneous equations is solved as a linear matrix equation. The values of M and N_e must be large enough to ensure convergence of the solution.

4.2.2 Gradual Transition

The step method extends the work of Bender (2001) by allowing a domain of arbitrary depth that contains a depth anomaly with gradual transitions (sloped sidewalls) between regions. Instead of having a "step down" from the upwave direction as in the Bender solution for a pit or a "step up" for the case of a shoal, in the step method a series of steps either up or down, of uniform depth, are connected by a uniform depth region for $r < r_{Ns}$. A sketch of a domain with a stepped pit is shown in Figure 4-3 indicating the location and definition of the velocity potentials and boundaries for a pit with $N_s = 3$.

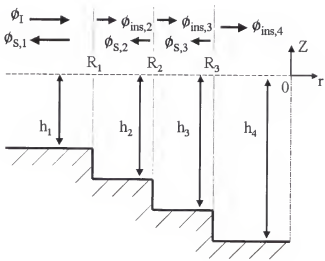

Figure 4-3: Definition sketch for boundaries of gradual depth transitions.

Each region has a specified depth and each interface between regions has a specified r location where the matching conditions must be applied. At each boundary

the matching conditions depend on whether the boundary is a "step up" or a "step down." With the incident wave specified, a set of equations with $2N_sN_e(M+1)$ unknown coefficients is formed.

The solution starts with the definition of an incident velocity potential defined by Eq. 4-17. The scattered velocity potential is defined at each boundary (R_j) and consists of a plane progressive wave and evanescent modes for $(j=1\rightarrow N_s+1)$:

$$\phi_{S,j}(r,\theta,z,t)=\left[\sum_{m=0}^{\infty}A_{j,m}\cos(m\theta)H_{1,m}(k_j,r)\right]\frac{\cosh\left[k_j(h_j+z)\right]}{\cosh(k_jh_j)}e^{-i\omega t}$$

$$+\left\{\sum_{m=1}^{\infty}\left[\sum_{n=1}^{\infty}\alpha_{j,m,n}K_m(\kappa_{j,n}r)\frac{\cos\left[\kappa_{j,n}(h_j+z)\right]}{\cos(\kappa_{j,n}h_j)}\right]\cos(m\theta)\right\}e^{-i\omega t} \qquad (4\text{-}28)$$

Inside the pit the velocity potential is given by the form

$$\phi_{ins,j}(r,\theta,z,t)=\left[\sum_{m=0}^{\infty}B_{j,m}\cos(m\theta)J_m(k_jr)\right]\frac{\cosh\left[k_j(h_j+z)\right]}{\cosh(k_jh_j)}e^{-i\omega t}$$

$$+\left\{\sum_{m=1}^{\infty}\left[\sum_{n=1}^{\infty}\beta_{j,m,n}I_m(\kappa_{j,n}r)\frac{\cos\left[\kappa_{j,n}(h_j+z)\right]}{\cos(\kappa_{j,n}h_j)}\right]\cos(m\theta)\right\}e^{-i\omega t} \qquad (4\text{-}29)$$

The velocity potentials in each region are determined in the following manner;

for $j=1\rightarrow N_s$:

if j = 1;

then $\phi_j=\phi_I+\phi_{S,1}$ and $\phi_{j+1}=\phi_{ins,2}+\phi_{S,2}$

or if j = N_s;

then $\phi_j=\phi_{ins,j}+\phi_{S,j}$ and $\phi_{j+1}=\phi_{ins,j}$

of if $1<j<N_s$;

then $\phi_j=\phi_{ins,j}+\phi_{S,j}$ and $\phi_{j+1}=\phi_{ins,j+1}+\phi_{S,j+1}$

The resulting integral equations are of the form: for $j = 1 \rightarrow N_s$:

if $\left(-h_j > -h_{j+1}\right)$ at r = R_j the depth anomaly is a pit and the boundary is a "step down" and the matching conditions are

$$\int_{-h_j}^{0} \phi_j(R_j,z)\cosh\left[k_j\left(h_j+z\right)\right]dz = \int_{-h_j}^{0} \phi_{j+1}(R_j,z)\cosh\left[k_j\left(h_j+z\right)\right]dz \quad (4\text{-}30)$$

$$\int_{-h_j}^{0} \phi_j(R_j,z)\cos\left[\kappa_{j,n}\left(h_j+z\right)\right]dz = \int_{-h_j}^{0} \phi_{j+1}(R_j,z)\cos\left[\kappa_{j,n}\left(h_j+z\right)\right]dz$$

$$\left(n = 1 \rightarrow N_e\right) \quad (4\text{-}31)$$

$$\int_{-h_j}^{0} \frac{\partial \phi_j}{\partial x}(R_j,z)\cosh\left[k_{j+1}\left(h_{j+1}+z\right)\right]dz = \int_{-h_{j+1}}^{0} \frac{\partial \phi_{j+1}}{\partial x}(R_j,z)\cosh\left[k_{j+1}\left(h_{j+1}+z\right)\right]dz \quad (4\text{-}32)$$

$$\int_{-h_j}^{0} \frac{\partial \phi_j}{\partial x}(R_j,z)\cos\left[\kappa_{j+1,n}\left(h_{j+1}+z\right)\right]dz = \int_{-h_{j+1}}^{0} \frac{\partial \phi_{j+1}}{\partial x}(R_j,z)\cos\left[\kappa_{j+1,n}\left(h_{j+1}+z\right)\right]dz$$

$$\left(n = 1 \rightarrow N_e\right) \quad (4\text{-}33)$$

if $\left(-h_j < -h_{j+1}\right)$ at r = R_j the depth anomaly is a shoal and the boundary is a "step up" and the matching conditions are

$$\int_{-h_{j+1}}^{0} \phi_j(R_j,z)\cosh\left[k_{j+1}\left(h_{j+1}+z\right)\right]dz = \int_{-h_{j+1}}^{0} \phi_{j+1}(R_j,z)\cosh\left[k_{j+1}\left(h_{j+1}+z\right)\right]dz \quad (4\text{-}34)$$

$$\int_{-h_{j+1}}^{0} \phi_j(R_j,z)\cos\left[\kappa_{j+1,n}\left(h_{j+1}+z\right)\right]dz = \int_{-h_{j+1}}^{0} \phi_{j+1}(R_j,z)\cos\left[\kappa_{j+1,n}\left(h_{j+1}+z\right)\right]dz$$

$$\left(n = 1 \rightarrow N_e\right) \quad (4\text{-}35)$$

$$\int_{-h_j}^{0} \frac{\partial \phi_j}{\partial x}(R_j,z)\cosh\left[k_j\left(h_j+z\right)\right]dz = \int_{-h_{j+1}}^{0} \frac{\partial \phi_{j+1}}{\partial x}(R_j,z)\cosh\left[k_j\left(h_j+z\right)\right]dz \quad (4\text{-}36)$$

$$\int_{-h_j}^{0} \frac{\partial \phi_j}{\partial x}(R_j, z)\cos\left[\kappa_{j,n}\left(h_j + z\right)\right] dz = \int_{-h_{j+1}}^{0} \frac{\partial \phi_{j+1}}{\partial x}(R_j, z)\cos\left[\kappa_{j,n}\left(h_j + z\right)\right] dz$$

$$\left(n = 1 \rightarrow N_e\right) \quad (4\text{-}37)$$

At each boundary (R_j) the appropriate evanescent mode contributions from the adjacent boundaries (R_{j-1}, R_{j+1}) must be taken into account. The resulting set of simultaneous equations is solved as a linear matrix equation with the values of M, N_e and N_s large enough to ensure convergence of the solution.

4.3 Exact Shallow Water Solution Method: Formulation and Solution

The exact shallow water solution method solves for the long wave transformation by an axisymmetric pit or shoal that reduces the governing equation to an equation with a known solution. Therefore this method is only valid within the shallow water limit for certain bathymetries containing a region where the depth is a function of the radius that connects two uniform depth regions.

The governing equation is developed with the continuity equation in cylindrical coordinates:

$$\frac{\partial V_r}{\partial r} + \frac{1}{r} V_r + \frac{1}{r}\frac{\partial V_\theta}{\partial \theta} + \frac{\partial V_z}{\partial z} = 0 \quad (4\text{-}38)$$

Integrating from –h to η, applying the Leibnitz rule, the kinematic free surface and bottom boundary conditions, and then multiplying by the depth to obtain the volume flow, q, results in

$$\frac{\partial \eta}{\partial t} + \frac{\partial q_r}{\partial r} + \frac{q_r}{r} + \frac{1}{r}\frac{\partial q_\theta}{\partial \theta} = 0 \quad (4\text{-}39)$$

The non-viscous equations of motion, averaged over depth and linearized give

$$\frac{\partial q_r}{\partial t} = -gh\frac{\partial \eta}{\partial r} \quad (4\text{-}40)$$

$$\frac{\partial q_\theta}{\partial t} = \frac{-gh}{r}\frac{\partial \eta}{\partial \theta} \tag{4-41}$$

Inserting Eqs. 4-40 and 4-41 into Eq. 4-39 after taking the derivative with time of each gives

$$\frac{\partial^2 \eta}{\partial t^2} - g\frac{\partial}{\partial r}\left(h\frac{\partial \eta}{\partial r}\right) - \frac{gh}{r}\frac{\partial \eta}{\partial r} - \frac{gh}{r^2}\frac{\partial^2 \eta}{\partial \theta^2} = 0 \tag{4-42}$$

The solution is assumed to be of the form

$$\eta(r,\theta,t) = F(r)\cos(m\theta)e^{i\sigma t} \tag{4-43}$$

which, when inserted into Eq. 4-42 results in the governing equation:

$$r^2F''(r) + rF'(r) + \frac{r^2}{h(r)}\frac{dh(r)}{dr}F'(r) + \left(r^2k(r)^2 - m^2\right)F(r) = 0 \tag{4-44}$$

The solution starts by specifying an incident wave form:

$$\phi_I(r,\theta,t) = \left[\sum_{m=0}^{\infty}\gamma_m \cos(m\theta)J_m(k_1 r)\right]e^{-i\omega t} \tag{4-45}$$

which is the shallow water form of Eq. 4-17. The velocity potential of the scattered wave and the wave inside the uniform depth region of the depth anomaly are given by the forms

$$\phi_S(r,\theta,t) = \left[\sum_{m=0}^{\infty}A_m \cos(m\theta)H_{1,m}(k_1 r)\right]e^{-i\omega t} \tag{4-46}$$

$$\phi_{ins}(r,\theta,t) = \left[\sum_{m=0}^{\infty}B_m \cos(m\theta)J_m(k_2 r)\right]e^{-i\omega t} \tag{4-47}$$

A definition sketch for the boundaries of the exact solution method is shown in Figure 4-4. As in the step method, matching conditions are used at the interface between different regions.

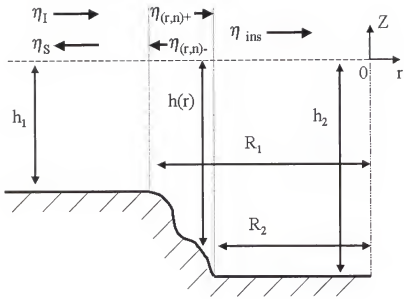

Figure 4-4: Definition sketch for boundaries of exact shallow water solution method.

The matching conditions ensure continuity of the water surface, η:

$$\eta_j = \eta_{j+1} \qquad (r = R_j),\ (j = 1 \to 2) \tag{4-48}$$

and continuity of the gradient of the water surface (equivalent to continuity of discharge):

$$\frac{\partial \eta_j}{\partial r_j} = \frac{\partial \eta_{j+1}}{\partial r_j} \qquad (r = R_j),\ (j = 1 \to 2) \tag{4-49}$$

where $\eta = \left.\frac{1}{g}\frac{\partial \phi}{\partial t}\right|_{z=0}$.

In order for Eq. 4-7 to be solved exactly, only specific bathymetries must be defined. Table 4-1 contains two bathymetries, one pit and one shoal, which solve the governing equation exactly. The resulting set of simultaneous equations is solved as a linear matrix equation with the number of Bessel function modes included, m, large enough to ensure convergence of the solution.

Table 4-1: Specifications for two bathymetries for exact shallow water solution method

h(r)	C	r_1 [m]	r_2 [m]	Solution ~ η(r,n)±	ξ	ζ
C/r (pit)	10	10	5	$\frac{\alpha(r,m)}{\sqrt{r}} \bullet \left[J(\xi,\zeta) \pm iY(\xi,\zeta)\right]$	$\sqrt{1+4m^2}$	$\frac{4\pi}{T}\sqrt{\frac{r}{gC}}$
C*r (shoal)	0.2	10	5	$\alpha(r,m) \bullet \sqrt{r} \bullet \left[J(\xi,\zeta) \pm iY(\xi,\zeta)\right]$	$\frac{\sqrt{1+4m^2}}{3}$	$\frac{4\pi}{3T}\sqrt{\frac{1}{gC}}r^{1.5}$

CHAPTER 5
2-DIMENSIONAL MODEL RESULTS AND COMPARISONS

5.1 Introduction

The step method was used to study wave transformation by 2-D trenches and shoals in arbitrary water depth with the Analytic 2-D Step Model ("2-D Step Model"). The focus of the study was trenches or shoals with sloped transitions, which for the step method was performed by approximating a slope as a series of steps of equal size. The focus of the 2-D results, as there is no variation in the longshore, is the energy reflection caused by the trench or shoal versus a dimensionless wave parameter.

For shallow water conditions the results of the step method were compared to the results of the slope method and the numerical method, which are long-wave models. The step method is also compared with the numerical model FUNWAVE 1.0 [1-D] (Kirby et al., 1998) with reasonable agreement for the cases presented.

5.2 Matching Condition Evaluation

Solution of the governing equations for the step method requires that the matching conditions for the pressure and the horizontal velocity, Eqs. 3-8 and 3-9, be satisfied over the depth, z, at each boundary between regions. For a bathymetric anomaly of infinite length with abrupt transitions the matching conditions are applied at the boundaries between the uniform depth region upwave and downwave of the anomaly and the uniform depth region that is the anomaly.

The matching conditions at the upwave boundary ($x = X_1$) for the case of a trench with abrupt transitions are shown in Figures 5-1 and 5-2. The trench, indicated in the inset diagram in each figure, has a width of 30 m with uniform depths outside and inside the trench of 2 m and 4 m, respectively, and a incident wave period of 12 s. Figure 5-1 plots the magnitudes of the horizontal velocity and the velocity potential with depth for two locations slightly inside and outside of the trench for 16 evanescent modes. The velocity potential can be used for the continuity of pressure condition as they have equivalent forms with depth.

The magnitude of the horizontal velocity shows good agreement between the solutions inside and outside the trench with zero velocity inside the trench along the vertical transition in depth ($z < -2$ m); where zero velocity is required. The oscillations in the values with depth arise from the inclusion of the evanescent modes in the solutions with more evanescent modes resulting in more oscillations with depth. The divergence in the velocities at $z = -2$ m can be explained by Gibb's phenomena when a Fourier series is used to approximate the behavior near the boundary. The magnitude of the velocity potentials inside and outside the trench shows good agreement with no requirement for the velocity potential to be zero for $z < -2$ m.

Plots of the phase with depth for the horizontal velocity and the velocity potential are shown in Figure 5-2. For $z > -2$ good agreement is shown for the solutions inside and outside the trench for both horizontal velocity and the velocity potential. The results of Figures 5-1 and 5-2 indicate that the matching conditions in the 2-D Step Model are met for this case and the Eqs. 3-14 through 3-17 correctly characterize the problem of an infinite trench with abrupt transitions in depth.

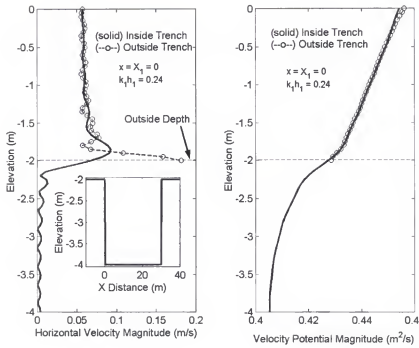

Figure 5-1: Matching conditions with depth for magnitude of the horizontal velocity and velocity potential for trench with abrupt transitions and 16 evanescent modes.

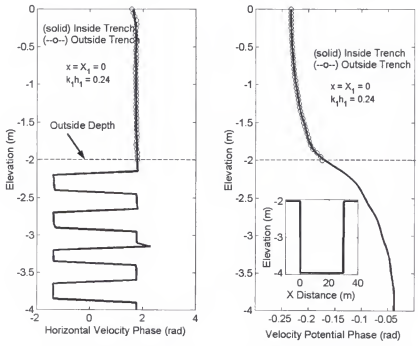

Figure 5-2: Matching conditions with depth for phase of the horizontal velocity and velocity potential for trench with abrupt transitions and 16 evanescent modes.

5.3 Wave Transformation

The wave transformation caused by a two-dimensional (infinitely long) bathymetric anomaly is usually shown through reflection and transmission coefficients as they are straightforward to calculate and can be plotted versus the wavelength thereby presenting values for many incident wave conditions. The reflection and transmission coefficients are calculated using the reflected and transmitted wave heights along with the specified incident wave conditions and Eqs. 3-10 and 3.11. The reflected and transmitted wave heights for a single wave period can be shown in a plot of the relative amplitude along a transect taken across the anomaly. Figure 5-3 shows the relative amplitude for a transect taken across the anomaly with the incident wave traveling in the positive X direction. The trench bathymetry is shown in the inset diagram with 10 steps approximating a transition slope of 0.1.

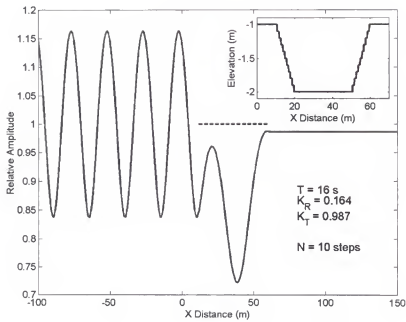

Figure 5-3: Relative amplitude for cross-trench transect for $k_1h_1 = 0.13$; trench bathymetry included with slope = 0.1.

Upwave of the trench a standing wave pattern comprised of the incident and reflected waves is observed; however, downwave of the trench only the transmitted wave is found. With the incident wave specified, the reflected and transmitted wave heights can be determined and the reflection coefficient ($K_R = 0.164$) and transmission coefficient ($K_T = 0.987$) can be calculated. Inside the trench, indicated by the dotted line in the main plot, the waveform must adjust to the new depth and therefore wave properties, causing the reflection from the trench.

The wave transformation caused by a shoal of infinite length for an incident wave period of 16 s is shown in Figure 5-4 with the inset diagram indicating the shoal bathymetry (slope = 0.05). As in the previous figure the dashed line in the main figure indicates the extent of the shoal and the "adjustment" of the waveform is shown. For this case the reflection and transmission coefficients are 0.115 and 0.993, respectively.

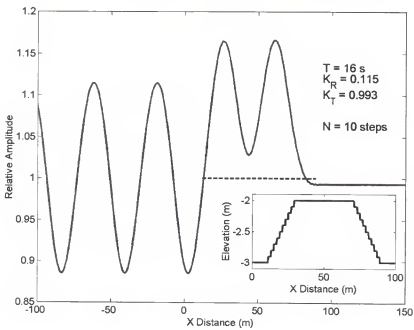

Figure 5-4: Relative amplitude for cross-shoal transect for $k_1h_1 = 0.22$; shoal bathymetry included with slope = 0.05.

5.3.1 Comparison of 2-D Step Model to Numerical Model FUNWAVE 1.0

To provide some verification for 2-D Step Model, a comparison can be made to the numerical model FUNWAVE 1.0 [1-D] (Kirby et al., 1998), which has shown good agreement with laboratory data (Kirby et al., 1998). FUNWAVE 1-D is based on the fully nonlinear Boussinesq model of Wei et al. (1995). The relative amplitude along a cross-trench transect is shown in Figure 5-5 for the 2-D Step Model and for FUNWAVE 1-D with wave heights of 0.2, 0.1 and 0.05 m and a wave period of 12 s. The trench bathymetry is indicated in the inset diagram with 10 steps approximating a transition slope of 0.1 for the 2-D Step Model. In FUNWAVE 1-D a space step of 1 m was used with a time step of 0.1 s. For the FUNWAVE 1-D results the relative amplitude was calculated using $\mathrm{Re}lAmp = \frac{H(x)}{H_I}$ where $H(x) = 2\sqrt{2}\sigma[\eta(x,t)]$ with σ equal to the standard deviation, η(x,t) equal to the water surface time series, and H_I equal to the incident wave height. To ensure that reflection from the end walls was not encountered the time steps used in the relative amplitude calculation were from 1500 to 2220 with a basin length of 900 m and 10001 total time steps.

The relative amplitude values from the 2-D Step Model agree with those of FUNWAVE 1-D with better agreement as wave height in FUNWAVE 1-D is reduced and the waves become more linear. For an incident wave height of 0.05 m the FUNWAVE 1-D results and the 2-D Step Model results nearly match at the crests and troughs of the standing wave in the upwave region and also in the downwave region. The maximum Ursell parameter $\left(U_r = \frac{HL^2}{h^3}\right)$, which is a measure of the wave nonlinearity, in the domain occurs outside the trench and is 74.2 and 19.6 for incident wave heights of 0.2

and 0.05 m, respectively. One measure of the wave nonlinearity is to ensure that second order Stokes wave expansion is valid with the limit $U_r < \frac{8\pi^2}{3}$.

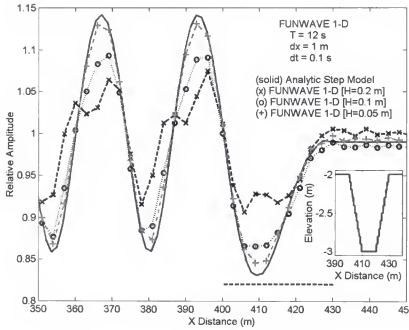

Figure 5-5: Relative amplitude along cross-trench transect for Analytic Model and FUNWAVE 1-D for $k_1h_1 = 0.24$; trench bathymetry included with slope = 0.1.

The relative amplitudes for an asymmetric shoal are shown in Figure 5-6 for the 2-D Step Model and for FUNWAVE 1-D with heights of 0.2, 0.1 and 0.05 m. The shoal has 10 steps approximating an upwave transition slope of 0.2 and a downwave transition slope of 0.05, with the waves incident from left to right. As in the previous diagram a period of 12 s was used with a space step of 1 m and a time step of 0.1 s in FUNWAVE 1-D with the relative amplitude calculations from time step 1500 to 2220.

The relative amplitude values from the 2-D Step Model and FUNWAVE 1-D compare well with much better agreement in the values as the wave height in FUNWAVE 1-D is reduced and the waves become more linear. For an incident wave

height of 0.05 m the FUNWAVE 1-D results and the 2-D Step Model results nearly match at the crests and troughs of the standing wave in the upwave region and also in the downwave region with FUNWAVE 1-D indicating somewhat larger values over the shoal. The maximum Ursell parameter in the domain occurs over the shoal and is 327.5 and 85.4 for incident wave heights of 0.2 and 0.05 m, respectively. The maximum U_r value outside of the shoal is 72.8 and 20.1 for wave heights of 0.2 and 0.05 m, respectively. These results of the last two figures indicate the two-dimensional 2-D Step Model can adequately represent a symmetric or asymmetric bathymetric anomaly.

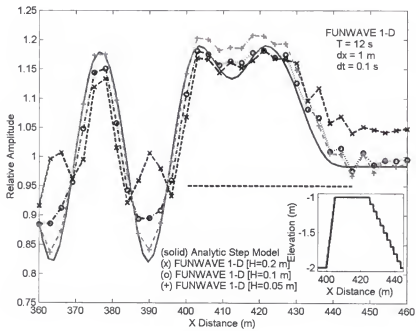

Figure 5-6: Relative amplitude along cross-shoal transect for Analytic Model and FUNWAVE 1-D for $k_1h_1 = 0.24$; shoal bathymetry included with upwave slope of 0.2 and downwave slope of 0.05.

5.4 Energy Reflection

5.4.1 Comparison to Previous Results

A comparison to results from Kirby and Dalrymple (1983a) was made to verify the step method (Figures 5-7 and 5-8). In these figures the magnitudes (i.e. the phases

are not reported) of the reflection coefficient, K_R, and magnitudes of the transmission coefficient, K_T, are plotted versus the dimensionless wave number, k_1h_1, using the step method for the case of a symmetric trench with abrupt transitions and normal wave incidence. Also plotted are the values (shown as "*") of K_r and K_t for three different k_1h_1, values taken from Table 1 in Kirby and Dalrymple (1983a) with good agreement between the results.

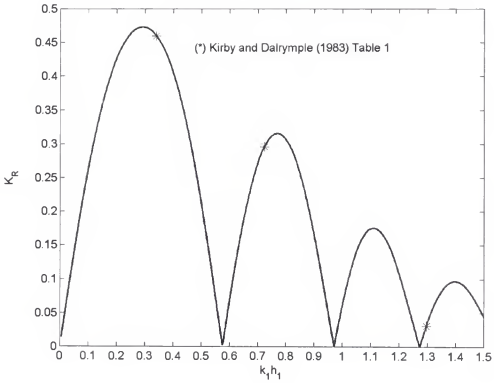

Figure 5-7: Comparison of reflection coefficients from step method and Kirby and Dalrymple (1983a Table 1) for symmetric trench with abrupt transitions and normal wave incidence: $h_3 = h_1$, $h_2/h_1 = 3$, $W/h_1 = 10$.

The results in the figure include 16 evanescent modes, an amount which was found by Kirby and Dalrymple (1983a) to provide adequate convergence for most values of k_1h_1.

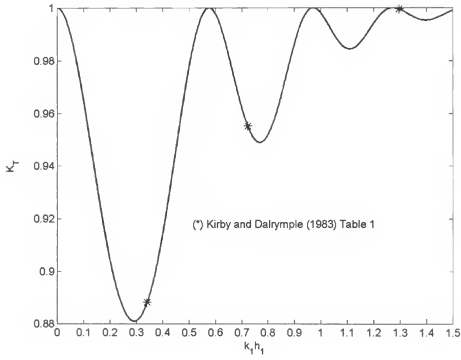

Figure 5-8: Comparison of transmission coefficients from step method and Kirby and Dalrymple (1983a Table 1) for symmetric trench with abrupt transition and normal wave incidence: $h_3 = h_1$, $h_2/h_1 = 3$, $W/h_1 = 10$.

A comparison to the results of Lee et al. (1981) was also carried out. Good agreement was found between the results of the step method and those from Lee et al. for several cases of a trench with abrupt transitions. A direct comparison between the results of the step method and data from the one case in Lee et al. (1981) for a trench with gradual transitions was not made as the complete dimensions of the trench were not specified in the article and could not be obtained.

5.4.2 Arbitrary Water Depth

To study the effects of sloped transitions on the wave transformation, a number of trench and shoal shapes were examined. For the first component of the analysis, the cross-sectional area was kept constant for several different symmetric trench

configurations. The objective was to investigate wave transformation for various slopes with a fixed cross-sectional trench area in a two-dimensional domain.

The first set of trench shapes has the same cross-sectional area and depth with different bottom widths and transition slopes as shown in Figure 5-9. The transition slopes range from an extreme value of 5000 that represents an abrupt transition, to a gradual transition with a slope of 0.1. In this figure of the bathymetry, and those that follow, the still water level is at elevation = 0 m. The trench with the abrupt transitions contains one step while ten equally sized steps approximate the slopes in the other three trenches.

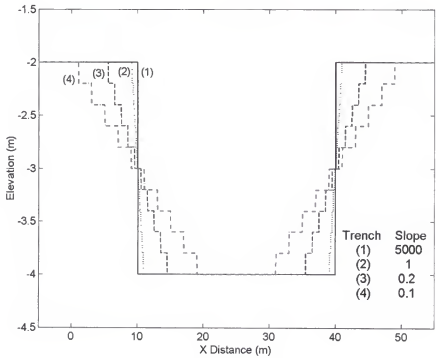

Figure 5-9: Setup for symmetric trenches with same depth and different bottom widths and transition slopes.

The reflection and transmission coefficients versus the dimensionless wave number, k_1h_1, are shown in Figures 5-10 and 5-11, respectively for the trenches with the

same depth. An inset figure of the trench through the centerline is included in each figure with four different line types indicating the corresponding trench configurations. The reflection coefficients oscillate with decreasing peaks as k_1h_1 increases and with k_1h_1 values of complete transmission ($K_R = 0$). Decreasing the transition slope is seen to reduce the reflection caused by the trench, especially at larger values of k_1h_1. As the slope is reduced, the location of the maximum value of K_R is shifted to a smaller k_1h_1 as the apparent width of the trench is increased with decreasing slope, even though the slope does not change the average width. The number of instances where complete transmission occurs is also seen to increase greatly as the slope is made more gradual.

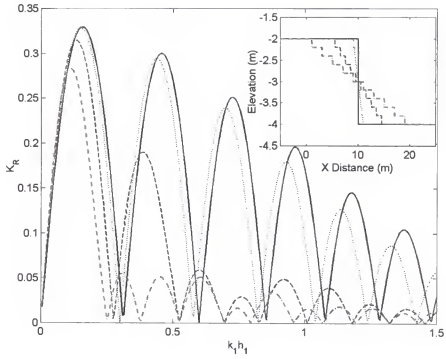

Figure 5-10: Reflection coefficients versus k_1h_1 for trenches with same depth and different bottom widths and transition slopes. Only one-half of the symmetric trench cross-section is shown with slopes of 5000, 1, 0.2 and 0.1.

The plot of the transmission coefficients shows the same features as the reflection coefficients with the effect on the wave field reduced as the slope is decreased. For all

four trench configurations and all values of k_1h_1, conservation of energy requirements were satisfied.

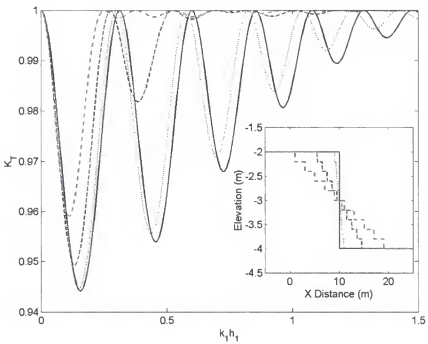

Figure 5-11: Transmission coefficients versus k_1h_1 for trenches with same depth and different bottom widths and transition slopes. Only one-half of the symmetric trench cross-section is shown with slopes of 5000, 1, 0.2 and 0.1.

The results shown in Figures 5-10 and 5-11 are for 16 evanescent modes taken in the summation and trenches with 10 steps approximating the sloped transitions.

The influence of the number of evanescent modes taken in the summation on the reflection coefficient is shown in Figure 5-12 for the same depth trenches with slopes of 5000, 1, and 0.1 at a specified value of k_1h_1. The reflection coefficient is seen to converge to a near constant value with increasing number of evanescent modes. A value of 16 modes is found to produce adequate results and was used for all the step method calculations.

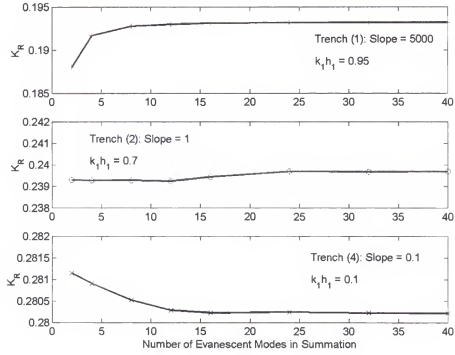

Figure 5-12: Reflection coefficient versus the number of evanescent modes used for trenches with same depth and transition slopes of 5000, 1, and 0.1.

The influence of the number of steps used in the slope approximation is shown in Figure 5-13 for the same depth trench configurations. The reflection coefficient is seen to converge to a steady value with increasing number of steps used for the trenches with slopes of 1 and 0.1; however, for the abrupt transition trench (slope = 5000) convergence with an increasing number of steps was not found. Convergence for the abrupt transition was found as the step number decreased to 1, which represents an almost vertical wall. This could be due to the small distance between points that results when dividing the nearly vertical wall into an increasing number of segments. For this reason the abrupt transition trenches were configured with 1 step, resulting in an almost vertical wall and for all other slopes 10 steps were used. This convention was followed for all the step method calculations.

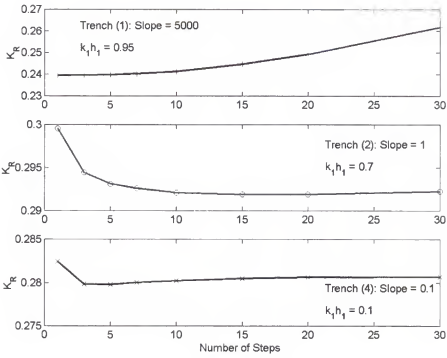

Figure 5-13: Reflection coefficient versus the number of steps for trenches with same depth and transition slopes of 5000, 1, and 0.1.

A second way to maintain a constant cross-sectional area is to fix the bottom width of the trench and allow the trench depth and transition slopes to vary. The reflection coefficients for four trenches developed in this manner with the same bottom width are shown in Figure 5-14. An inset figure is included to show the trench dimensions through the centerline with slopes of 5000, 1, 0.2 and 0.05 being used. For this case, as the slope decreases, the depth of the trench must also decrease to maintain the fixed value of the cross-sectional area. The maximum reflection coefficient is seen to decrease and shift towards a smaller value of k_1h_1 as the slope decreases, due to the associated decrease in the depth of the trench. Generally the depth of the trench determines the magnitude of K_R and the trench width determines the location of the maximum value of K_R.

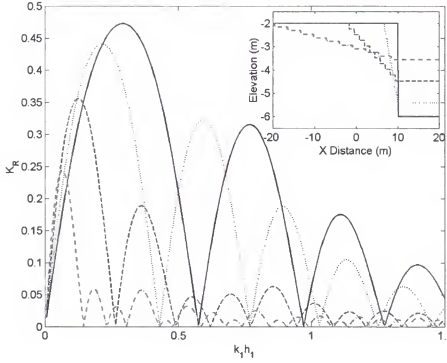

Figure 5-14: Reflection coefficients versus k_1h_1 for trenches with same bottom width and different depths and transition slopes. Only one-half of the symmetric trench cross-section is shown with slopes of 5000, 1, 0.2 and 0.05.

Maintaining the trench cross-sectional area and top width fixed while allowing the transition slopes and depths to change, results in another series of trench configurations. The reflection coefficients for four trenches with the same cross-sectional areas and top width are shown in Figure 5-15. The slopes of the transitions are 5000, 5, 2, and 1. The trench with the smallest slope is found to produce the largest value of K_R due to the large depth associated with that slope; however, the abrupt transition results in the largest K_R values after the first maximum. For this case, decreasing the slope does not shift the locations of the maximum values of K_R as much as in the same depth and same bottom width cases, although no slopes less than one were used as they do not satisfy the constraints of the domain. These three cases have demonstrated that trenches with the

same cross-sectional area can have very different reflective properties depending on the trench configuration.

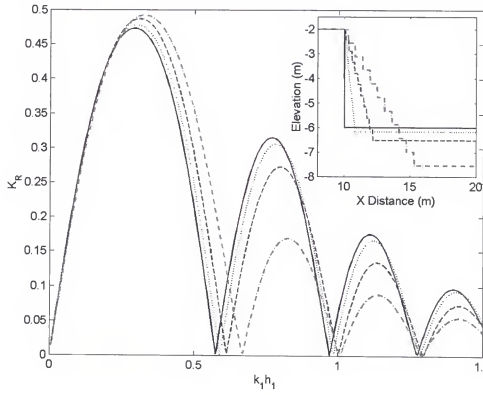

Figure 5-15: Reflection coefficients versus k_1h_1 for trenches with same top width and different depths and transition slopes. Only one-half of the symmetric trench cross-section is shown with slopes of 5000, 5, 2, and 1.

The effect of the transition slope can be viewed in another manner when the cross-sectional area of the trench is not fixed. For a fixed depth and bottom width, decreasing the transition slope results in a trench with a larger cross-sectional area. Plots of the reflection coefficients versus k_1h_1 for four trenches with the same depth and bottom width, but slopes of 5000, 0.2, 0.1, and 0.05 are shown in Figure 5-16. Decreasing the transition slope is seen to reduce K_R, even though the trench cross-sectional area may be much larger.

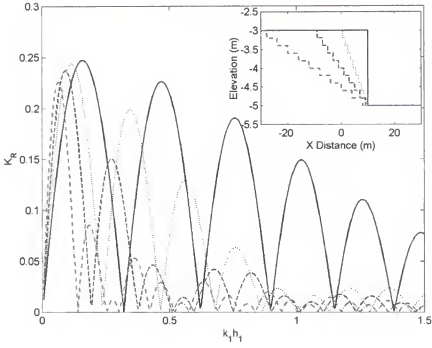

Figure 5-16: Reflection coefficients versus k_1h_1 for trenches with same depth and bottom width and different transition slopes. Only one-half of the symmetric trench cross-section is shown with slopes of 5000, 0.2, 0.1, and 0.05.

The step method is also valid for the case of a submerged shoal with sloped transitions approximated by a series of steps. Figure 5-17 shows the reflection coefficients versus k_1h_1 for four different shoal configurations with transition slopes of 5000, 0.5, 0.2 and 0.05. Decreasing the transition slope is found to reduce the value of K_R as was the case for the trench; however, the reduction in K_R is not as significant for large k_1h_1 as in the trench cases.

A planar transition slope, approximated by a series of uniform steps, was used in the previous cases for the wave transformation caused by symmetric trenches and shoals. In the following cases the wave transformation by depth anomalies with variable transition slopes is investigated. The domain was created by inserting a Gaussian form for the bottom depth into an otherwise uniform depth region.

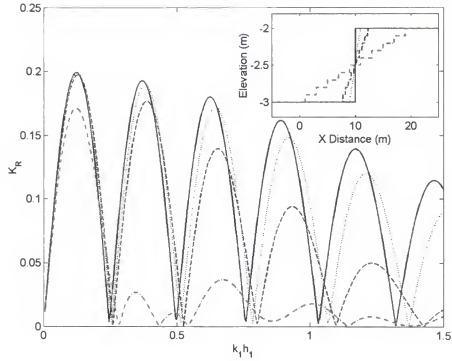

Figure 5-17: Reflection coefficients versus k_1h_1 for shoals with same depth and different top widths and transition slopes. Only one-half of the symmetric shoal cross-section is shown with slopes of 5000, 0.5, 0.2 and 0.05.

The equation for the Gaussian shape centered at x_o was

$$h(x) = h_o + C_1 e^{\frac{(x-x_o)^2}{2C_2^2}} \tag{5-1}$$

where h_o is the water depth in the uniform depth region and C_1 and C_2 are shape parameters with dimensions of length. To implement the step method, steps were placed at a fixed value for the change in depth to approximate the Gaussian shape. Two extra steps were placed near h_o where the slope is very gradual and one extra step was placed near the peak of the "bump" to better simulate the Gaussian form in these regions. The reflection coefficients versus k_1h_1 for a Gaussian trench with C_1 and C_2 equal to 2 m and 12 m, respectively, and a uniform water depth, h_o, equal to 2 m is shown in Figure 5-18. An inset figure is included to show the configuration of the stepped trench and the

form of the Gaussian trench. The Gaussian form is approximated by the step method with a step at every 0.05 m change in depth. The reflection caused by the Gaussian trench is seen to differ considerably from that for the trenches with constant transition slopes shown previously where K_R showed significant oscillations that diminished as k_1h_1 increased, even with gradual transition slopes. The reflection coefficient for the Gaussian trench is seen to have one peak near k_1h_1 equal to 0.1 with minimal reflection for larger values of k_1h_1.

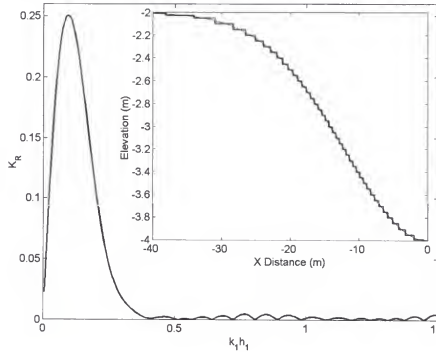

Figure 5-18: Reflection coefficients versus k_1h_1 for Gaussian trench with $C_1 = 2$ m and $C_2 = 12$ m and $h_o = 2$ m. Only one-half of the symmetric trench cross-section is shown with 43 steps approximating the non-planar slope.

The reflection caused by a Gaussian shoal is shown in Figure 5-19 for C_1 and C_2 values of 1 m and 8 m, respectively. The steps approximating the Gaussian form are placed at 0.05 m depth intervals. As for the case of the Gaussian trench, a single peak in K_R occurs followed by minimal reflection at larger values of k_1h_1.

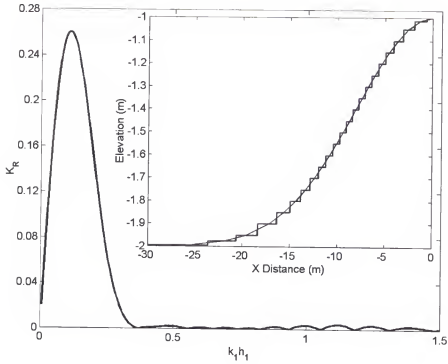

Figure 5-19: Reflection coefficients versus k_1h_1 for Gaussian shoal with $C_1 = 1$ m and $C_2 = 8$ m and $h_o = 2$ m. Only one-half of the symmetric shoal cross-section is shown with 23 steps approximating the non-planar slope.

The trenches considered previously have been symmetric with the upwave and downwave water depths equal and the same slope for the upwave and downwave transitions. Figure 5-20 shows the reflection coefficients versus k_1h_1 for 3 trenches with the same depth upwave and downwave of the trench: a symmetric trench with an abrupt transition, an asymmetric trench with a steep ($s_1 = 1$) upwave transition and gradual ($s_2 = 0.1$) transition and a mirror image of the asymmetric trench with a gradual ($s_1 = 0.1$) upwave transition and steep ($s_2 = 1$) downwave transition. The trench configurations are shown in the inset diagram with dashed and dotted lines. The order of the transition slopes (steep slope first versus gradual slope first) is seen to have no effect on the value of K_R; therefore only one dotted line is plotted in the K_R versus k_1h_1 plot. Stated differently, the direction of the incident wave (positive x direction versus negative x

direction) does not matter for this case. Kreisel (1949) proved this analytically for the case of a trench or shoal, either symmetric or asymmetric, in arbitrary water depth. For the asymmetric trenches with the different transition slopes, complete transmission only occurs at $k_1h_1 = 0$, which is different from the case for the abrupt transitions and the previous cases where s_1 equals s_2.

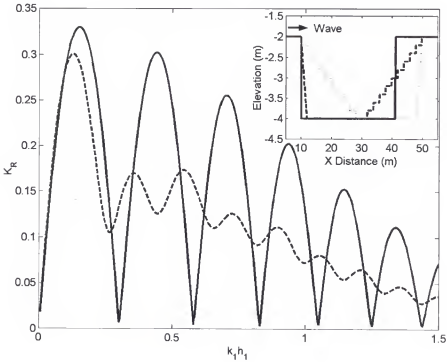

Figure 5-20: Reflection coefficients versus k_1h_1 for a symmetric abrupt transition trench, an asymmetric trench with $s_1 = 1$ and $s_2 = 0.1$ and a mirror image of the asymmetric trench.

Asymmetric trenches can also be studied with different depths upwave and downwave of the trench. Figure 5-21 plots K_R versus k_1h_1 for domains with different depths upwave (h_1) and downwave (h_J) of the trench. The case of an abrupt transition (solid line) with the downwave depth greater than the upwave depth can be compared to the case with transition slopes of 0.2 (dashed line) with the same cross-sectional area. Complete transmission does not occur for either the trench with the abrupt transition or

the trench with sloped transitions. The trench with sloped transitions is found to cause less reflection with an irregular oscillation in K_R with increasing k_1h_1 as compared to the abrupt transition.

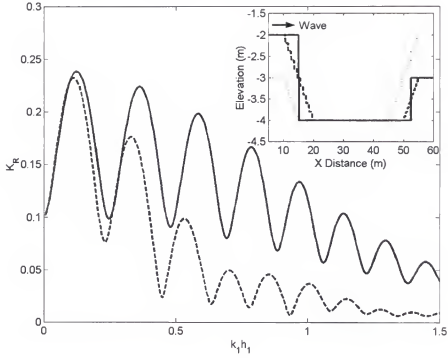

Figure 5-21: Reflection coefficients versus k_1h_1 for an asymmetric abrupt transition trench ($h_1 \neq h_5$), an asymmetric trench with gradual depth transitions ($h_1 \neq h_5$ and $s_1 = s_2 = 0.2$) and a mirror image of the asymmetric trench with $s_1 = s_2$.

For this asymmetric case K_R does not approach zero as k_1h_1 approaches zero as was found when h_1 was equal to h_J, but approaches the long wave value for a single abrupt step (either up or down) of elevation $|h_1 - h_J|$. Also plotted (dotted line) are the results for an asymmetric trench with the depth upwave of the trench greater than the depth downwave of the trench with transition slopes of 0.2, which is a mirror image of the trench shown with the dashed line. The reflection coefficients for this case are identical in magnitude to (but differ in phase from) the mirror image trench if K_R is plotted versus the shallower constant depth, k_Jh_J; therefore only one dashed line for K_R is

plotted. This result is another case of the incident wave direction not affecting the magnitude of the reflection coefficients for an asymmetric trench as shown in Figure 5-20.

Another asymmetric trench case is shown in Figure 5-22 where the upwave and downwave depths and transition slopes are different with a larger upwave depth and slope. In this figure two asymmetric trenches with the same cross-sectional area are compared: a trench with an abrupt transition (solid line) and a trench with an upwave transition slope (s_1) equal to 1 and a downwave slope (s_2) of 0.2 (dashed line). The sloped transitions are seen to reduce significantly the value of K_R, especially as k_1h_1 increases.

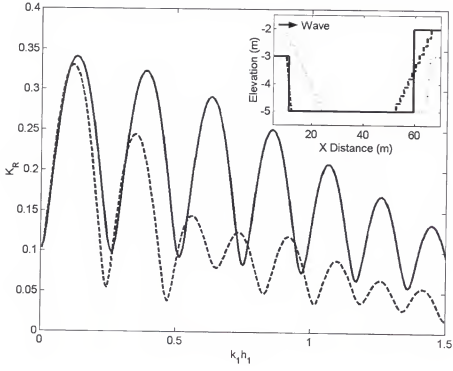

Figure 5-22: Reflection coefficients versus k_1h_1 for an asymmetric abrupt transition trench ($h_1 \neq h_5$), an asymmetric trench with gradual depth transitions ($h_1 \neq h_5$ and $s_1 = 1$ and $s_2 = 0.2$) and a mirror image of the asymmetric trench with $s_1 \neq s_2$.

As shown in the previous figure, K_R does not approach zero as k_1h_1 approaches zero for this case where the upwave and downwave depths are not equal. Also plotted is a mirror image of the asymmetric trench with the sloped transitions (dotted line).Only one dashed line for K_R is plotted, as the reflection coefficients for this case are identical to that for the mirror image trench if K_R is plotted versus the deeper constant depth, k_5h_5. This result is another example of the independence of K_R to the incident wave direction as shown in Figures 5-20 and 5-21 and proven by Kreisel (1949).

5.4.3 Long Waves

Direct comparison of the step method to the slope and numerical methods can only be made in the long wave region. While the slope method and numerical method are limited by the long wave restrictions, it is in this region that changes in bathymetry are most effective at modifying the wave field.

The slope method does not contain any variables that will affect the accuracy of the results such as the number of evanescent modes or the number of steps as in the last section. The numerical method, however, is sensitive to the spacing between points used in the backward space stepping procedure described in Section 4. Figure 5-23 shows the value of K_R versus the step spacing, dx, using the numerical method for three trench configurations at a single value of k_1h_1 for the three of the same depth cases (Figure 5-9) presented earlier. The reflection coefficient is seen to converge for $dx < 1$ m and a value of $dx = 0.5$ m was found to be adequate for the numerical model.

To compare the three solution methods, the same depth trench configurations shown in Figure 5-9 were used. In order to maintain long wave conditions throughout the domain the limit of $k_3h_3 \leq \pi/10$ was taken with the subscript 3 indicating the constant

depth region inside the trench between the transitions. Figure 5-24 shows K_R versus k_3h_3 for the three solution methods for the same depth trench case with a slope of 5000. The slope method and the numerical method are found to yield nearly the same value of K_R at each point with the peak value occurring at a slightly smaller k_3h_3 than for the step method. Overall, the agreement between the three models is found to be very good for this case.

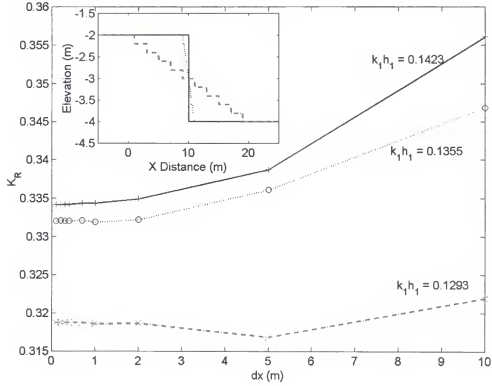

Figure 5-23: Reflection coefficient versus the space step, dx, for trenches with same depth and different bottom width and transition slopes. Only one-half of the symmetric trench cross-section is shown with slopes of 5000, 1 and 0.1.

Figures 5-25 and 5-26 show K_R versus k_3h_3 for a slope of 1 and 0.1, respectively for the same depth trench case with all three models results plotted. Good agreement is found for the results of the three models. In Figure 5-26 the numerical model results match those of the slope method up to the peak value for K_R, but as k_3h_3 increases beyond

the peak the numerical results match those of the step method and the slope method results diverge slightly. The similarity in the results of Figures 5-24 through 5-26 provides reasonable verification for the three solution methods in the shallow water region.

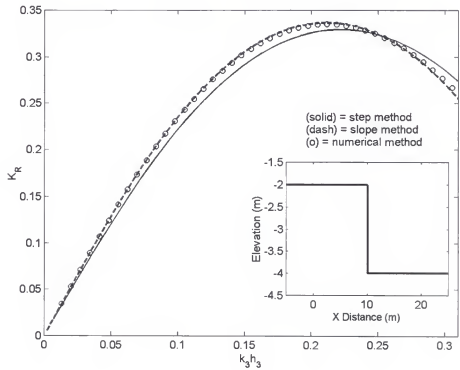

Figure 5-24: Reflection coefficients versus k_3h_3 for three solution methods for the same depth trench case with transition slope equal to 5000. Only one-half of the symmetric trench cross-section is shown.

While the conservation of energy requirement is satisfied exactly in the step method and the slope method, for the cases studied, the numerical method is found to have some variance in the conservation of energy requirement for the space step used in Figures 5-24 through 5-26. Figure 5-27 shows the conservation of energy parameter versus the dimensionless wave number inside the pit, k_3h_3,for the same depth trench with a slope of 1.

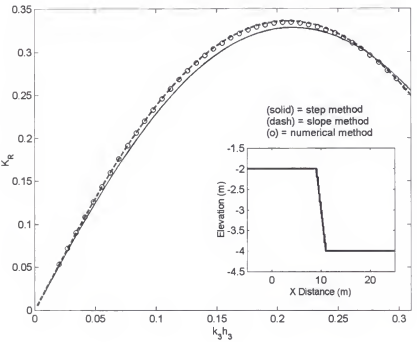

Figure 5-25: Reflection coefficients versus k_3h_3 for three solution methods for same depth trench case with transition slope equal to 1. Only one-half of the symmetric trench cross-section is shown.

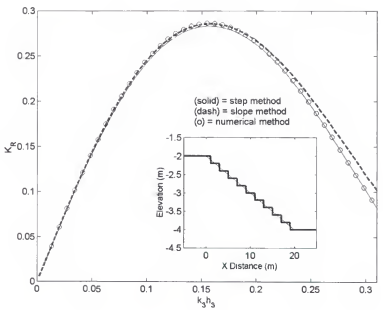

Figure 5-26: Reflection coefficients versus k_3h_3 for three solution methods for same depth trench case with transition slope equal to 0.1. Only one-half of the symmetric trench cross-section is shown.

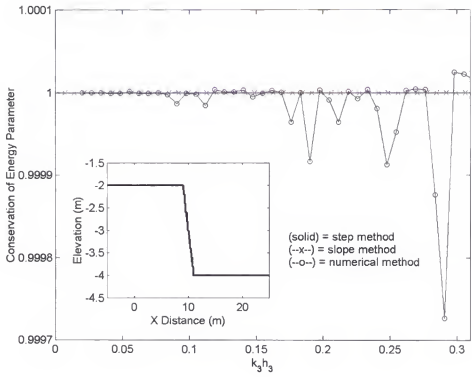

Figure 5-27: Conservation of energy parameter versus k_3h_3 for three solution methods for same depth trench case with transition slope equal to 1. Only one-half of the symmetric trench cross-section is shown.

As noted, the step method and the slope method have values exactly equal to 1, while the numerical method results are equal to one for small k_3h_3 with increasing deviation from one, although very small, as k_3h_3 increases.

Using the step method the reflection coefficients for Gaussian trenches and shoals were shown to have a single peak followed by minimal reflection as k_1h_1 increased. Figure 5-28 shows a comparison of the step method and numerical method results for a shoal with $h_o = 2$ m, $C_1 = 1$ m, and $C_2 = 8$ m. The results for the step method were shown previously in Figure 5-19. The slope method can only contain two slopes and therefore cannot be employed to model a Gaussian form and is not included in the following

comparisons. The numerical results show good agreement with those of the step method with a slight divergence at higher k_1h_1 values near the shallow water limit.

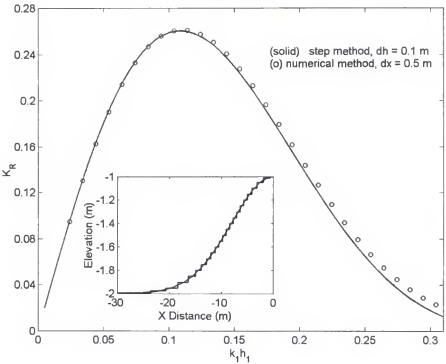

Figure 5-28: Reflection coefficients versus k_1h_1 for step and numerical methods for Gaussian shoal ($h_o = 2$ m, $C_1 = 1$ m, $C_2 = 8$ m). Only one-half of the symmetric shoal cross-section is shown with 23 steps approximating the non-planar slope.

Figure 5-29 is a comparison of the results of the step method and the numerical method for a Gaussian trench in shallow water. The step method has a step for every 0.01 m in elevation and the numerical method has a space step of 0.1 m. The domain is in very shallow water ($h_o = 0.25$ m, $C_1 = 0.2$ m, $C_2 = 3$ m) to extend the numerical method results into the region of minimal reflection following the initial peak in K_R. The numerical method results agree closely to those of the step method and verify the small K_R values of the step method that occur as k_3h_3 increases after the initial peak in K_R.

The case of a trench with unequal upwave and downwave slopes as shown in Figure 5-20 is now compared for the three solution methods. In order to maintain shallow water conditions throughout the domain a limit of $k_3h_3 \leq \pi/10$ was set for the slope and numerical methods. Figure 5-30 shows the value of K_R versus k_3h_3 for the same depth trench with an abrupt transition (solid line) and for s_1 and s_2 equal to 1 and 0.1, respectively. The bottom width for all three cases was maintained the same. The slope and numerical method results show good agreement with the step method solution for both cases. Due to the location of the shallow water limit, the increase of K_R for the step method at k_3h_3 equal to 0.4 cannot be verified directly.

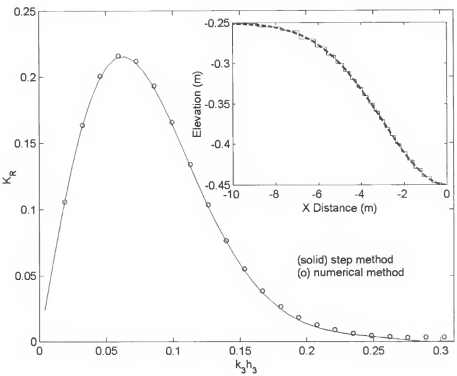

Figure 5-29: Reflection coefficients versus k_3h_3 for step and numerical methods for Gaussian trench in shallow water ($h_o = 0.25$ m, $C_1 = 0.2$ m, $C_2 = 3$ m). Only one-half of the symmetric trench cross-section is shown with 23 steps approximating the non-planar slope.

The case of an asymmetric trench with unequal upwave and downwave slopes and depths as shown in Figure 5-22 is now compared for the three solution methods. For the slope and numerical methods a limit of $k_3h_3 \leq \pi/10$ was taken to maintain shallow water conditions.

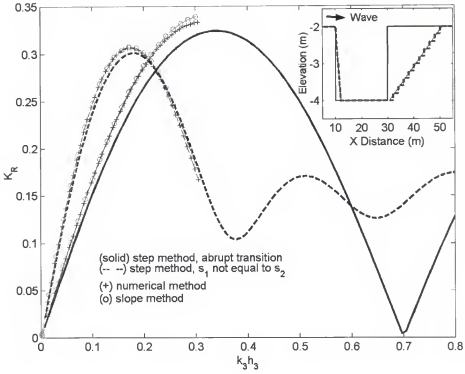

Figure 5-30: Reflection coefficients versus k_3h_3 for three solution methods for same depth trench case with symmetric abrupt transition trench and asymmetric trench with unequal transition slopes equal to 1 and 0.1.

Figure 5-31 shows the value of K_R versus k_3h_3 for an asymmetric trench with an abrupt transition (solid line) and s_1 and s_2 equal to 1 and 0.2, respectively (dash line). The bottom width was changed to maintain a constant cross-sectional area. The slope and numerical method results show good agreement with the step method solution for both cases with less divergence in the K_R values at larger k_3h_3 for the sloped transition trench.

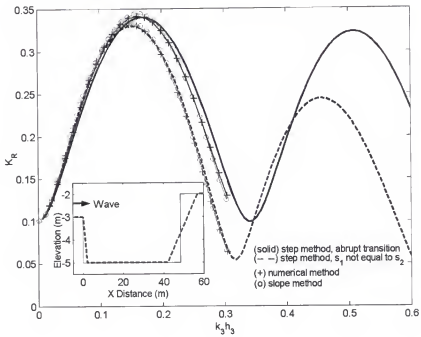

Figure 5-31: Reflection coefficients versus k_3h_3 for three solution methods for same depth trench case with asymmetric abrupt transition trench and asymmetric trench with unequal transition slopes equal to 1 and 0.2.

CHAPTER 6
3-DIMENSIONAL MODEL RESULTS AND COMPARISONS

6.1 Introduction

Solution of the three-dimensional models establishes the complex velocity potential anywhere in the fluid domain. From the complex velocity potential the wave height, wave angle and energy flux can be determined and used to show the wave field modification and energy reflection caused by a bathymetric anomaly. Using the Analytic 3-D Step Model ("3-D Step Model") the effect of the depth transition slope on the wave field modification was investigated. The wave field modification is indicated by changes in the wave height and wave direction. The effect of the transition slope on the energy reflected by a 3-D bathymetric anomaly is approximated using a far-field method developed in the study.

To extend the 3-D Step Model to the nearshore region where the depth is non-uniform, an analytic shoaling and refraction method was developed to determine the breaking wave height and angle for arbitrary nearshore slopes. Estimates of the longshore transport and shoreline change are made by combining the 3-D Step Model, the analytic shoaling and refraction model and the shoreline change model. The shoreline change model uses the conservation of sand (continuity) equation with the breaking wave height and angle from the nearshore model driving the longshore transport.

Comparisons between the 3-D Step Model and the exact analytic model were made in shallow water conditions for two bathymetries. The 3-D Step Model is also

validated through comparison with the laboratory data of Chawla and Kirby (1996), the numerical models REF/DIF-1 (Kirby and Dalrymple, 1994) and FUNWAVE 1.0 [2-D] (Kirby et al., 1998) and the numerical model of Kennedy et al. (2000) for arbitrary depth conditions.

6.2 Matching Condition Evaluation

Solution of the governing equations for the step method requires the matching conditions for the pressure and the horizontal velocity, Eqs. 4-14 and 4-15, to be satisfied over the depth, z, at each boundary between regions. For a bathymetric anomaly with abrupt transitions the matching conditions are applied at the boundary between the uniform depth region outside the anomaly and the uniform depth region that is the anomaly.

The matching conditions for the case of a pit with abrupt transitions are shown in Figures 6-1 and 6-2. The pit has a radius of 20 m with uniform depths outside and inside the pit of 2 m and 4 m, respectively, and an incident wave period of 12 s. Figure 6-1 plots the magnitude of the horizontal velocity and the velocity potential with depth for two locations slightly inside and outside of the pit for 10 evanescent modes. The velocity potential can be used for the continuity of pressure condition as they have equivalent forms with depth. The magnitude of the horizontal velocity shows good agreement between the solutions inside and outside the pit. The requirement of zero velocity inside the pit along the vertical transition in depth ($z < -2$ m) is met to good approximation. The oscillations in the values with depth arise from the inclusion of the evanescent modes with the divergence in the velocities at $z = -2$ m explained by Gibb's phenomena. The magnitude of the velocity potentials inside and outside the pit shows reasonable agreement with no requirement for the velocity potential to be zero for $z < -2$ m.

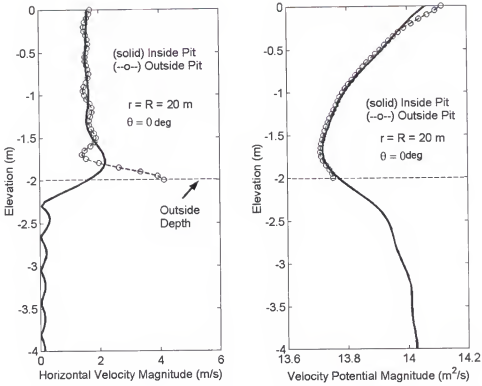

Figure 6-1: Matching conditions with depth for magnitude of the horizontal velocity and velocity potential for pit with abrupt transitions and 10 evanescent modes.

Figure 6-2 plots the phase with depth for the horizontal velocity and the velocity potential with good agreement for $z > -2$. The results of Figures 6-1 and 6-2 indicate that the matching conditions in the 3-D Step Model are met for this case and Eqs. 4-20 through 4-23 correctly characterize the problem of a bathymetric anomaly in the form of a pit with abrupt transitions in depth.

6.3 Wave Height Modification

Using the 3-D Step Model, a wave field that encounters a bathymetric anomaly will be modified by the three wave transformation processes identified earlier. In a three-dimensional domain the modified wave field can be viewed as a contour plot of the relative amplitude for the wave envelope where the modified wave field is normalized by

the incident wave height. Figure 6-3 shows a contour plot of the relative amplitude for a circular pit with sloped sidewalls (truncated cone). In this figure and all that follow the incident waves propagate from left to right. A cross section of the pit taken through the centerline is shown in the inset diagram for one-half of the pit and a transition slope of 0.1 where 10 equally sized steps approximate the slope. The divergence of the wave field caused by the pit is shown clearly in Figure 6-3 with a large area of wave sheltering evident directly shoreward of the pit. This area is flanked by two bands of relative amplitude greater than one caused as the waves converge or focus at these locations. The relative amplitude values are found to be symmetric about Y = 0.

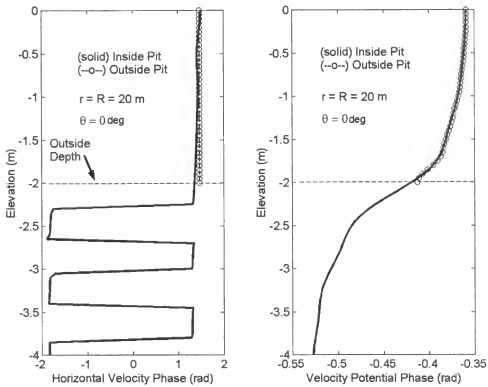

Figure 6-2: Matching conditions with depth for phase of the horizontal velocity and velocity potential for pit with abrupt transitions and 10 evanescent modes.

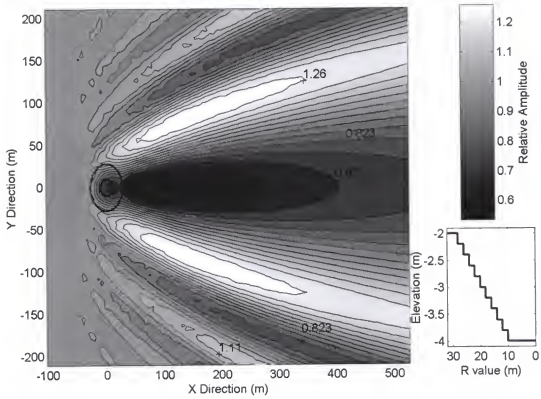

Figure 6-3: Contour plot of relative amplitude with $k_1h_1 = 0.24$ for pit with transition slope = 0.1; cross-section of pit bathymetry through centerline included.

The wave field modification can be viewed in another way by taking transects in the cross-shore and longshore directions. Figures 6-4 and 6-5 show the relative amplitude along transects taken in the cross-shore direction at Y = 0 and in the longshore direction at X = 300 m, respectively. In each figure a cross-section of the pit taken through the centerline is included in an inset diagram and the extent of the pit shown by the dotted line in the main plot. The cross-shore transect of the relative amplitude highlights the sheltering caused by pit with the sheltering effect diminishing with distance shoreward of the pit. A partial standing wave pattern is evident in the upwave direction indicating the reflection caused by the pit.

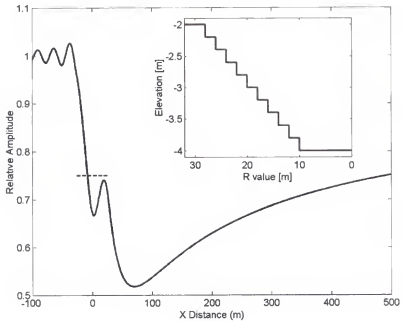

Figure 6-4: Relative amplitude for cross-shore transect at Y = 0 with $k_1h_1 = 0.24$ for pit with transition slope = 0.1; cross-section of pit bathymetry through centerline included. Note small reflection.

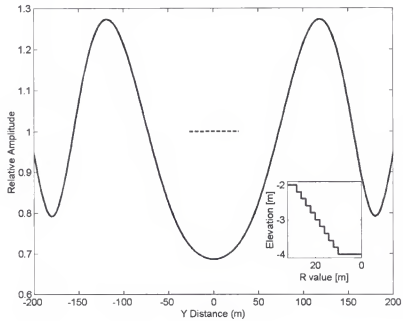

Figure 6-5: Relative amplitude for longshore transect at X = 300 m with $k_1h_1 = 0.24$ for pit with transition slope = 0.1; cross-section of pit bathymetry through centerline included.

The longshore transect (Figure 6-5) shows sheltering directly shoreward of the pit and oscillations in the relative amplitude that decay with distance in the longshore direction. The oscillations in the longshore direction indicate the refraction and diffraction of the wave field created by the bathymetric anomaly.

In the previous plots of the relative amplitude the number of evanescent modes and Bessel function modes were 4 and 120, respectively, with these values providing reasonable convergence of the solution. In the 3-D Step Model the convergence of the solution depends on three parameters: the number of evanescent modes included, the number of Bessel function modes included and the number of steps approximating the transition in depth. The convergence of the solution with respect to the number of Bessel functions modes included was found to depend on the distance from the center of the bathymetric anomaly and its radius; a dependency that was not found for the number of evanescent modes and the number of steps.

The influence of the number of evanescent (N_e) and Bessel function (Mval) modes on the solution is shown in Figure 6-6 for case of a circular pit with a radius of 20 m and abrupt transitions in depth. Abrupt transitions were used to remove the influence of the number of steps approximating the transition slope. The uniform water depth outside the pit, h, is 2 m, and the uniform depth in the center of the pit, d, is 4 m as before. To illustrate the dependence of the solution on distance from the center of the pit two plots are shown; one for a point located 100 m shoreward of the pit center and one for a point located 800 m shoreward. The plots indicate convergence of the relative amplitude value with increasing number of evanescent modes and increasing number of Bessel function modes. For both locations using 4 evanescent modes was found to

provide adequate convergence. The point located at X = 100 m was found to require between 30 and 50 Bessel function modes for convergence of the solution while the point located at X = 800 m required between 120 and 140 modes. This indicates that for convergence of the solution the number of Bessel function terms must be increased as distance from the bathymetric anomaly increases.

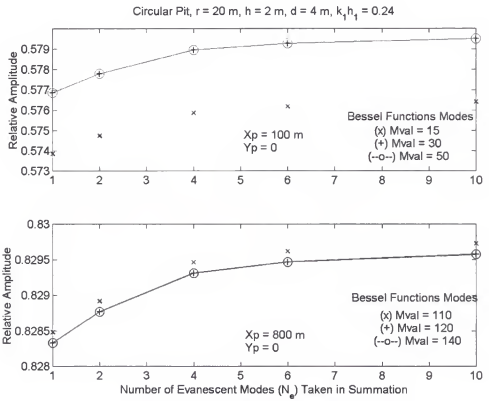

Figure 6-6: Relative amplitude versus number of evanescent modes included for different Bessel function summations at two locations directly shoreward of a pit with abrupt transitions in depth.

The influence of the number of steps, N_s, approximating a linear, gradual transition in depth is shown in Figure 6-7. Two plots are included in the figure for circular pits with transitions slopes of 1 and 0.1, respectively. The uniform water depth outside the pit, h, is 2 m, and the uniform depth in the center of the pit, d, is 4 m. The relative amplitudes are taken at a point located 400 m shoreward from the first step used

to approximate the gradual transition in depth. For both pits the solution converges as the number of steps approximating the slope increases, with 10 steps providing adequate convergence. The number of Bessel function modes needed to ensure converge is between 60 and 90 for both pit configurations. With these results the base conditions for the 3-D Step Model were 4 evanescent modes, 10 steps approximating the linear depth transitions and 90 or 120 Bessel function modes depending on the distance from the anomaly.

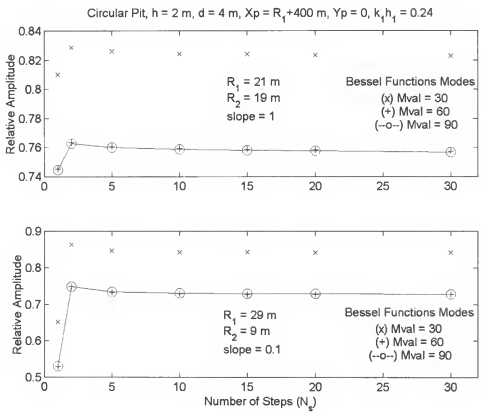

Figure 6-7: Relative amplitude versus number of steps approximating slope for different Bessel function summations for two pits with gradual transitions in depth.

The wave field modification caused by a shoal can also be studied using the 3-D Step Model. A contour plot of the relative amplitude for a domain containing a shoal in the form of a truncated cone with a transition slope equal to 0.1 is shown in Figure 6-8.

The shoal causes an area of wave focusing, and a resulting increase in relative amplitude directly shoreward of the shoal. Two areas with relative amplitude less than one flank this area of increased relative amplitude. These results demonstrate the difference in the wave field modification caused by a shoal versus a pit (Figure 6-3) with shoals causing wave sheltering/focusing where a pit causes focusing/sheltering.

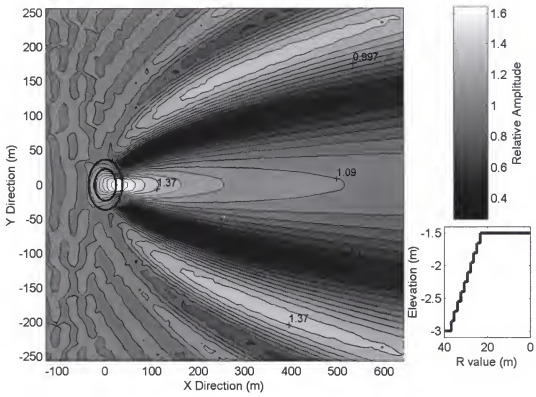

Figure 6-8: Contour plot of relative amplitude for shoal with $k_1h_1 = 0.29$ and transition slope = 0.1; cross-section of shoal bathymetry through centerline included.

A focal point of the current study was to investigate the effect of the transition slope on wave field modification. In an attempt to isolate the effect of the sidewall slope, different truncated cones of constant volume were created. Starting from a pit of uniform depth with abrupt depth transitions (cylinder), three other pits (truncated cones) with the same volume and depth were created by allowing the transition slope to decrease. A

cross-section of these "same depth" pits taken through the centerline is shown in Figure 6-9 where the slopes used were abrupt, 1, 0.2 and 0.07. The main plot shows the relative amplitude along a cross-shore transect through the center of each pit for $k_1h_1 = 0.15$ with the extent of the abrupt pit indicated by the dotted line. Upwave of the pit a more gradual transition slope is seen to reduce the reflection caused by the pit. The sheltering downwave of the pit is seen to increase as the transition slope decreases.

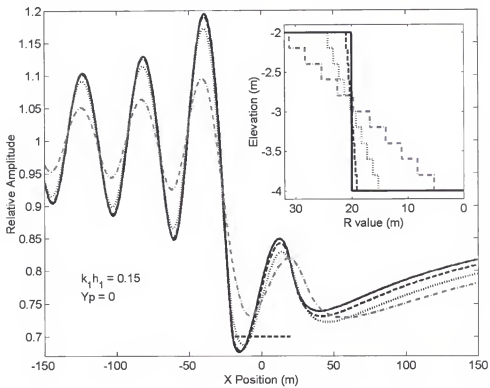

Figure 6-9: Relative amplitude for cross-shore transect at Y = 0 for same depth pits for $k_1h_1 = 0.15$; cross-section of pit bathymetries through centerline included with slopes of abrupt, 1, 0.2 and 0.07.

The wave field modification caused by an incident wave with $k_1h_1 = 0.3$ is shown in Figure 6-10. In this figure the greatest reflection upwave of the pit is associated with transition slopes of 1 and 0.2 with minimal reflection for a slope of 0.07. The effect of the slope on the reflection is different in Figure 6-10 than in Figure 6-9 indicating that the

incident wave characteristics can significantly affect the wave field modification caused by the bathymetric anomaly. This result will be further discussed in Section 6.8. The sheltering caused by all four pit bathymetries is greater for $k_1h_1 = 0.3$ than for $k_1h_1 = 0.15$ with the most gradual slopes having the greatest sheltering effect.

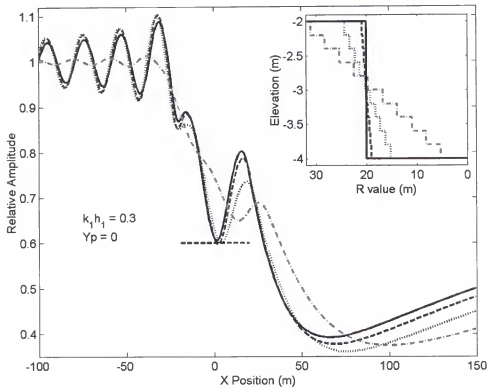

Figure 6-10: Relative amplitude for cross-shore transect at Y = 0 for same depth pits for $k_1h_1 = 0.3$; cross-section of pit bathymetries through centerline included with slopes of abrupt, 1, 0.2 and 0.07.

The effect of the transition slope on the wave field can also be viewed in the longshore direction. Figure 6-11 shows the relative amplitude versus longshore distance for $k_1h_1 = 0.15$ at X = 200 m. Only one-half of the longshore transect is plotted as the results are symmetric about Y = 0. As indicated in Figure 6-9, as the transition slope becomes more gradual the sheltering directly shoreward of the pit increases indicating a greater divergence in the wave field near the pit. The focusing caused by the pit at Y =

120 m is seen to increase as the transition slope decreases, which follows from the more gradual slopes causing a greater divergence in the wave field.

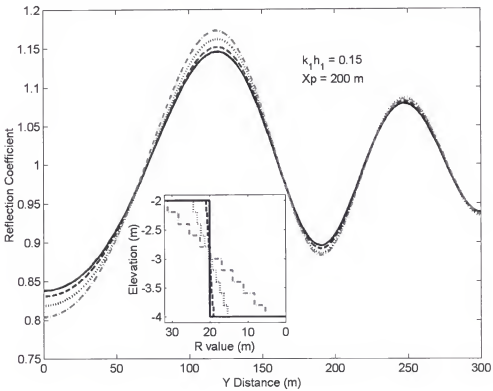

Figure 6-11: Relative amplitude for alongshore transect at X = 200 m for same depth pits for $k_1h_1 = 0.15$; cross-section of pit bathymetries through centerline included with slopes of abrupt, 1, 0.2 and 0.07.

The results from Figure 6-11 can be compared to those of Figure 6-12 which show the relative amplitude in the longshore direction for $k_1h_1 = 0.3$. As shown previously, the more gradual transition slopes result in the greatest sheltering of the waves directly shoreward of the pit with Figure 6-12 indicating more wave sheltering and greater wave focusing than for the case of Figure 6-11.

The effect of the transition slope for the case of a shoal can be viewed in Figures 6-13 and 6-14 in the cross-shore and longshore direction, respectively. A cross-section of the shoal configurations taken through the centerlines is shown in each figure with each

shoal in the form of a truncated cone with constant volume. The slopes for the transitions are abrupt, 1, 0.2 and 0.05. Figure 6-13 shows the relative amplitude for a transect in the cross-shore direction through the center of the shoal for $k_1h_1 = 0.15$ with the extent of the shoal indicated by the dashed line. The features of the contour plot of relative amplitude for a shoal (Figure 6-8) are shown with an increase in the relative amplitude over the shoal and shoreward of the shoal where wave focusing occurs. The shoal with a transition slope of 0.05 is seen to cause less focusing shoreward of the shoal, significantly smaller relative amplitudes over the shoal and a reflected wave that is out of phase, but similar in magnitude to the other transitions slopes.

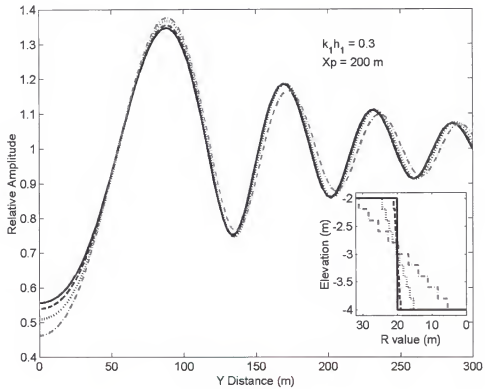

Figure 6-12: Relative amplitude for alongshore transect at X = 200 m for same depth pits for $k_1h_1 = 0.3$; cross-section of pit bathymetries through centerline included with slopes of abrupt, 1, 0.2 and 0.07.

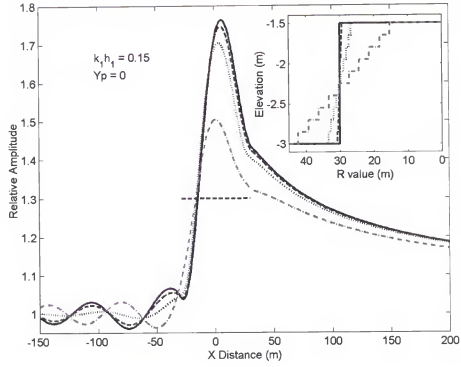

Figure 6-13: Relative amplitude for cross-shore transect located at Y = 0 for same depth shoals with $k_1h_1 = 0.15$; cross-section of shoal bathymetries through centerline included with slopes abrupt, 1, 0.2 and 0.05.

In Figure 6-14 the transition slope is shown to reduce the magnitude in the longshore oscillations of the relative amplitude in the regions of wave focusing. The longshore transect is located at a cross-shore distance of 300 m and only one-half of the longshore transect is plotted as the results are symmetric about Y = 0.

Up to this point all of the transitions in depth have been linear. Nonlinear transitions in depth can also be studied using the step method and provide a more realistic representation of bathymetric anomalies found in nature. In Figure 6-15 a transition slope with a Gaussian form connects two regions of uniform depth. The equation of the Gaussian form centered at x_o was $h(x) = h_o + C_1 e^{\frac{(x-x_o)^2}{2C_2^2}}$ where the shape factors C_1 and C_2 were taken as 1 m and 20 m, respectively.

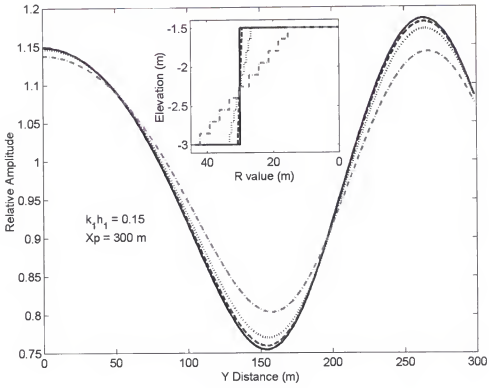

Figure 6-14: Relative amplitude for alongshore transect located at X = 300 m for same depth shoals with $k_1h_1 = 0.15$; cross-section of shoal bathymetries through centerline included abrupt, 1, 0.2 and 0.05.

The Gaussian slope connects the uniform depth region outside the pit to a uniform depth region of radius equal to 20 m at the center of the pit. A cross-section of the pit bathymetry taken through the centerline is shown in an inset diagram with the parameters for the pit. For this example 23 steps approximate the nonlinear slope of the Gaussian transitions in depth. The main plot shows the relative amplitude for a cross-shore transect through the center of the pit for $k_1h_1 = 0.24$. The pit is shown to cause minimal reflection in the upwave direction with significant sheltering at the shoreward extent of the pit and shoreward of the pit.

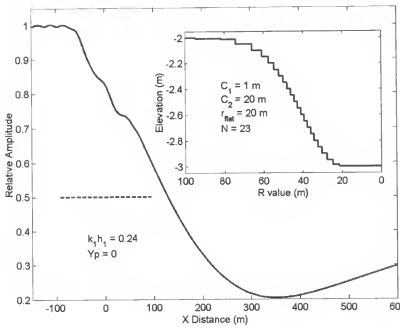

Figure 6-15: Relative amplitude for cross-shore transect at Y = 0 for pit with Gaussian transition slope for $k_1h_1 = 0.24$; cross-section of pit bathymetry through centerline included.

6.3.1 Comparison of 3-D Step Model and Analytic Shallow Water Exact Model

For certain shallow water bathymetries the 3-D Step Model can be compared to the exact shallow water analytic model (exact analytic model) described in Section 4.3. Table 4-1 indicates two bathymetric forms that satisfy the requirements of the exact analytic model. To specify a bathymetry for the exact analytic model the value of C, h_1, h_2, R_1, R_2 and T (wave period) must be selected such that shallow water conditions are maintained.

Figure 6-16 shows the relative amplitude in the cross-shore direction through the center of the pit for the 3-D Step Model ($N_s = 10$ steps) and the exact analytic model. The inset diagram shows a cross-section of the pit bathymetry through the centerline for the dimensions indicated in the figure, which satisfy the exact analytic model for the first case in Table 4-1, h = C/r. Good agreement between the models is indicated in all

regions (upwave, over the pit and downwave) providing verification for the 3-D Step Model in shallow water. A transect in the longshore direction comparing the two models for this bathymetry is shown in Figure 6-17. The transect is located at Xp = 100 m with good agreement between the models indicated in the longshore direction for this case.

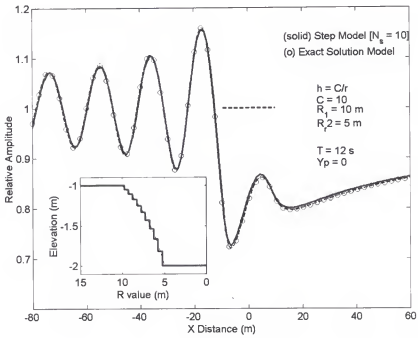

Figure 6-16: Relative amplitude for cross-shore transect at Y = 0 for pit with for h = C/r in region of transition slope; cross-section of pit bathymetry through centerline included.

The 3-D Step Model and the exact analytic model can also be compared for the case of a shoal with Case 2 in Table 1. Figures 6-18 and 6-19 show the relative amplitude in the cross-shore and longshore directions for the case of a shoal that satisfies the requirements of the exact analytic model with h = C*r (linear slope) in the region connecting the two uniform depth regions. In each figure the inset diagram shows a cross-section of the shoal bathymetry through the centerline. In Figure 6-18 good agreement is shown between the models in the upwave region with the exact analytic model indicating slightly less focusing over the shoal and in the downwave region.

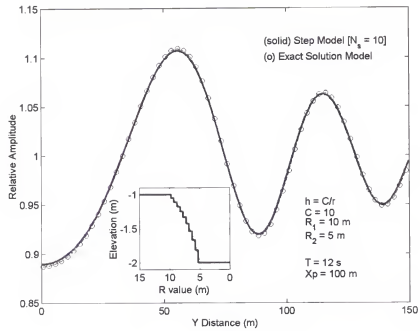

Figure 6-17: Relative amplitude for longshore transect at X = 100 m for pit with for h = C/r in region of transition slope; cross-section of pit bathymetry through centerline included.

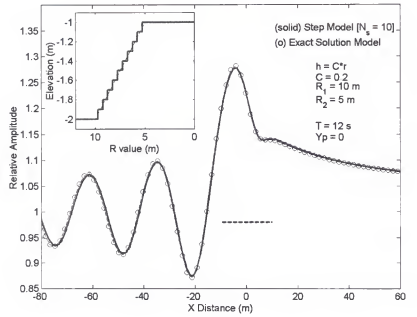

Figure 6-18: Relative amplitude for cross-shore transect at Y = 0 for shoal with for h = C*r in region of transition slope; cross-section of shoal bathymetry through centerline included.

Figure 6-19 shows reasonable agreement between the models with the exact model having smaller oscillation magnitudes in the longshore direction with differences between the results less than 1%.

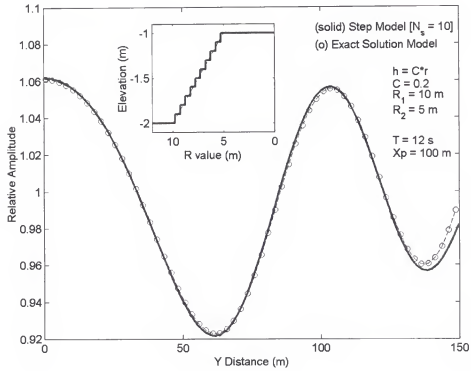

Figure 6-19: Relative amplitude for longshore transect at X = 100 m for shoal with for h = C*r in region of transition slope; cross-section of shoal bathymetry through centerline included.

6.4 Wave Angle Modification

Previous plots of the relative amplitude in a domain with a bathymetric anomaly have demonstrated the divergence and convergence of the wave field near the anomaly due to wave sheltering and focusing, respectively. The divergence and convergence of the wave field can also be viewed by examining the wave angle modification near a bathymetric anomaly. The method for calculating the wave angles is contained in Appendix A.

A contour plot of the wave angle for a pit with a gradual depth transition is shown in Figure 6-20. As in the previous figures the waves are incident from left to right with an incident angle equal to 0 with positive wave angles measured counter clockwise. Leeward of the pit a divergence in the wave field occurs with the waves "spreading out" due to the increase in depth over the pit. The wave angles inside the pit were not calculated due to the complex nature of the solution in this region. The wave directions are anti-symmetric in the longshore direction about the center of pit with oscillations in the wave angle occurring in the longshore indicating the diffraction pattern caused by the pit, as in the relative amplitude results.

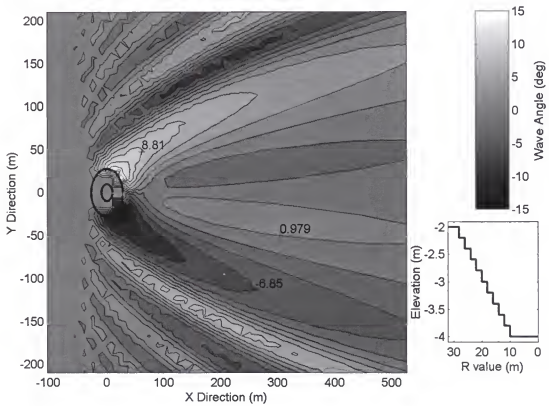

Figure 6-20: Contour plot of wave angles in degrees for pit with $k_1h_1 = 0.24$ and transition slope = 0.1; cross-section of pit bathymetry through centerline included.

The wave angle modification caused by a shoal with a Gaussian transition in depth and a uniform depth inner region is shown in Figure 6-21 with the inset diagram showing the shoal bathymetry. The Gaussian shoal is seen to cause a focusing of the wave field in the lee of the shoal as the waves converge over the decreased depth of the shoal. Although not clearly indicated by the resolution of the contour plot, the results were found to be anti-symmetric in the longshore about the center of the shoal. The shoal is seen to cause less wave field modification than the pit in the previous plot with much smaller wave angles resulting leeward of the shoal.

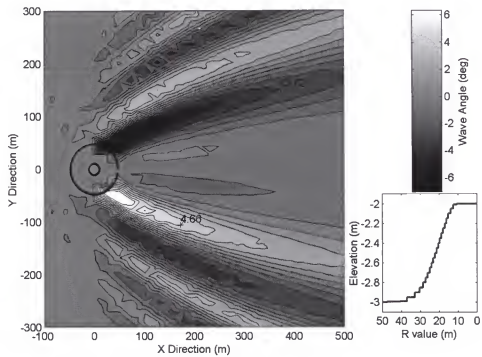

Figure 6-21: Contour plot of wave angles for Gaussian shoal with C_1 =1 and C_2 = 10 for k_1h_1 = 0.22; cross-section of shoal bathymetry through centerline included with 23 steps approximating slope.

The impact of the transition slope on the wave angle was investigated using the constant volume, constant depth pits first shown in Figure 6-9. The wave angle for a longshore transect located 300 m from the center of the pits is shown in Figure 6-22 for

$k_1h_1 = 0.15$. Decreasing the transition slope is seen to increase slightly the magnitude of the wave angle oscillations in the longshore.

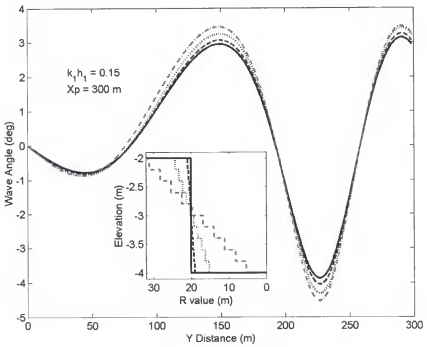

Figure 6-22: Wave angle for alongshore transect at X = 300 m for same depth pits for $k_1h_1 = 0.15$; cross-section of pit bathymetries through centerline included with slopes of abrupt, 1, 0.2 and 0.07. Negative angles indicate divergence of wave rays.

6.5 Comparison of 3-D Step Model to Numerical Models

Three-dimensional numerical models for nearshore wave transformation can be employed to validate the 3-D Step Model for similar bathymetries. As in comparing any models, care must be taken to ensure the models are representing comparable processes and are used within their limits. The widely used numerical model REF/DIF-1 (Kirby and Dalrymple, 1994) and a 2-D fully nonlinear Boussinesq model (Kennedy et al., 2000) were employed to assess the results of the 3-D Step Model for a uniform domain containing a bathymetric anomaly. REF/DIF-1 has been compared to laboratory data from Berkhoff et al. (1982) for a submerged shoal on a sloped, plane beach. Using its

composite nonlinear wave theory REF/DIF-1 was shown to be quite accurate in predicting the wave field. Boussinesq models have shown very good agreement to laboratory data for numerous bathymetries including the Berkhoff et al. (1982) shoal with the results being quite reasonable. Thus, while the 3-D Step Model can only be compared to the laboratory data from a single experiment (Chawla and Kirby, 1996) for the wave field modification by a bathymetric anomaly with gradual transitions in an otherwise uniform domain, comparing the 3-D Step Model to numerical models can provide a certain level of validation for many domains as the numerical models have been compared successfully to laboratory data.

6.5.1 3-D Step Model Versus REF/DIF-1

REF/DIF-1 (Kirby and Dalrymple, 1994) is a parabolic model for monochromatic water waves that is weakly-nonlinear and accounts for wave refraction, diffraction, shoaling, breaking, and bottom friction. REF/DIF-1 assumes a mild bottom slope and has been found to remain accurate for slopes up to 1 on 3 by Booij (1983). REF/DIF-1 was run with no wave energy dissipation and with linear wave theory in order to most closely match the limitations of the 3-D Step Model. One difference between REF/DIF-1 and the 3-D Step Model is that upwave scattering (reflection) caused by a bathymetric anomaly is not handled by REF/DIF-1.

The 3-D Step Model and REF/DIF-1 results for a cross-shore transect of the relative amplitude are shown in Figure 6-23. A cross-section of the bathymetric anomaly used in the 3-D Step Model taken through the centerline for this comparison is shown in the inset diagram where 23 steps approximate the slope. A grid spacing of 5 m was used in the x and y directions for REF/DIF-1, which resulted in a coarser resolution for the anomaly than in the 3-D Step Model. The solid line in the main plot shows the relative

amplitude for the 3-D Step Model and indicates slight reflection upwave of the pit and significant wave sheltering shoreward of the pit that diminishes with distance from the pit. The circles show the REF/DIF-1 results for the case of linear wave theory, and generally shows good agreement with the 3-D Step Model results; however, upwave of the pit the REF/DIF-1 results identically equal 1 as reflection is not considered.

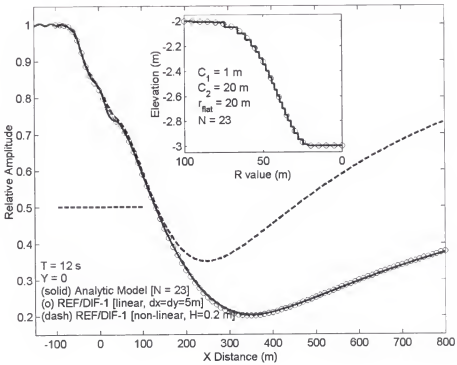

Figure 6-23: Relative amplitude using 3-D Step Model and REF/DIF-1 for cross-shore transect at Y = 0 for Gaussian pit with $k_1 h_1 = 0.24$; cross-section of pit bathymetry through centerline included.

The dashed line indicates results from REF/DIF-1 using composite nonlinear wave theory (Kirby and Dalrymple, 1986) for an incident wave height of 0.2 m. The nonlinear results follow the linear results over the pit and at small (< 50 m) downwave distances. At large downwave distances the nonlinear results diverge significantly from the linear results and indicate much less wave sheltering due to the pit. The nonlinear REF/DIF-1 results were

found to approach the linear results as the wave height was decreased to very small values and the waves become more linear.

The 3-D Step Model and REF/DIF-1 results were also compared for transects in the longshore direction. Figure 6-24 shows the relative amplitude for a longshore transect located at Xp = 100 m. The 3-D Step Model and REF/DIF-1 (linear) results overlay each other for longshore distance less than ±150 m. The REF/DIF-1 (nonlinear) results show good agreement with the models using linear wave theory as the cross-shore location of the transect is not in the region shown in Figure 6-23 where the nonlinear and linear results diverge. At large longshore distances the 3-D Step Model and REF/DIF-1 (linear and nonlinear) results diverge as the minimax wide-angle parabolic approximation (Kirby, 1986) used in REF/DIF-1 is violated at these locations.

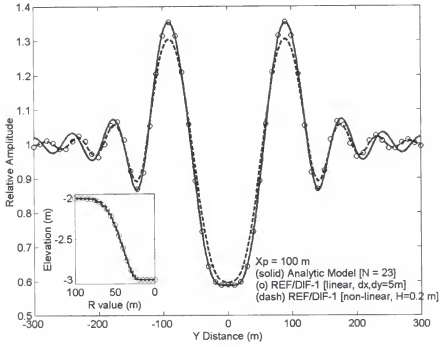

Figure 6-24: Relative amplitude using 3-D Step Model and REF/DIF-1 for longshore transect at X = 100 m for Gaussian pit with $k_1h_1 = 0.24$; cross-section of pit bathymetry through centerline included.

A transect of the relative amplitude at Xp = 400 m is shown in Figure 6-25. This transect lies in the region where the REF/DIF-1 (nonlinear) results diverge from the REF/DIF-1 (linear) and 3-D Step Model results and significant differences are shown for longshore distances, |Y| < 300 m. The difference between the nonlinear and linear results is seen to diminish for large longshore distances.

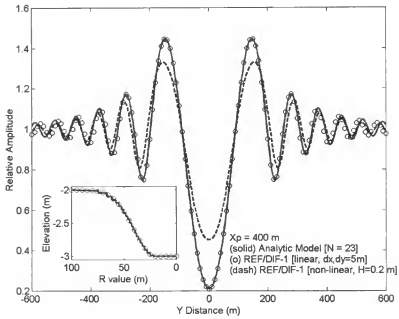

Figure 6-25: Relative amplitude using 3-D Step Model and REF/DIF-1 for longshore transect at X = 400 m for Gaussian pit with $k_1 h_1 = 0.24$; cross-section of pit bathymetry through centerline included.

As in the previous figure the 3-D Step Model and REF/DIF-1 (linear) results show good agreement. The divergence in the results seen in the previous figure at ±200 m due to the wide angle approximation being violated does not occur until longshore distances greater than 500 m due to the cross-shore location of the transect in Figure 6-25.

REF/DIF-1 can also be used to validate the wave angles calculated using the 3-D Step Model. Figure 6-26 shows the wave angles for a longshore transect located at Xp = 400 m for the same bathymetry as for the last 3 figures. The results are only plotted for

one-half of the longshore transect as the wave angles are anti-symmetric about Yp = 0. The 3-D Step Model and REF/DIF-1 (linear) results show good agreement with a slight divergence in the results at the larger longshore distances. The REF/DIF-1 (nonlinear) results show significant differences in the magnitude of the wave angle at longshore distances less than 100 m with better agreement in the magnitude as longshore distance increases.

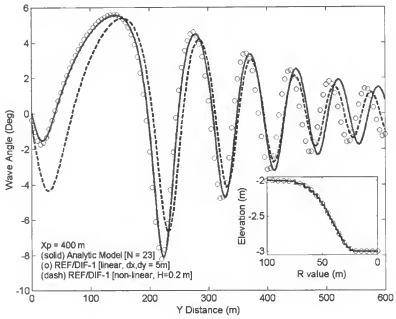

Figure 6-26: Wave angle using 3-D Step Model and REF/DIF-1 for longshore transect at X = 100 m for Gaussian pit with $k_1h_1 = 0.24$; cross-section of pit bathymetry through centerline included.

The 3-D Step Model was also compared to REF/DIF-1 for a pit with linear transitions in depth with a slope equal to 0.1. The intent was to create a bathymetry that would cause significant reflection and to compare the results of the 3-D Step Model, which accounts for reflection, to REF/DIF-1, which does not allow reflection in the upwave direction. Figure 6-27 shows the relative amplitude for a transect taken in the cross-shore direction with a cross-section of the pit taken through the centerline shown in

the inset. In this example 10 steps approximate the linear slope in the 3-D Step Model and a grid spacing of 4 m in the x and y directions was employed in REF/DIF-1.

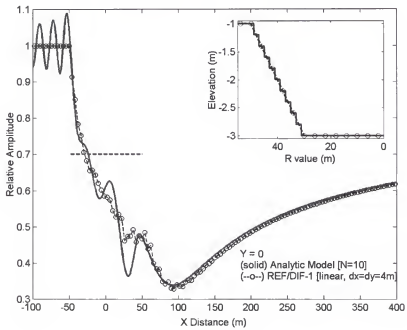

Figure 6-27: Relative amplitude using 3-D Step Model and REF/DIF-1 for cross-shore transect at Y = 0 for pit with linear transitions in depth with $k_1 h_1 = 0.24$; cross-section of pit bathymetry through centerline included with slope = 0.1.

The 3-D Step Model results (solid line) indicate significant upwave reflection in the upwave region with wave sheltering in the downwave region. The relative amplitude values for REF/DIF-1 employing linear wave theory show good agreement with the 3-D Step Model results in the downwave region with a slight divergence inside and just downwave of the pit. Thus, the reflection captured by the 3-D Step Model does not result in significant differences in the relative amplitude in the downwave region for the two models for this cross-shore transect.

The relative amplitude can also be viewed in the longshore direction for a transect at Xp = 300 m in Figure 6-28. The results are only plotted for one-half of the longshore transect as the relative amplitude values are symmetric about Yp = 0. The 3-D Step

Model and REF/DIF-1 results show good agreement for small longshore distances in the main region of wave sheltering. As the relative amplitude oscillates in the longshore direction the peak values of REF/DIF-1 show greater focusing and sheltering (around 3 %) than for the 3-D Step Model. The difference in the results of the two models in the longshore direction might be attributed to the reflection that is included in the 3-D Step Model, but not REF/DIF-1. Divergence in the results of the 3-D Step Model and REF/DIF-1 at these locations is not apparent in the longshore transects shown in Figures 6-24 and 6-25, which are for a gradual pit with little reflection.

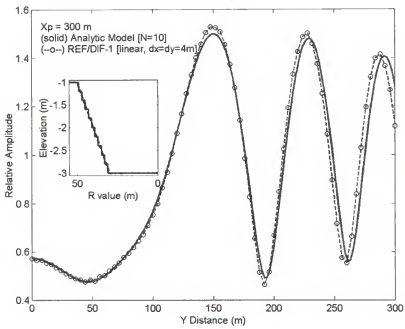

Figure 6-28: Relative amplitude using 3-D Step Model and REF/DIF-1 for longshore transect at X = 350 m for pit with linear transitions in depth with $k_1 h_1 = 0.24$; cross-section of pit bathymetry through centerline included with slope = 0.1.

6.5.2 3-D Step Model Versus 2-D Fully Nonlinear Boussinesq Model

The 3-D Step Model was also compared to a 2-D fully nonlinear Boussinesq numerical model developed by Kennedy et al. (2000). The Boussinesq model used in the comparison accounts for wave refraction, diffraction, reflection, shoaling, breaking,

nonlinear wave-wave interactions and bottom friction. Boussinesq models have been shown to give good estimates of the wave height, direction, shape and transformation when compared to a growing collection of laboratory data (Kirby et al., 1998).

The 3-D Step Model was compared to the Boussinesq model for an abrupt circular shoal of radius and height equal to 1 m and 0.15 m respectively, lying in an uniform domain of depth equal to 0.3 m. Figure 6-29 shows the relative amplitude for a transect taken in the cross-shore direction with the inset diagram showing a cross-section of the shoals used, taken through the centerline. An abrupt shoal is not an applicable domain for a Boussinesq model so a smoothing filter was used to create more gradual transitions in depth.

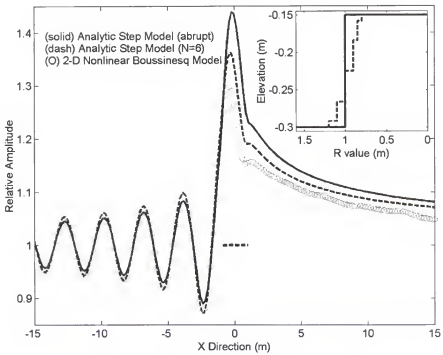

Figure 6-29: Relative amplitude using 3-D Step Model and 2-D fully nonlinear Boussinesq model for cross-shore transect at Y = 0 for shoal with $k_1h_1 = 0.32$; cross-section of pit bathymetry through centerline included.

The inset diagram shows two shoals with the solid line indicating an abrupt shoal and the dashed line representing the abrupt shoal after two smoothing passes in the both the longshore and cross-shore directions. The "smoothed" shoal was evaluated using the 3-D Step Model with 6 steps approximating the form, which is similar to the one used in the Boussinesq model. The solid and dashed lines in the main plot show the relative amplitude for the abrupt and smoothed shoals, respectively, using the 3-D Step Model. The circles show the results of the Boussinesq model for an incident wave height and period of 0.01 m and 3.5 s, respectively. It should be noted that Boussinesq models were not derived for steep slopes used in this comparison.

To calculate the relative amplitude from the Boussinesq model, the wave height was determined from $\mathrm{Re}lAmp = \frac{H(x)}{H_I}$ where $H(x) = 2\sqrt{2}\sigma[\eta(x,t)]$ with σ equal to the standard deviation, $\eta(x,t)$ equal to the water surface time series, and H_I equal to the incident wave height. In both the upwave region where significant reflection occurs and in the downwave focusing, the 3-D Step Model and Boussinesq model results compare well with the stepped, smoothed shoal showing better agreement than the abrupt shoal. The Boussinesq model results upwave of the shoal indicate a mean value above unity, a result of dividing the nonlinear waveform upwave of the shoal by the linear incident wave height. The maximum value of the Ursell parameter for the Boussinesq model over the shoal and upwave of the shoal are 68.3 and 14.2, respectively.

6.6 Comparison to Laboratory Data of Chawla and Kirby (1996)

The requirement of uniform depth outside of the bathymetric anomaly in the Step Method greatly limits the available laboratory data for comparison. The laboratory experiment of Chawla and Kirby (1996) is the only experiment known to the author with

wave measurements in a domain of uniform depth that contains a bathymetric anomaly. The bathymetric anomaly in Chawla and Kirby is a shoal of 2.57 m radius with the shape of the shoal being the upper portion of a sphere with a radius of 9.1 m. The dimensions for the basin used in the experiment were18.2 m in the longshore direction and 20 m in the cross-shore direction. Further details of the experiment and the collected data can be found in Chawla and Kirby (1996).

The data collected during the experiment of Chawla and Kirby that fits within the constraints of the Step Method are comprised of 3 different tests (Tests 1, 2, and 4) for monochromatic, non-breaking, incident waves with wave heights collected along seven transects. To compare with the step method the data from Test 4 were used along four of the seven transects. A schematic of the laboratory setup with the transect locations used in the comparisons is shown in Figure 6-30 with the shoal is centered at (0,0).

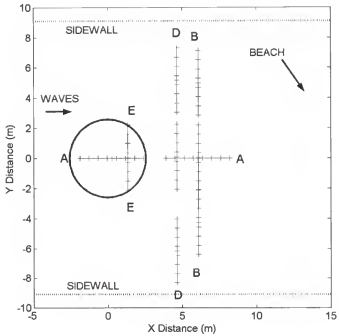

Figure 6-30: Experimental setup of Chawla and Kirby (1986) for shoal centered at (0,0) with data transects used in comparison shown.

The relative amplitudes along Transect A-A for the Analytic Model and the Chawla and Kirby (1986) data are shown in Figure 6-31. An inset diagram is including showing the bathymetry with the shoal being approximated by 15 steps in the 3-D Step Model. Also included in the main plot is the relative amplitude from FUNWAVE 1.0 [2-D] (Kirby et al., 1998). FUNWAVE 2-D is a two-dimensional fully nonlinear Boussinesq model based on the equations of Wei et al. (1995), which has been successfully compared with the data of Chawla and Kirby (1986). The specifications of the inputs for FUNWAVE 2-D necessary to model the experiment of Chawla and Kirby (1986) are included in the freely distributed code for the numerical model and were used to generate the FUNWAVE 2-D results shown here. The incident wave height and period are 0.0233 m and 1 s, respectively.

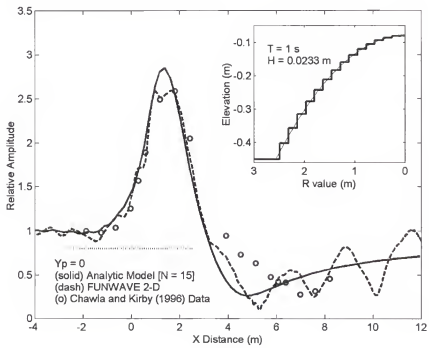

Figure 6-31: Relative amplitude using 3-D Step Model, FUNWAVE 2-D and data from Chawla and Kirby (1996) for cross-shore transect A-A with $k_1h_1 = 1.89$; cross-section of shoal bathymetry through centerline included.

Good agreement is shown in Figure 6-31 between the 3-D Step Model and the data of Chawla and Kirby. FUNWAVE 2-D is found to agree well with the data up to X = 5 m, where oscillations in the relative amplitude commence. Nonlinear effects could cause the difference in the maximum relative amplitude values over the shoal for the Step Model and those of the data and FUNWAVE 2-D. The maximum value of the Ursell parameter for the FUNWAVE 2-D results over the shoal is 83.13, while the maximum value upwave of the shoal is 0.60. Both the 3-D Step Model and FUNWAVE 2-D indicate smaller relative amplitude values shoreward of the shoal (4 < X < 6 m).

The relative amplitude values for longshore Transect E-E, which lies over the shoreward side of the shoal, are found in Figure 6-32. For each data point, the 3-D Step Model results show good agreement with the data of Chawla and Kirby (1996).

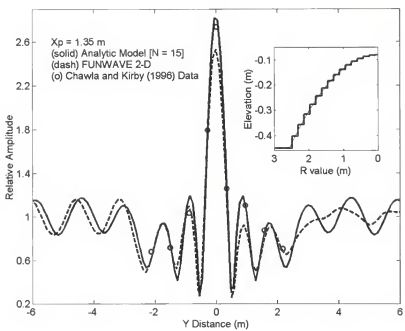

Figure 6-32: Relative amplitude using 3-D Step Model, FUNWAVE 2-D and data from Chawla and Kirby (1996) for longshore transect E-E with $k_1h_1 = 1.89$; cross-section of shoal bathymetry through centerline included.

The FUNWAVE 2-D results nearly match those of the 3-D Step Model with a smaller peak value at Y = 0 and a slight asymmetry in the values due to a slight asymmetry in the experimental setup (sidewall locations), and therefore the FUNWAVE 2-D domain. The relative amplitudes along Transects D-D and B-B are shown in Figures 6-33 and 6-34, respectively. In each figure the 3-D Step Model is seen to have relative amplitude values that are comparable to the data of Chawla and Kirby (1996) and FUNWAVE 2-D.

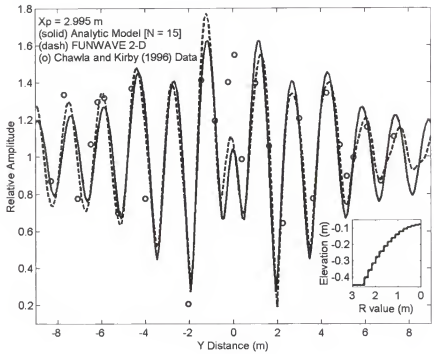

Figure 6-33: Relative amplitude using 3-D Step Model, FUNWAVE 2-D and data from Chawla and Kirby (1996) for longshore transect D-D with $k_1h_1 = 1.89$; cross-section of shoal bathymetry through centerline included.

In Figure 6-33 the data of Chawla and Kirby (1996) show large (> 1.4) values directly shoreward of the shoal where the 3-D Step Model and FUNWAVE 2-D results indicate values around 1.1; a result first shown in Figure 6-31. Overall the agreement between the Analytic Step Method and experimental data of Chawla and Kirby (1996) is found to be acceptable.

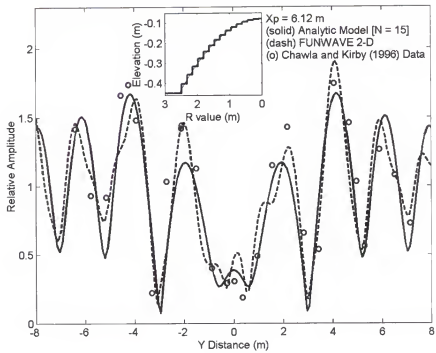

Figure 6-34: Relative amplitude using 3-D Step Model, FUNWAVE 2-D and data from Chawla and Kirby (1996) for longshore transect B-B with $k_1h_1 = 1.89$; cross-section of shoal bathymetry through centerline included.

6.7 Direction Averaged Wave Field Modification

The results presented thus far have been for a monochromatic incident wave from a single direction; however, a natural wave field is known to consist of many wave directions and periods. Since the 3-D Step Model employs linear wave theory, solutions can be superimposed to create a wave field that is averaged over several directions or periods, thereby creating more realistic incident wave conditions.

Figure 6-35 is a plot of the relative amplitude for a longshore transect where the relative amplitudes are an average of the values obtained with incident wave directions from –10 to 10 deg taken every 2 deg. Two averaging procedures were used. The solid line is the average relative amplitude with each incident direction having the same weight or frequency while the dashed line is the average relative amplitude where the incident

directions were weighted in the following manner: 0 deg (30%), ±2 deg (15%), ±4 deg (10%), ±6 deg (6%), ±8 deg (3%), ±10 deg (1%). The dotted line on the plot is the relative amplitude for an incident wave directed normal to the transect (0 deg). A cross-section of the pit used in the models taken through the centerline is shown in the inset diagram. The transect was located 300 m shoreward of the pit and $k_1h_1 = 0.24$.

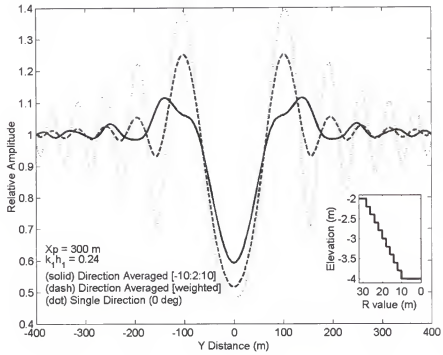

Figure 6-35: Relative amplitude averaged over incident direction (centered at 0 deg) for alongshore transect at X = 300 m for pit with $k_1h_1 = 0.24$; cross-section of pit bathymetries through centerline included with slope = 0.1.

The weighted average (dashed line) is shown to reduce the oscillations in longshore direction with the reduction increasing with longshore distance away from the pit and the phasing of the oscillations unchanged. There is only a slight reduction in the wave sheltering directly shoreward of the pit using the weighted average. Averaging over the 11 directions with no weighting (solid line) greatly reduces the oscillations in the longshore directions and also changes the phasing of the oscillations. The unweighted

averaging technique is shown to result in a significant reduction in the sheltering shoreward of the pit and in the focusing bands that border the sheltering. Averaging over a few periods around 12 s, while also averaging over the 11 directions, was found to produce slightly more dampening of the oscillations in the longshore while maintaining the features directly shoreward of the pit.

The effect of averaging over incident wave direction on the wave angle is shown in Figure 6-36 for the same incident wave conditions as for the previous figure. Both averaging procedures are shown to reduce the wave angles along the entire transect, with the greatest reduction at large longshore distances.

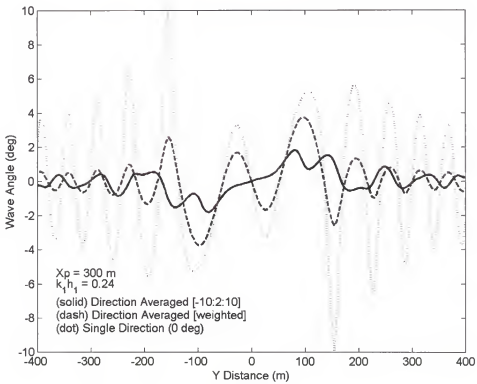

Figure 6-36: Wave angle averaged over incident direction (centered at 0 deg) for alongshore transect at X = 300 m for pit with $k_1h_1 = 0.24$ with bathymetry indicated in inset diagram of previous figure.

As in the previous figure, the weighted averaging results in a reduction of the longshore oscillations with the effect increasing with longshore distance, and no change to phase of the oscillations. The unweighted averaging is shown to reduce the wave angles significantly along the entire transect, with changes to the phasing of the oscillations. The unweighted average wave angles indicate a divergence in the wave field shoreward of the pit without the small area of convergence seen for the case of normally incident waves.

Averaging around an incident wave direction of 20 degrees was performed for Figures 6-37 and 6-38, which show the longshore transects of the relative amplitude and wave angle, respectively. As in the previous example two averaging procedures were used with the solid line indicating the average value with each incident direction having the same weight or frequency and the dashed line is the weighted average value: 20 deg (30%), 20±2 deg (15%), 20±4 deg (10%), 20±6 deg (6%), 20±8 deg (3%), 20±10 deg (1%).

Figure 6-37 shows the relative amplitude values with the area of wave sheltering shifted in the longshore direction due to the incident wave angle. The weighted averaging technique is shown to result in a dampening of the longshore oscillations with no changes to the phasing, while the unweighted averaging results in a larger reduction in the relative amplitude values, especially at small longshore distances, and changes in the phasing. The oscillations in the negative Y direction are found to have a smaller wavelength than the oscillations in the other longshore direction, a result of the transect orientation for oblique wave incidence. Figure 6-38 shows similar features for the wave angles with the area of wave divergence being shifted in the longshore direction.

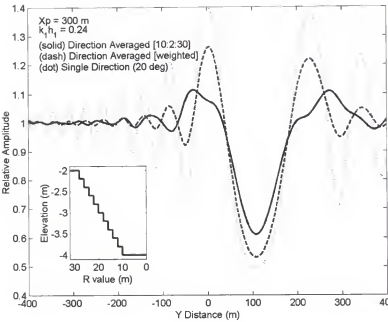

Figure 6-37: Relative amplitude averaged over incident direction (centered at 20 deg) for alongshore transect at X = 300 m for pit with $k_1h_1 = 0.24$; cross-section of pit bathymetries through centerline included with slope = 0.1.

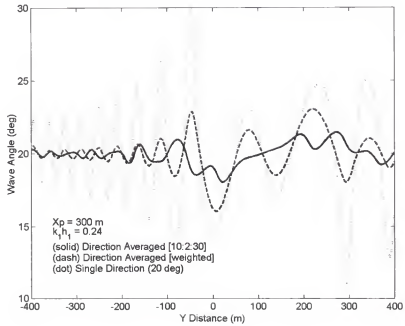

Figure 6-38: Wave angle averaged over incident direction (centered at 20 deg) for alongshore transect at X = 300 m for pit with $k_1h_1 = 0.24$ with bathymetry indicated in inset diagram of previous figure.

6.8 Energy Reflection

Unlike the two-dimensional case of waves over a trench or shoal of infinite length, determining the energy reflection from a bathymetric anomaly in three dimensions is not trivial. To determine the energy reflection caused by a three-dimensional bathymetric anomaly a method was developed using far-field approximations of the Bessel functions along a half-circular arc bounding the region of reflected energy. A reflection coefficient was obtained by summing the reflected energy through this arc and comparing it to the amount of energy incident on the anomaly. The complete formulation of the far-field energy reflection method is presented in Appendix B.

6.8.1 Comparison to Prior Results

The far-field energy reflection method will first be compared to a shallow water method that sums the energy flux through a transect. In Bender (2001) a method to calculate the energy reflection caused by bathymetric anomalies in shallow water was developed. This method used a time-averaged energy flux approach in which a transect was created outward from the center of the anomaly in the longshore direction and parallel to the incident wave fronts. At each location in the transect the energy flux was determined, which allowed for the total energy flux through the transect to be summed and compared with the energy flux through the transect if no pit were present, resulting in a reflection coefficient.

Figure 6-39 shows the reflection coefficient, K_R, versus pit diameter divided by the wavelength outside the pit for the far-field approximation method and the shallow water transect method. In order to maintain shallow water conditions the transect method

requires increasing the pit radius to obtain K_R for larger values of the non-dimensional diameter; therefore 4 different pit radii are included for the transect method results.

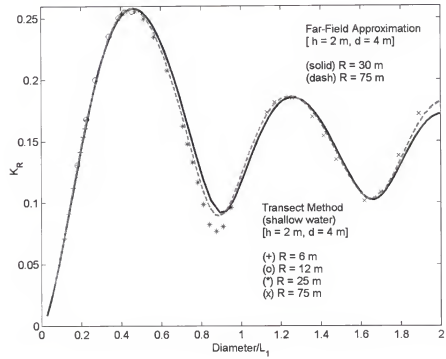

Figure 6-39: Reflection coefficient versus non-dimensional diameter; comparison between shallow water transect method and far-field approximation method.

Two different pit radii were used for the far-field approximation method with little difference in the values indicated in the results. The transect method values for each of the four radii used show good agreement with the results of the far-field approximation method with the largest difference at a non-dimensional diameter of 0.9.

6.8.2 Effect of Transition Slope on Reflection

The effect of the transition slope on the reflection was investigated using the step method and the far-field approximation for the reflection coefficient. In an attempt to isolate the effect of the transition slope, bathymetric anomalies of constant volume were created either by keeping the depth or the bottom radius constant. Figure 6-40 shows the

reflection coefficient versus k_1h_1 for four pits in the shape of truncated cones with constant volume and equal depth; these are the same pit configurations used in Section 6.3 in Figures 6-9 to 6-12. The gradual transition slopes are seen to greatly change the reflection properties of the pits. The K_R values for each pit are seen to oscillate with k_1h_1 with the trend of K_R decreasing as k_1h_1 increases. For the more gradual transition slopes the oscillations are almost completely damped for the larger k_1h_1 values. The only occurrence of complete transmission ($K_R = 0$) is the trivial solution of $k_1h_1 = 0$. This differs from the result for symmetric two-dimensional trenches of infinite length with the same depth on both sides of the trench, where for each oscillation there is an instance of complete transmission.

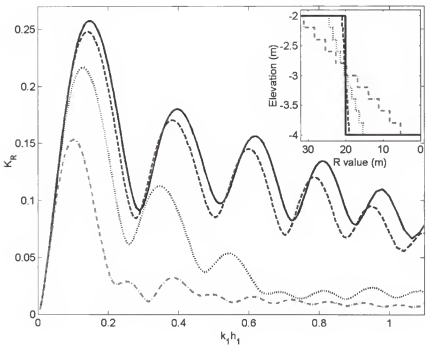

Figure 6-40: Reflection coefficient versus k_1h_1 based on far-field approximation and constant volume and depth pits; cross-section of pit bathymetries through centerline included with slopes of abrupt, 1, 0.2 and 0.07.

The reflection caused by a pit is shown to depend greatly on the pit bathymetry and the non-dimensional wave number. The abrupt pit is shown to have the largest K_R value at $k_1h_1 = 0.15$; however, at $k_1h_1 = 0.30$ the pit with a transition slope of 1 has the largest K_R value and the pit with a slope of 0.2 has a value that approaches the more abrupt pits. The wave field for these instances is shown in Figures 6-9 and 6-10, which show the relative amplitude along a cross-shore transect at $k_1h_1 = 0.15$ and 0.3, respectively. Reviewing Figure 6-9 indicates that the abrupt pit clearly causes the largest reflection upwave of the pit, and Figure 6-10 shows that the pits with slopes of 1 and 0.2 cause a slightly larger reflected wave than the abrupt pit.

The reflection coefficients for four pits (truncated cones) of equal volume with constant bottom radius (slope: abrupt, 1, 0.2, 0.05) are shown in Figure 6-41.

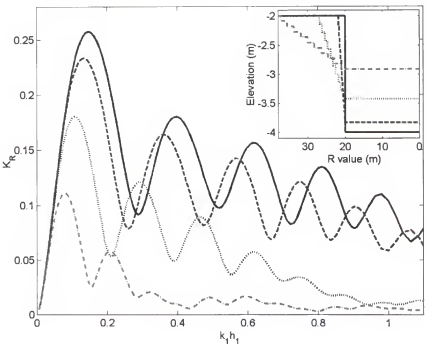

Figure 6-41: Reflection coefficient versus k_1h_1 based on far-field approximation and constant volume bottom width pits; cross-section of pit bathymetries through centerline included with slopes of abrupt, 1, 0.2 and 0.05.

The smaller transition slopes are seen to reduce greatly the reflection caused by the pit for most values of k_1h_1. The pit with transition slope of 0.2 is shown for all the pits with $k_1h_1 \approx 0.27$ to have the largest K_R. As in the previous figure, K_R is shown to oscillate with k_1h_1 with a decreasing trend as k_1h_1 increases and no instances of complete transmission other than $k_1h_1 = 0$.

The reflection coefficients for four shoals of equal volume and depth are shown in Figure 6-42. The same shoal configurations were used as in Figure 6-13. The more gradual transition slopes are seen to produce less reflection than the more abrupt slopes, as seen previously. The reflection coefficient is seen to oscillate with k_1h_1 with the general trend of the K_R values increasing with k_1h_1 for all slopes except the most gradual; a result that differs from the case for a pit.

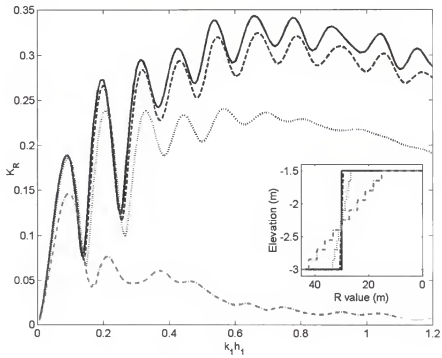

Figure 6-42: Reflection coefficient versus k_1h_1 based on far-field approximation and constant volume and depth shoals; cross-section of shoal bathymetry through centerline included with slopes of abrupt, 1, 0.2 and 0.07.

6.9 Analytic Nearshore Shoaling and Refraction Method

The 3-D Step Model requires a uniform depth outside of the bathymetric anomaly, which limits its use in the nearshore zone where shoaling and refraction occur due to changes in depth. To overcome this limitation an analytic nearshore shoaling and refraction method was developed. The Analytic Shoaling and Refraction Model (Analytic S/R Model) uses wave height and direction values determined from the 3-D Step Model as the initial conditions at a cross-shore location where a region of uniform depth joins with a nearshore region with a defined slope. The Analytic S/R Model propagates the waves in the nearshore region up the slope the to the point where depth limited breaking occurs; the theory and formulation for the model are found in Appendix C.

The bathymetries for two cases used in the Analytic S/R Model are shown in Figure 6-43. In both cases the center of the pit lies in a region of uniform depth and is centered at X = 0 m with the nearshore region commencing at X = 600 m. For Pit 1 both the transition slopes and the nearshore slope are linear with values of 0.1 and 0.02, respectively with 10 steps defining the transition slope and a cross-shore spacing of 1 m in the nearshore region. For the second case, Pit 2, the side wall slopes are of Gaussian form with C_1 and C_2 equal to 1 m and 10 m, respectively with 23 steps defining the slope. The nearshore region for this case has an Equilibrium Beach Profile form defined by $h = Ax^{\frac{2}{3}}$ with A equal to 0.1 $m^{1/3}$ and a cross-shore spacing, dx, equal to 1. In all models run the base conditions were an incident wave height and period of 1 m and 12 s, respectively.

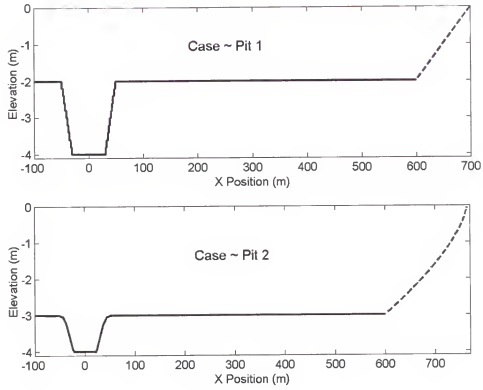

Figure 6-43: Bathymetry for two nearshore regions used in analytic shoaling and refraction model: Pit 1; linear transition slopes with linear nearshore slope and Pit 2; Gaussian transition slopes with Equilibrium Beach form for nearshore slope.

The results of the Analytic S/R Model for Pit 1 are shown in Figure 6-44. The upper plot in Figure 6-44 shows the wave height values at the start of the nearshore region (X = 600 m) and at the breaking location after the wave transformation processes of shoaling and refraction have altered the waves in the surfzone. The middle plot shows the wave angles at these locations. Only one-half of the longshore region is plotted as the wave height values are symmetric about Y = 0 while the wave angle values are anti-symmetric. The upper plot indicates that the greatest amount of shoaling occurs directly shoreward of the pit where the smallest initial waves coincide with an area of wave convergence. Very little shoaling is found where the largest initial waves occur near Y = 200 m. It is apparent that as the wave height oscillates in the longshore direction there

are regions of minimal shoaling followed by regions of significant shoaling that coincide in longshore location with areas of wave divergence and convergence, respectively.

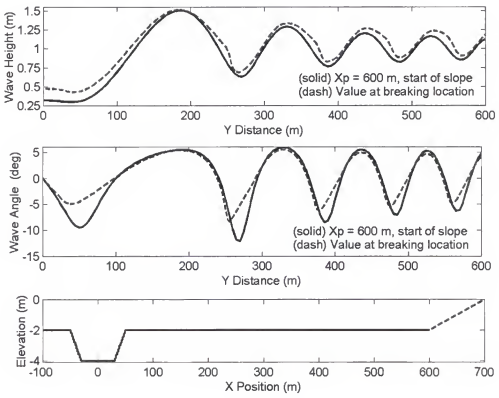

Figure 6-44: Wave height and wave angle values at start of nearshore region and at breaking for longshore transect with bathymetry with H = 1 m and T = 12 s for Pit 1.

The most significant refraction is shown to occur where the initial wave heights are the smallest, which allows for the wave to propagate farther into the surf zone before depth limited breaking commences.

In Figure 6-45 the wave heights in the nearshore region are shown in a contour plot with the breaking location indicated. This plot reveals the differences in the cross-shore location of the breaking point, which is a consequence of the non-uniform alongshore wave height shoreward of the pit. The waves with the smallest heights are

seen to travel well into the nearshore region, while in the regions of wave focusing, where the initial wave heights are larger, breaking commences much farther offshore.

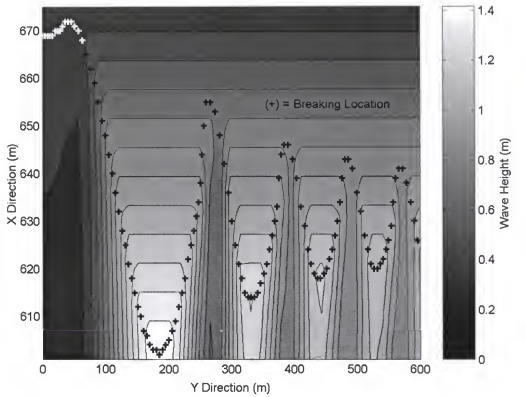

Figure 6-45: Contour plot of wave height for Pit 1 in nearshore region with breaking location indicated with H = 1 m and T = 12 s.

The initial and breaking values of the wave height and wave angle for Pit 2 are shown in Figure 6-46. The upper plot of the wave height shows considerably more wave shoaling than for the case of Pit 1. There are two reasons for the increased shoaling: the water depth in the region of uniform depth is greater for Pit 2 and initially the nearshore slope is smaller for Pit 2, both of which allow for greater shoaling to occur before wave breaking. As in Figure 6-44 for Pit 1, there are both regions of considerable wave shoaling and regions of minimal wave shoaling, which correspond to regions of wave convergence and divergence shown in the middle plot of the wave angles in the

longshore. The wave angles at the start of the slope for the case of Pit 2 are shown to be much smaller than for Pit 1 due to Pit 2 lying in greater water depth and having a less abrupt change in depth, a result of the Gaussian transition slopes.

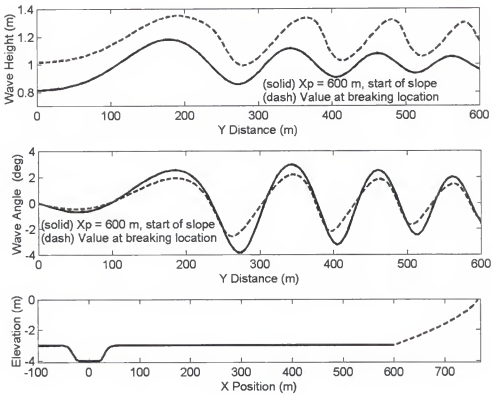

Figure 6-46: Wave height and wave angle values at start of nearshore region and at breaking for longshore transect with bathymetry with H = 1 m and T = 12 s for Pit 2 bathymetry.

A contour plot of the wave height and breaking location for Pit 2 is shown in Figure 6-47. The figure indicates that all of the waves shoal significant distances into the surf zone before breaking commences as compared to Figure 6-45 for Pit 1. The distance between locations of the first wave breaking and last wave to break is 26 m, which can be compared to the 70 m difference for the case of Pit 1. The longshore gradient in the breaking wave height is shown to be much smaller than for the case of Pit 1.

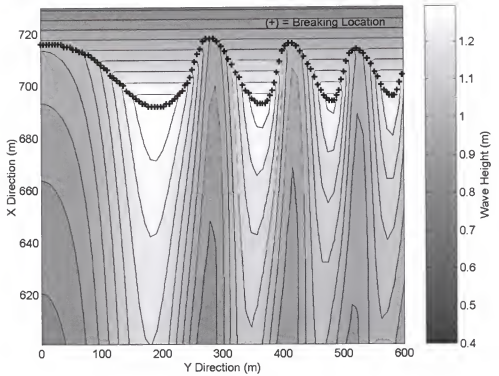

Figure 6-47: Contour plot of wave height for Pit 2 in nearshore region with breaking location indicated with H = 1 m and T = 12 s.

6.9.1 Comparison of Analytic Method to REF/DIF-1

The 3-D Step Model can be compared to the numerical model REF/DIF-1 (Kirby and Dalrymple, 1994), as demonstrated in Section 6.5.1 for cases of a uniform depth domain containing a bathymetric anomaly. Comparisons can also be drawn for the Analytic S/R Model and REF/DIF-1 for the domains shown in Figure 6-43, which mesh a uniform depth region containing a bathymetric anomaly to a sloped region representing the nearshore. For the comparisons the wave height and wave angle from each model were compared at the start of the slope representing the nearshore and at two locations in the nearshore region for both Pit 1 and Pit 2.

The REF/DIF-1 modeling was performed using linear wave theory with no bottom dissipation and with cross-shore and longshore spacing equal to 4 m. REF/DIF-1

uses the Dally et al. (1985) model for wave breaking, which is based on the premise that there is a stable wave height within the surf zone for each water depth. The stable wave height is reached after the breaking threshold is met and breaking commences.

The wave height and wave angle values for the Analytic S/R Model and REF/DIF-1 (linear) at the start of the nearshore region for Pit 1 are shown in Figure 6-48. The bottom plot shows the bathymetry for the two regions and the cross-shore location for the wave heights and angles. The upper plot indicates that the REF/DIF-1 values nearly match the analytic values with a slight divergence at large longshore distances. The wave angles (middle plot) show good agreement with the REF/DIF-1 results showing some scatter, but with a trend that nearly matches the analytic results.

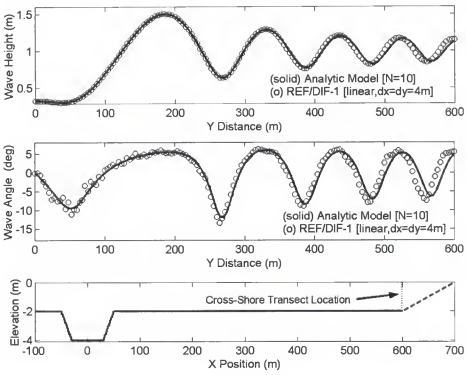

Figure 6-48: Wave height and wave angle values at start of nearshore region from 3-D Step Model and REF/DIF-1 (linear) with H = 1 m and T = 12 s for Pit 1.

The wave height and angle values for the Analytic S/R Model and REF/DIF-1 at a location on the nearshore slope with a depth of 1.68 m (X = 616 m) are shown in Figure 6-49. As in the previous figure the cross-shore location of the wave height and angle transects is indicated in the bottom plot. At this cross-shore location, wave breaking has commenced for the largest waves as shown in the upper plot. In the Analytic S/R Model wave breaking is depth limited and after breaking the wave height is simply the breaking criterion (0.78) times the depth, while for REF/DIF-1 the broken waves reach a stable wave height with a smaller breaking criterion. At the two longshore sections where breaking has occurred the Analytic S/R Model and REF/DIF-1 show similar values for breaking height and breaking location.

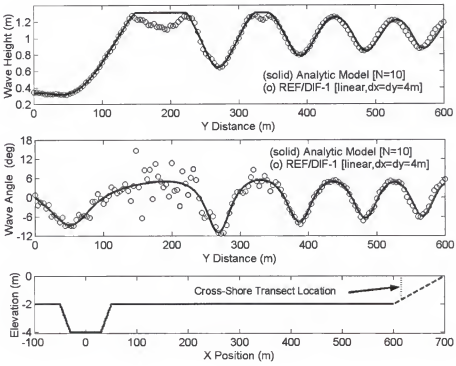

Figure 6-49: Wave height and wave angle values at h = 1.68 m (X = 616 m) from 3-D Step Model and REF/DIF-1 (linear) with H = 1 m and T = 12 s for Pit 1.

The values for the unbroken waves show similar shoaled wave heights with more divergence between the models at large longshore distances. The wave angle values in the middle plot show good agreement between the models in the areas of unbroken waves with the REF/DIF-1 results showing significant scatter in two sections of broken waves. The wave angle in the Analytic S/R Model is controlled by Snell's Law refraction throughout the nearshore region, both before and after breaking.

Figure 6-50 shows the wave height and angle for a longshore transect located farther into the surf zone (h = 1.44 m, X = 628 m), which induces widespread depth-limited breaking is found. The lower plot shows the location of the cross-shore transect in the nearshore region.

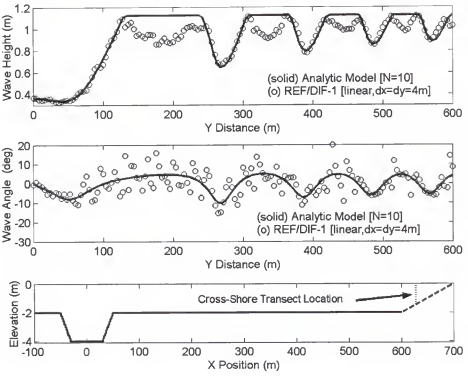

Figure 6-50: Wave height and wave angle values at h = 1.44 m (X = 628 m) from 3-D Step Model and REF/DIF-1 (linear) with H = 1 m and T = 12 s for Pit 1.

The wave height values for the two models show good agreement for the breaking height and location in the longshore for this location with significant breaking. The REF/DIF-1 wave angle values show considerable scatter in the areas of wave breaking, which is the majority of the transect, with the Analytic S/R Model wave angles generally following the trend of the scattered REF/DIF-1 values.

The Analytic S/R Model and REF/DIF-1 were also compared for the case of Pit 2 for three cross-shore locations (h = 3 m (slope start), h = 2.04 m, h = 1.6 m). Figure 6-51 shows the wave height and angle at the start of the nearshore region with the cross-shore location indicated in the bottom plot. The wave height (upper plot) and wave angle (middle plot) values show good agreement with a slight divergence in the values that grows with longshore distance.

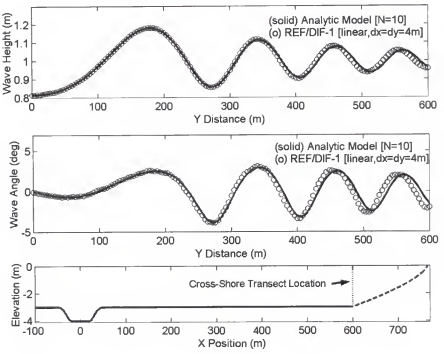

Figure 6-51: Wave height and wave angle values at start of nearshore region from 3-D Step Model and REF/DIF-1 (linear) with H = 1 m and T = 12 s for Pit 2.

The wave height and wave angle shown in Figure 6-52 occur at a depth of 2.04 m before breaking has been initiated at any longshore location. The upper plot shows the wave height values of the Analytic S/R Model with larger values in the peaks and smaller values in the troughs of the oscillations that occur in the longshore, as compared to the REF/DIF-1 values, with the largest differences being less than 5%. The wave angles (middle plot) show similar magnitudes for the two models but with a phase shift of approximately 15 m.

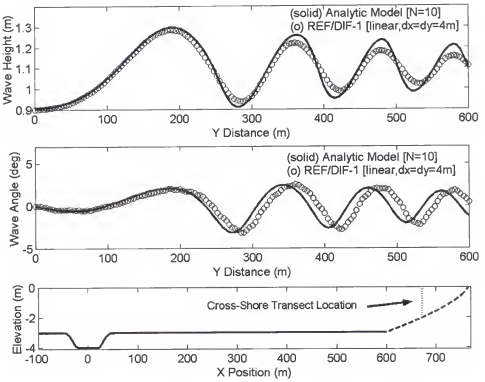

Figure 6-52: Wave height and wave angle values at h = 2.04 m (X = 672 m) from 3-D Step Model and REF/DIF-1 (linear) with H = 1 m and T = 12 s for Pit 2.

The wave height and angle values at a cross-shore location for Pit 2 with significant breaking are shown in Figure 6-53. The cross-shore location is at X = 672 m (h = 1.6 m) and is indicated in the bottom plot. The wave height values in the upper plot

show similar values for the breaking wave height and location for the two models with the Analytic S/R Model showing slightly larger values before breaking and generally smaller values in the non-breaking waves. The REF/DIF-1 values for the wave angles show large scatter for the broken waves with similar values for the non-broken waves with the Analytic S/R Model.

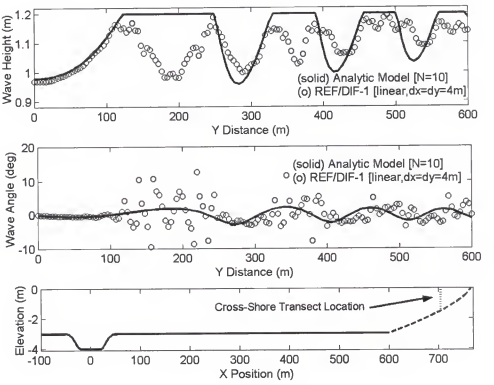

Figure 6-53: Wave height and wave angle values at h = 1.6 m (X = 704 m) from 3-D Step Model and REF/DIF-1 (linear) with H = 1 m and T = 12 s for Pit 2.

Overall the Analytic S/R Model is found to agree quite well the results from REF/DIF-1 for linear waves for the cases shown. The Analytic S/R Model will be used to determine the nearshore wave transformation needed for the shoreline change model of Section 6.10.

6.9.2 Wave Averaged Results

As was demonstrated in Section 6.7, averaging over several directions centered on a central value generates a more realistic incident wave climate and greatly reduces the longshore oscillations in the wave height and angle found using a single monochromatic incident wave. The weighted averaging technique described in Section 6.7 was used for the bathymetries of Pit 1 and Pit 2 with H = 1 m and T = 12 s to determine the breaking values for an averaged wave field.

Figure 6-54 shows the wave height and angle values at the start of the nearshore region and at breaking for the case of Pit 1 with the bathymetry indicated in the bottom plot. The values of the wave height at breaking shown in the upper plot indicate fairly uniform shoaling for the entire transect with little longshore variation for the larger longshore distances; the desired consequence of the averaging procedure. The wave angle values show minimal refraction except for longshore distances less than 100 m. The magnitudes of the values and the variation in the longshore for the averaged values can be compared to those of Figure 6-44 for a normally incident wave.

The weighted average values of the wave height and angle at the start of the nearshore region and at breaking for Pit 2 are shown in Figure 6-55. The bathymetry for this case is detailed in the bottom plot. Significant shoaling is seen in the upper plot of the wave height, which also indicates minimal variation in the values for large longshore distances. The wave angles are small in magnitude with slight refraction occurring at most longshore locations. Using the weighted averaging technique these values can be compared for the bathymetry of Pit 2 in Figure 6-46 where the waves are normally incident.

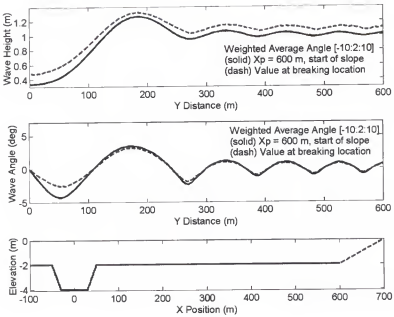

Figure 6-54: Weighted wave averaged values of wave height and wave angle at start of nearshore region and at breaking for longshore transect with H = 1 m and T = 12 s and bathymetry for Pit 1.

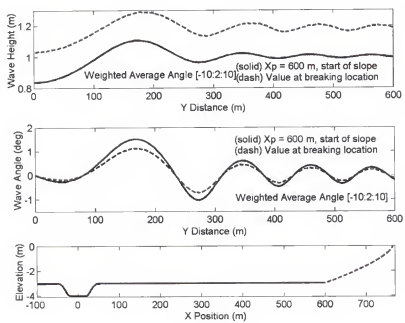

Figure 6-55: Weighted wave averaged values of wave height and wave angle at start of nearshore region and at breaking for longshore transect with H = 1 m and T = 12 s and bathymetry for Pit 2.

To make sure that the weighted average method was valid with the Analytic S/R Model a study of when to implement the averaging procedure was made. The first procedure ran the 3-D Step Model for 11 wave directions from –10 deg to 10 deg every 2 deg and obtained the results at a transect representing the start of the nearshore zone. Next, the weighted averaging technique was used to determine the averaged values, which were then used in the Analytic S/R Model. The other procedure ran the Analytic S/R Model 11 different times, one for each incident wave direction. Then the weighted averaging technique was employed on the shoaled and refracted values for each wave direction to determine the averaged values. Little difference was found in the values obtained by the two procedures with the wave height values almost equal and only small differences for the wave angles. From this comparison it was determined that only shoaling the weighted average values was sufficient.

6.10 Shoreline Evolution Model

Up to this point only the wave field modification caused by bathymetric anomalies has been demonstrated. The development of the Analytic S/R Model extends the bathymetry altered wave field into the nearshore region where shoaling and refraction induced by the sloping bottom modify the waves until depth limited breaking occurs. In order to calculate the shoreline planform evolution shoreward of a bathymetric anomaly the Analytic S/R Model is employed to calculate the breaking wave height and angle as well as the breaking location, which are then used to drive the longshore transport and, with the continuity equation, the change in shoreline position. Details of the Shoreline Evolution Model can be found in Appendix D. The Shoreline Evolution Model provides a means to determine the shoreline evolution near an axisymmetric bathymetric anomaly

lying in uniform depth, which has gradual transitions in depth, and a nearshore region that may be defined with a linear slope or an Equilibrium Beach Profile (EBP) form.

6.10.1 Shoreline Change Estimates Shoreward of Bathymetric Anomalies

The Shoreline Evolution Model was used with several domains containing different bathymetric anomaly shapes, as well as nearshore forms, in an attempt to develop the equilibrium planform for a variety of conditions. The base conditions for the modeling were an incident wave height and period of 1 m and 12 s, respectively with the first longshore transport term, K_1, equal to 0.77. The time step was 50 seconds with 12600 time steps, for a total modeling time of 175 hours (7.3 days). The boundary conditions for the model were closed boundarys (longshore transport, Q, equal to 0) at Yp = +/- 800 m. The weighted averaging procedure described in Section 6.7 was used on the initial wave height and angle values determined by the 3-D Step Model.

The shoreline evolution for the case of Pit 1 is shown in Figure 6-56 with $K_2 = 0.4$ with the bathymetry shown in inset diagram. The weighted average wave height and angles used as the initial values at the offshore limit of the nearshore region are found in Figure 6-54. The shoreline planforms are plotted every 4 hours for the first 16 hours and thereafter every 12 hours. The initial shoreline position is indicated by the dotted line and the final shoreline position is indicated with "o" for every third longshore point. Accretion (shoreline advancement) is in the negative X direction. The shoreline plot indicates a large salient forming directly shoreward of the pit, which is bordered by two areas of erosion with the cross-shore extent of the shoreline advancement approximately twice that of the shoreline retreat. Some areas of interest are directly shoreward of the pit (Yp +/- 50 m) where the shape of the planform changes concavity as the shoreline evolves, and the oscillations in the longshore at Yp > +/- 250 m where the shoreline

advances at first and then retreats as material leaves the area. The system is seen to approach equilibrium as the change in the shoreline position with each 12 hour step is seen to decrease dramatically.

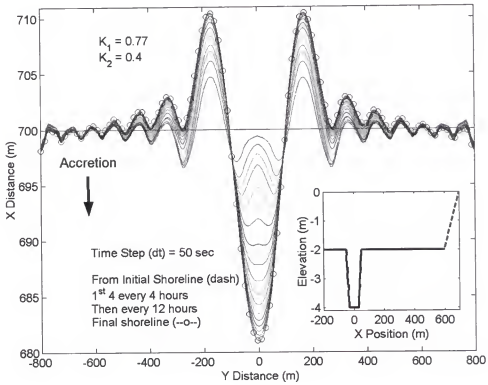

Figure 6-56: Shoreline evolution for case Pit 1 with $K_1 = 0.77$ and $K_2 = 0.4$ for incident wave height of 1 m, wave period of 12 s, and time step of 50 s with shoreline advancement in the negative X direction; Pit 1 bathymetry along cross-shore transect included.

Studying the longshore transport terms (K_1 and K_2) individually allows investigation of the mechanics of the shoreline evolution. Figure 6-57 shows the shoreline position, longshore transport (Q), breaking wave height, and breaking wave angle within subplots to isolate their behavior after one time step for the model shown in the previous figure. Only one-half of the domain is shown as the results are either symmetric (shoreline position, wave height) or anti-symmetric (wave angle, Q) about Yp

= 0. The upper plot shows the shoreline position versus longshore distance with accretion indicated shoreward of the pit, flanked by an area of erosion and then shoreline advancement. The second plot shows the longshore transport, which causes the change in the shoreline position, with the total transport (K_1 & K_2), transport driven by the breaking wave angle (K_1), and transport driven by the gradient in the breaking wave height (K_2) plotted separately. The K_2 transport term is seen to dominate the total transport in most areas with few regions where the terms reinforce. Regions where the gradient in the longshore transport is negative (0<Yp<130 m) are shown to correspond to regions of shoreline advancement with shoreline retreat for a positive gradient in transport.

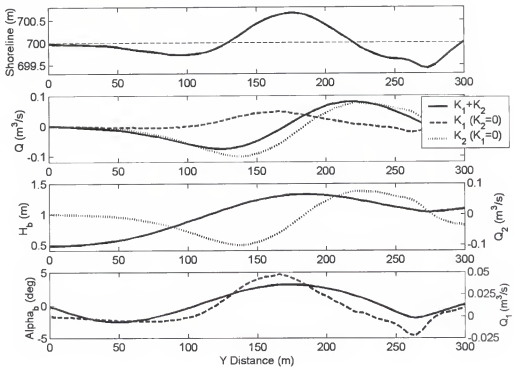

Figure 6-57: Parameters for shoreline change after 1st time step showing shoreline position, and longshore transport terms for case Pit 1 with $K_1 = 0.77$ and $K_2 = 0$.

The third plot shows the relationship between the breaking wave height and the K_2 driven transport (Q_2) with the left axis and solid line indicating H_b and the right axis and dotted line indicating Q_2. A positive gradient in H_b is shown to cause negative transport, which is intuitive as a gradient in H_b will cause a flow from the section with the larger wave height to the smaller wave height. The bottom plot shows the breaking wave angle (α_b) and the longshore transport driven by the angle (Q_1) with the transport having the same form as the wave angle.

The effect of the second transport coefficient, K_2, on the equilibrium planform is shown in Figure 6-58 for the case of Pit 1 with $K_1 = 0.77$. Only one-half of the domain is plotted as the results are symmetric about $Yp = 0$.

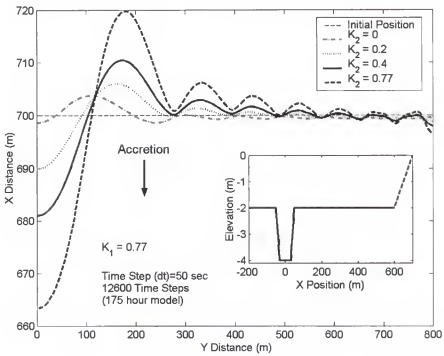

Figure 6-58: Final shoreline planform for case Pit 1 with $K_1 = 0.77$ and $K_2 = 0$, 0.2, 0.4, and 0.77 for incident wave height of 1 m and T = 12 s, with shoreline advancement in the negative X direction; Pit 1 bathymetry along cross-shore transect included.

The final shoreline planforms are plotted for four different K_2 values: $K_2 = 0$ indicating only wave angle driven transport, the base condition of $K_2 = 0.4$, $K_2 = 0.77$ taken as the upper limit for effect of the longshore gradient in the breaking wave height, and $K_2 = 0.2$. The final shoreline planform is shown to vary greatly with the value of K_2. The shoreline advance that occurs directly shoreward of the pit ($Yp = 0$) ranges from approximately 2 m for $K_2 = 0$ to 36 m for $K_2 = 0.77$. All of the equilibrium planforms are shown to pass through a point at $Yp = 110$ m with the value of K_2 determining the magnitude of the shoreline advancement and retreat.

Plotting the change in shoreline position versus time indicates approach of the system to an equilibrium planform. Figure 6-59 shows the change in shoreline position with modeling time for 4 longshore locations for the case of Pit 1 with $K_1 = 0.77$ and $K_2 = 0.4$ and the bathymetry indicated in the inset diagram. The longshore locations were directly behind the pit ($Yp = 0$) and then every 100 m out to 300 m. At all four longshore locations the change in shoreline position with time is seen to approach 0 for the larger modeling times. For $Yp = 0$ m the change in shoreline position with time indicates accretion (negative X) at an increasing rate up to 23 hours and then at a rate that decrease asymptotically towards 0. For the transects located at 100 and 300 m the shoreline first advances greatly and then retreats at a diminishing rate, while at $Yp = 200$ m the shoreline retreats monotonically at a decreasing rate.

The assumption of small changes in the wave height and angle in the cross-shore at the beginning of the nearshore zone is contained in the Shoreline Evolution Model. This allows the same initial wave height and wave angle values to be used, even as the shoreline translates onshore or offshore. To check the assumption of small changes in the

cross-shore a comparison was made of the wave height and angle at the start of the nearshore zone for the case of Pit1 and at locations +/- 20 m from the start of the nearshore zone (Figure 6-60). The bottom plot indicates the bathymetry for Pit 1 and the locations of the two transects for 600 m +/- 20 m. The top plot shows the wave height at the three cross-shore locations with little variation indicated. The middle plot shows the wave angle values with longshore distance for the 3 locations with differences from the value at Xp = 600 m less than 0.5 degrees at all locations. These results indicate that the assumption of small cross-shore variations in the wave height and wave angle where the uniform depth region joins the nearshore region is valid.

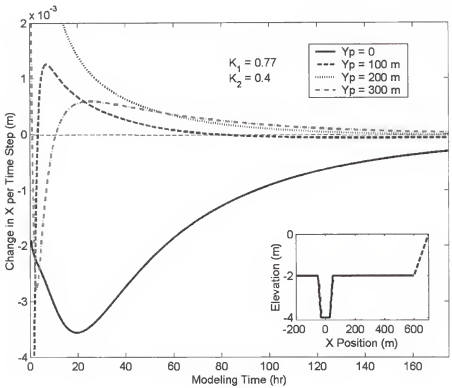

Figure 6-59: Change in shoreline position with modeling time at 4 longshore locations (Yp = 0, 100, 200, 300 m) for case Pit 1 with $K_1 = 0.77$ and $K_2 = 0.4$ with shoreline advancement in the negative X direction; Pit 1 bathymetry along cross-shore transect included.

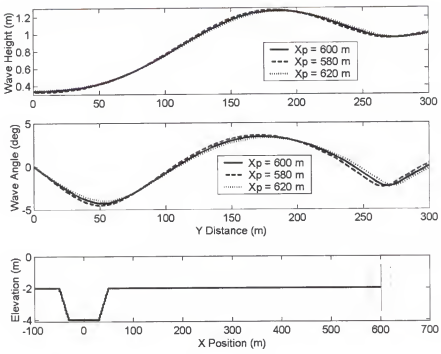

Figure 6-60: Comparison of wave height and wave angle values at 600 m and 600 m +/- 20 m for case of Pit 1 for T = 12 s with bathymetry and transect locations indicated in bottom plot.

The final shoreline planforms for the case of Pit 2 are shown in Figure 6-61 for 4 values of K_2 (0, 0.2, 0.4, 0.77) with the bathymetry indicated in the inset diagram. The nearshore region for this case is an Equilibrium Beach Profile form with coefficient "A" equal to 0.1 $m^{1/3}$ corresponding to a sediment diameter of 0.1 mm. The weighted average wave height and angles used as the initial values at the start of the nearshore region are found in Figure 6-55. The final shoreline planform is found to vary greatly with K_2, as for the case of Pit 1; however, there are some differences between the two cases. For K_2 = 0 the shoreline is found to retreat directly shoreward of the pit, due to the divergence of the wave field. This result indicates that depending on whether the gradient in the breaking wave height term is included or what value it is assigned, the shoreline response directly landward of the pit can change from erosion to accretion or vice versa. Due to

the smaller breaking wave angles and breaking wave height gradients, the magnitude of the shoreline changes are smaller than for the case of Pit 1; this provides many more locations where all 4 final planforms pass through the same point with the K_2 value determining the cross-shore extent of the deflections.

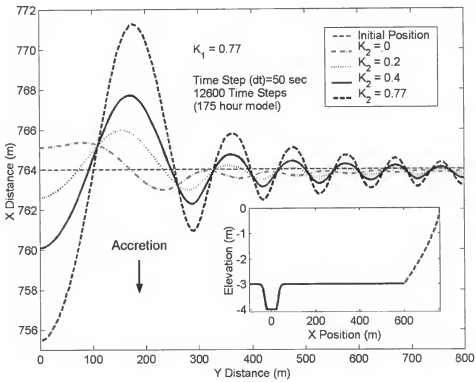

Figure 6-61: Final shoreline planform for case Pit 2 with $K_1 = 0.77$ and $K_2 = 0$, 0.2, 0.4, and 0.77 for incident wave height of 1 m, wave period of 12 s, and time step of 50 s with shoreline advancement in the negative X direction; Pit 2 bathymetry along cross-shore transect included.

The shoreline evolution for the case of Pit 2 with K_1 and K_2 equal to 0.77 and 0, respectively is shown in Figure 6-62. The shoreline planforms are plotted every 4 hours for the first 16 hours and then every 12 hours with the initial shoreline position indicated by the dotted line and the final shoreline position is indicated with "o" for every third longshore point. The plot indicates that directly shoreward of the pit the shoreline

advances initially and then retreats at a decreasing rate. Inspecting the final shoreline position at the two regions of maximum advancement reveals that the shoreline advances to a point and then retreats as the planform must compensate for the large region of erosion shoreward of the pit.

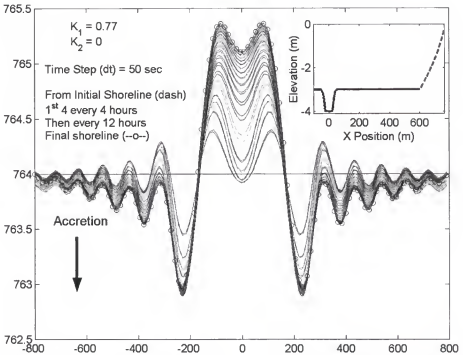

Figure 6-62: Shoreline evolution for case Pit 2 with $K_1 = 0.77$ and $K_2 = 0$ for incident wave height of 1 m, wave period of 12 s, and time step of 50 s with shoreline advancement in the negative X direction; Pit 2 bathymetry along cross-shore transect included.

The change of the shoreline planform with time for Pit 2 with $K_1 = 0.77$ and K_2 equal to 0 can be viewed in Figure 6-63 at longshore distances of 0, 100, 200, and 300 m. At Yp = 0 the large initial shoreline advancement followed by the gradual decrease in the retreat is indicated, while at Yp = 100 m only erosion occurs. For Yp = 200 m (region of maximum advancement) the shoreline is shown to advance and then retreat very gradually. The complex nature of reorganization of the sediment in response to the

forcing of the waves is highlighted at Yp = 300 m where a large initial shoreline advance is followed by a gradual shoreline retreat, which at a modeling time of 500 hours, the shoreline starts to advance at a very small rate.

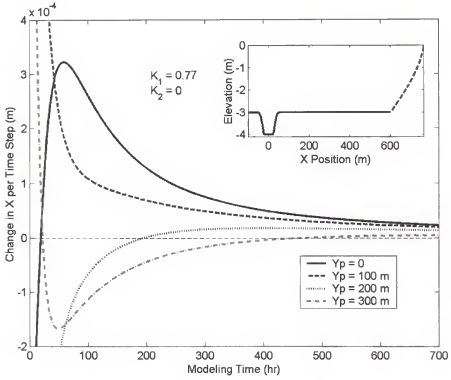

Figure 6-63: Change in shoreline position with modeling time at 4 longshore locations (Yp = 0, 100, 200, 300 m) for case Pit 2 with $K_1 = 0.77$ and $K_2 = 0$ with shoreline advancement in the negative X direction; Pit 2 bathymetry along cross-shore transect included.

The equilibrium shoreline planform for the case Shoal 1 for K_2 equal to 0, 0.2, 0.4, and 0.77 is shown in Figure 6-64 for $K_1 = 0.77$. The bathymetry for the case of Shoal 1 is shown in the inset diagram. The equilibrium planforms show two cases of erosion occurring directly shoreward of the shoal ($K_2 = 0.4, 0.77$) and two cases of accretion occurring ($K_2 = 0.2, 0$). For this case the wave angles converge directly shoreward of the shoal, a result of the refraction and diffraction caused by the anomaly, thus causing the K_1 term, when taken individually, to create a salient. With K_2 equal to 0.2 the gradient in

the wave height term, which is negative directly shoreward of the shoal, is not strong enough to overcome the wave angle term, but with $K_2 = 0.4$ the gradient in the breaking wave height overcomes the breaking wave angle term, and erosion occurs directly shoreward of the shoal.

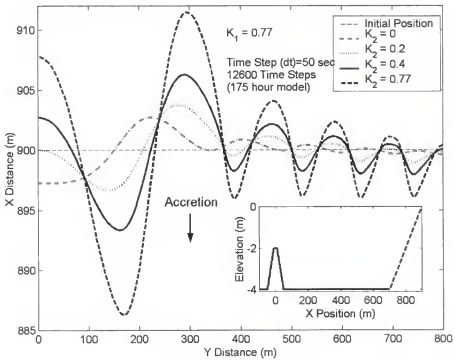

Figure 6-64: Final shoreline planform for case Shoal 1 with $K_1 = 0.77$ and $K_2 = 0$, 0.2, 0.4, and 0.77 for incident wave height of 1 m, wave period of 12 s, and time step of 50 s with shoreline advancement in the negative X direction; Shoal 1 bathymetry along cross-shore transect included.

The shoreline evolution for the case of $K_1 = 0.77$ and $K_2 = 0.2$ with Shoal 1 is shown in Figure 6-65. For this plot the shoreline position is shown at 4 hour intervals for the first 16 hours by dotted lines, with the shoreline position every 12 hours after that indicated by solid lines. The initial shoreline position is plotted as a dashed line. The shorelines indicate that an area of erosion occurs directly shoreward of the shoal in the first 20 hours. After 20 hours the shoreline starts to advance and at 90 hours the shoreline

crosses the initial location and advances 0.5 m before reaching an equilibrium position. The other areas of significant shoreline movement all either only advance or only retreat.

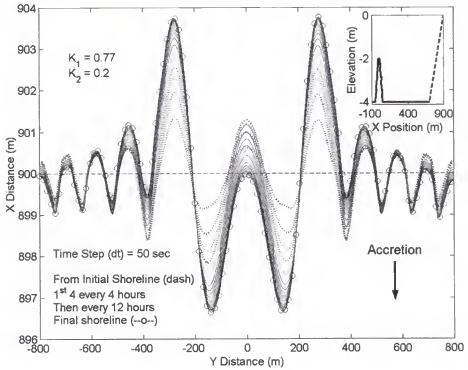

Figure 6-65: Shoreline evolution for case Shoal 1 with $K_1 = 0.77$ and $K_2 = 0.2$ for incident wave height of 1 m, wave period of 12 s, and time step of 50 s with shoreline advancement in the negative X direction; Shoal 1 bathymetry along cross-shore transect included.

6.10.2 Effect of Nearshore Form on Shoreline Change

The effect of the nearshore form (linear slope or Equilibrium Beach Profile) on the shoreline evolution was investigated using the cases of Pit 1 and Shoal 1. Pit 1 (nearshore 1) has linear transitions in depth and a nearshore region with a linear slope of 0.2, resulting in a cross-shore extent of 100 m. Pit 1 (nearshore 2) was characterized by an EBP form that fit the depth and cross-shore distance constraints of case Pit 1 (nearshore 1), which require a coefficient "A" value of 0.0928 $m^{1/3}$ corresponding to a sediment diameter of 0.08 mm. Figure 6-66 shows the final equilibrium shoreline

position for the cases of Pit 1 with the two nearshore forms for two different values of K_2 with the bathymetry for the two cases indicated in the bottom plot. The upper plot shows the final shoreline position for K_1 and K_2 equal to 0.77 and 0, respectively with the equilibrium planforms shown to be almost identical. The middle plot is for K_1 and K_2 equal to 0.77 and shows that case Pit 1 (nearshore 1) results in more shoreline advancement directly shoreward of the pit and more erosion in the bordering areas; however, the differences are relatively small. With $K_2 = 0$ indicating no difference in the planforms and $K_2 = 0.77$ showing a divergence in the final planforms, suggests that the change in the shoaling of the waves over the two nearshore forms is more pronounced than the variation in the wave refraction.

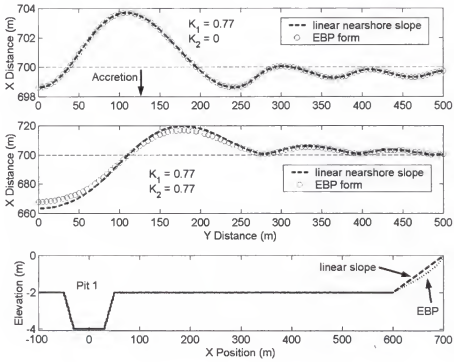

Figure 6-66: Final shoreline planform for case Pit 1 with linear nearshore slope and EBP form for T = 12 s and with $K_1 = 0.77$ and $K_2 = 0$ and 0.77 with shoreline advancement in the negative X direction; Pit 1 and Pit 1b bathymetry along cross-shore transect included.

The case of Shoal 1 was also used to investigate the impact of the nearshore form. Figure 6-67 shows the final shoreline planform for Shoal 1 with a linear nearshore slope and with an EBP form with $K_1 = 0.77$ and $K_2 = 0$ and 0.77 in the top and middle plots, respectively.

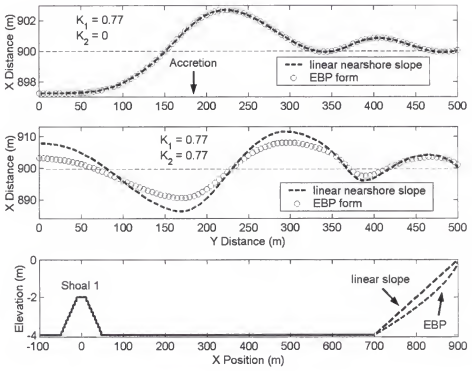

Figure 6-67: Final shoreline planform for case Shoal 1 (linear nearshore slope) and Shoal 1b (Equilibrium Beach Profile) for T = 12 s and with $K_1 = 0.77$ and $K_2 = 0$ and 0.77 with shoreline advancement in the negative X direction; Shoal 1 and Shoal 1b bathymetry along cross-shore transect included.

The bathymetry for the two nearshore forms is shown in the bottom plot. The EBP form has an "A" value of 0.117 $m^{1/3}$ for the Equilibrium Beach Profile coefficient, which provides an equivalent nearshore distance to Shoal 1. The case of $K_2 = 0$ shows that both bathymetries provide similar final shoreline planforms. The middle plot with $K_2 = 0.77$ indicates that Shoal 1 with a linear nearshore slope leads to a larger shoreline change with more erosion directly shoreward of the shoal and more accretion in the first salient in the

longshore direction. The case of a linear nearshore slope was also found to produce larger shoreline change for the case of Pit 1 in Figure 6-66.

6.10.3 Investigation of Boundary Conditions

In Appendix D two different boundary conditions at the longshore extent of the domain are discussed: no longshore transport (Boundary Condition 1) and fixed cross-shore location (Boundary Condition 2). All of the prior shoreline change results have used the no longshore transport boundary condition. Neither boundary condition fully depicts a natural shoreline where transport can occur and the cross-shore location is not fixed. However for domains with large longshore extents the impact of the pit near the end of the domain should be minimal and little shoreline effects should be expected, thereby reducing the influence of the boundary condition that is used..

Figure 6-68 shows the final shoreline planform for the case of Pit 1 for $K_1 = 0.77$ and $K_2 = 0.4$ for both boundary conditions. The average shoreline position for the entire domain is included on the plot to quantify the gain or loss of sediment from the system. For the no longshore transport boundary condition (Boundary Condition 1) a closed system is requisite, and the average shoreline position should equal the starting position, a result not expected for the fixed cross-shore location condition, which allows sediment flow at the longshore limits of the domain. As expected, the plot indicates that the final shoreline planform for longshore distances less than ±300 m are not very sensitive to the boundary condition. At larger longshore distances, Boundary Condition 2 is shown to result in an average shoreline position of 700.62 m, which is greater than the initial shoreline position of 700 m, indicating a net loss of sediment from the system. Assuming that the nearshore zone is translated in the cross-shore direction, this equates to a net

sediment loss of 3968 m^3 (0.62 m * 1600 m * 4 m) from the system. Boundary Condition 1 leads to a build up of sediment at the longshore ends of the domain with the average shoreline position of 700.03 m indicating no significant loss of sediment from the system.

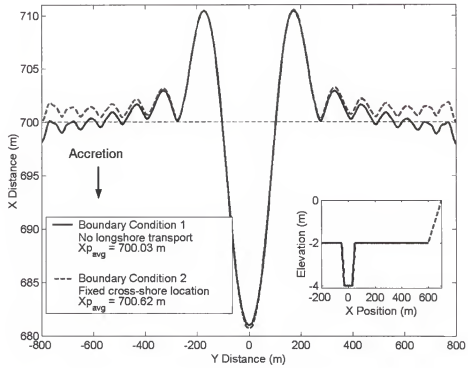

Figure 6-68: Final shoreline planform for case Pit 1 for T = 12 s and with $K_1 = 0.77$ and $K_2 = 0.4$ for two boundary conditions with shoreline advancement in the negative X direction; Pit 1 bathymetry along cross-shore transect included.

The case of Shoal 1 was also used to demonstrate the impact of the boundary condition on the shoreline evolution. Figure 6-69 shows the final shoreline position for the case of Shoal 1 with $K_1 = 0.77$ and $K_2 = 0.4$ for both boundary conditions. For this case no significant difference is indicated between the final shoreline positions for the two boundary conditions, except at large longshore distances. Boundary Condition 2 (fixed cross-shore location) is shown to result in a net gain of the sediment to the system with the average shoreline position of 899.81 m, which is less than the initial location.

For Boundary Condition 1 (no longshore transport) no significant amount of sediment is lost from the system.

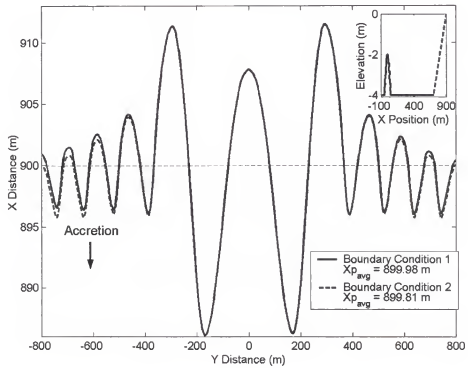

Figure 6-69: Final shoreline planform for case Shoal 1 for T = 12 s and with $K_1 = 0.77$ and $K_2 = 0.77$ for two boundary conditions with shoreline advancement in the negative X direction; Shoal 1 bathymetry along cross-shore transect included.

6.10.4 Investigation of Transition Slope on Shoreline Evolution

The effect of the transition slope on the wave transformation and energy reflection has been investigated previously using the constant volume pits first shown in Figure 6-9. Using the same constant volume, constant depth pits in the form of truncated cones (slope = abrupt, 1, 0.2, 0.07) the effect of the transition slope on the shoreline evolution was studied. The incident wave conditions were averaged over direction using the weighted averaged procedure discussed in Section 6.7.

The Shoreline Evolution Model was run for the base conditions described in Section 6.10.1 with the longshore boundaries at ±600 m. The shoreline was located 500 m from the center of the pits, with a nearshore slope of 0.2. The final shoreline planforms for the 4 pits of constant volume with K_1 and K_2 equal to 0.77 and 0, respectively are shown in Figure 6-70 for half of the domain. An inset plot is included to show the bathymetry for the 4 slopes with the line type corresponding to the slope value on the main plot.

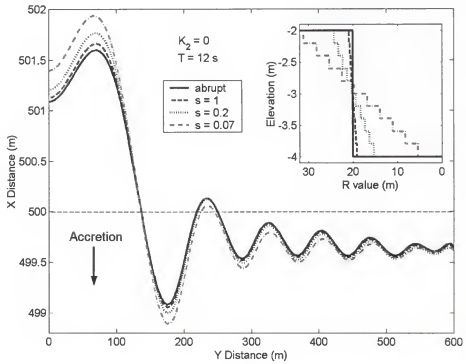

Figure 6-70: Final shoreline planform for constant volume pits for T = 12 s and with K_1 = 0.77 and K_2 = 0 with shoreline advancement in the negative X direction; cross-section of pit bathymetries through centerline included with slopes of abrupt, 1, 0.2, 0.07.

The pit with the most gradual transition slope is shown to cause the largest shoreline retreat directly shoreward of the pit for this case, bordered by the largest shoreline advancement. Generally, the more gradual the slope, the larger the shoreline

displacement. For this case with $K_2 = 0$ the longshore transport direction will be driven by the wave angle only and the more gradual transition slopes resulted in greater refraction and larger modification to the wave angles shoreward of the bathymetric anomaly. Due to the no-flow boundary condition a build up of sediment is found at the larger longshore distances of the domain. This area of shoreline advancement must occur to balance the large area of shoreline retreat directly shoreward of the pits with the continuity principle confirmed by the average shoreline position.

The Shoreline Evolution Model was also employed with $K_2 = 0.4$ for the constant volume pits. To compare the magnitude of the shoreline response with K_2 equal to 0 and 0.4, the final planforms for both values are shown in Figure 6-71. With $K_2 = 0.4$ all four pit configurations are shown to result in shoreline advancement directly shoreward of the pits with the advancement increasing for more gradual transition slopes. This is another demonstration of the significance of the transport coefficients on the shoreline response with either shoreline advancement or retreat possible depending on the magnitude of the coefficients.

The impact of the wave period on the shoreline response was also investigated for the same depth pits. The final shoreline planform for 5 periods (8, 10, 12, 14, 16 s) for the constant volume pit with a transition slope of 0.2 is shown in Figure 6-72 for $K_2 = 0$. A period of 10 s is shown to produce the largest shoreline displacement, with a shoreline retreat of 1.8 m. The largest shoreline advancement occurs for a period of 16 s, the period with the smallest shoreline retreat. This is due to the final planform for a period of 16 s having a wider area of erosion, which forces the area of accretion to be larger, resulting in the largest shoreline advancement.

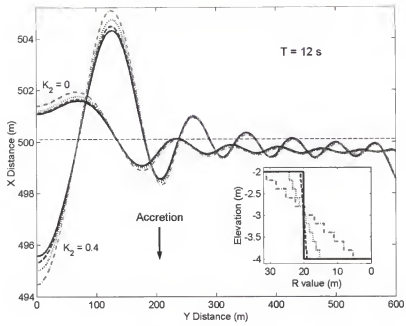

Figure 6-71: Final shoreline planform for constant volume pits for T = 12 s and with K_1 = 0.77 and K_2 = 0 and 0.4 with shoreline advancement in the negative X direction; cross-section of pit bathymetries through centerline included with slopes of abrupt, 1, 0.2, 0.07.

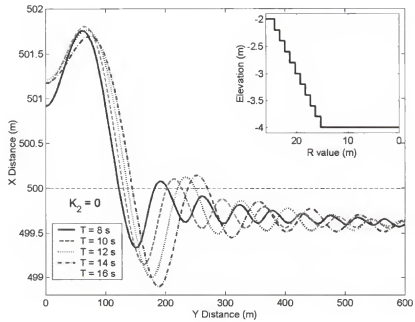

Figure 6-72: Final shoreline planform for 5 periods for constant volume pits with K_1 = 0.77 and K_2 = 0 with shoreline advancement in the negative X direction; cross-section of pit bathymetry through centerline included with slope 0.2.

The magnitude of the maximum shoreline advancement and shoreline retreat are plotted for the 4 pit bathymetries shown in the inset diagram and periods of 8, 10, 12, 14, 16 seconds with $K_2 = 0$ in Figure 6-73. For $K_2 = 0$ the maximum shoreline retreat occurs shoreward of the pits with the locations of maximum advancement bordering this area, as shown in Figure 6-70 for T = 12 s. A period of 10 s is shown to produce the largest shoreline displacement (-2 m) with the most gradual transition slope producing the largest displacement for each period.

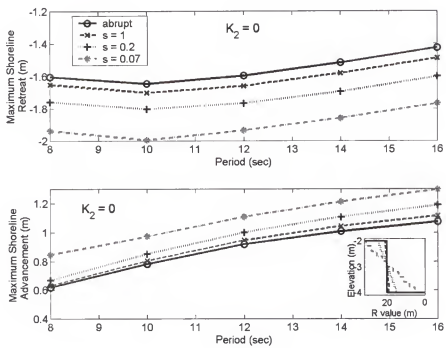

Figure 6-73: Maximum shoreline advancement and retreat versus period for constant volume pits with $K_1 = 0.77$ and $K_2 = 0$; cross-section of pit bathymetries through centerline included with slopes of abrupt, 1, 0.2, 0.07.

The maximum shoreline advancement values show that a period of 16 s produces the largest shoreline advancement with a transition slope of 0.07 producing the largest values. Figure 6-74 plots the magnitude of the maximum shoreline advancement and retreat for the 4 constant volume pit bathymetries shown in the inset diagram with $K_2 =$

0.4. With $K_2 = 0.4$ a period of 8 seconds results in the largest shoreline advancement and retreat. A transition slope of 0.07 is shown to produce the largest shoreline displacements for each period.

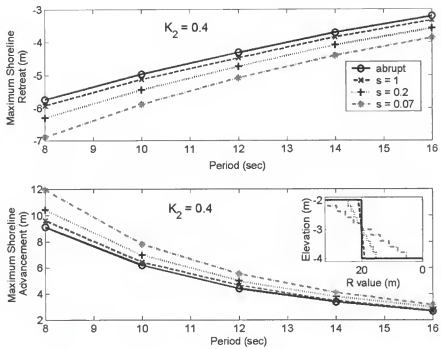

Figure 6-74: Maximum shoreline advancement and retreat versus period for constant volume pits with $K_1 = 0.77$ and $K_2 = 0.4$; cross-section of pit bathymetries through centerline included with slopes of abrupt, 1, 0.2, 0.07.

CHAPTER 7
CONCLUSIONS AND DIRECTIONS FOR FUTURE STUDY

7.1 Conclusions

Recent interest in extracting large volumes of nearshore sediment for beach nourishment and construction purposes has increased the need for reliable predictions of the wave transformation and associated shoreline changes caused by the resulting bathymetric anomalies. This predictive capacity would assist the designer of such projects in minimizing undesirable shoreline changes.

The available laboratory and field data suggest that the effect of wave transformation by an offshore pit can result in substantial shoreward salients. Of the four wave transformation processes caused by a bathymetric anomaly, a significant number of wave models include only the effects of wave refraction and diffraction, with few models incorporating wave reflection and/or dissipation over a soft medium in the pit. Computational results incorporating only refraction and diffraction and accepted values of sediment transport coefficients appear incapable of predicting the observed salient landward of borrow pits. Therefore, improved capabilities to predict wave transformation and shoreline response to constructed borrow pits will require improvements in both: (1) wave modeling, particularly in representing wave reflection and dissipation, and (2) longshore sediment transport particularly by the breaking wave angle and wave height gradient terms.

The interaction of linear water waves with two-dimensional trenches and shoals has been demonstrated using three methods (2-D Analytic Step Method, Analytic Slope Method, Numerical Method) for both symmetric and asymmetric anomalies. The three methods show good agreement for the cases presented for various bathymetric anomalies with abrupt and gradual transitions between changes in depth. The numerical model FUNWAVE 1.0 [1-D] compares reasonably well with the 2-D Analytic Step Model, with better agreement as the linearity of the waves increases.

Gradual transitions in the depth for both symmetric and asymmetric bathymetric changes are seen to reduce the reflection coefficients, especially for non-shallow water waves. Linear transitions are shown to result in instances of complete wave transmission for symmetric trenches and shoals, while for asymmetric trenches and shoals complete transmission does not occur other than for the trivial solution ($k_1h_1=0$) . Changes in depth that are Gaussian in form are demonstrated to result in a single peak of the reflection coefficient in the long wave region, followed by minimal reflection for shorter wavelengths.

Several new results for 2-D domains have been demonstrated in this study: (1) The wave field modifications are shown to be independent of the incident wave direction for asymmetric changes in depth; a result proven by Kreisel (1949), (2) For asymmetrical bathymetric anomalies with $h_1 = h_J$, a zero reflection coefficient occurs only at $k_1h_1 = 0$, and (3) For asymmetrical bathymetric anomalies with $h_1 \neq h_J$, the only k_1h_1 value at which $K_R = 0$ is that approached asymptotically at deep-water conditions.

The wave field transformation by 3-D bathymetric anomalies was demonstrated by two methods (3-D Analytic Step Method and Analytic Exact Solution Method)

developed in this study with good agreement shown between the methods for shallow water conditions. The 3-D Step Method compared well with the laboratory data of Chawla and Kirby (1996) as well as the numerical models REF/DIF-1 (Kirby and Dalrymple, 1994) and FUNWAVE 1.0 [2-D] (Kirby et al., 1998) and a 2-D fully nonlinear Boussinesq model (Kennedy et al., 2000) for several bathymetries and linear incident waves. The agreement between numerical and the 3-D Step Model can be used to the benefit of past and future numerical models, with the numerical models employing the analytic model for verification of the numerical scheme contained in the numerical model.

The impact of the configuration of the bathymetric anomaly on the wave transformation was demonstrated using pits or shoals (in the form of truncated cones) of constant volume. Gradual transition slopes were found to cause greater wave sheltering shoreward of a pit, with the degree of upwave reflection dependent on incident wave and pit characteristics. The energy reflected by anomalies of constant volume was found to be greatly reduced for gradual transition slopes. The reflection coefficients for a pit were found to oscillate with the dimensionless wavelength (kh) with a decreasing trend in the magnitude as kh increased and the only value of complete transmission for the trivial solution at $kh = 0$. For the shoals of constant volume the reflection coefficients were found to oscillate with an increasing trend in the magnitude, except for the most gradual transition slope, where little reflection occurred. The reflection coefficient versus the non-dimensional quantity kr', where k is the wave number and r' is the apparent radius, would provide another means to view the reflection caused by various pit geometries. A method to determine r' must incorporate the depth dependency of the solution as the

apparent radius should be larger than the average radius for the case of a pit since the waves "feel" the upper part of the pit more than the bottom of the pit.

An analytic shoaling and refraction model (Analytic S/R Model) was developed to extend the 3-D Analytic Step Model into the nearshore region where the depth is non-uniform (linear slope or Equilibrium Beach Profile form) in the cross-shore direction. The Analytic S/R Model was found to produce breaking wave heights, breaking wave angles and breaking locations (cross-shore and longshore) similar to REF/DIF-1 (Kirby and Dalrymple, 1994) for the same bathymetries.

Shoreline changes shoreward of a bathymetric anomaly were calculated using the Analytic Shoreline Change Model, which uses the breaking wave height, angle and location values determined from the Analytic S/R Model. Several bathymetries were studied and results indicate that the shoreline evolution landward of a bathymetric anomaly is highly dependent on the longshore transport coefficients used with either shoreline advancement or retreat possible at the same location depending on the coefficient values.

7.2 Future Work

Extending the 3-D Step Model to allow elliptic bathymetric anomalies will allow the study of borrow areas of more realistic shape, which usually have a much larger longshore extent than cross-shore. In elliptic coordinates the solution is developed from a series of Mathieu functions, instead of Bessel functions for the case of a circular anomaly. The general setup for the 3-D Step Model matching conditions and matrix solution should remain generally unchanged for the elliptic anomaly case.

The range of longshore sediment transport coefficient, K_2, must be better constrained in order to predict the shoreline response caused by an actual bathymetric

anomaly. At this point the values of the longshore transport coefficients must be considered site specific with values obtained after laboratory or field study. This limits the use of the Shoreline Response Model to calibrating models based on known planform changes. Laboratory or small-scale field studies examining the shoreline response landward of a bathymetric anomaly would be beneficial in better constraining the range of values for the longshore transport coefficients and improve the predicative capacity of future shoreline change models. For laboratory studies the effect of scale on the second longshore transport term (Q_2) must be considered with regard to the wave height and longshore distance in the $\frac{dH_b}{dY_b}$ term.

APPENDIX A
ANALYTIC WAVE ANGLE CALCULATION

The wave angles are calculated using a procedure outlined in Bender (2001) using the time-averaged energy flux based on the total velocity potential outside the bathymetric anomaly. The time averaging is obtained by taking the conjugate of one of the complex variables:

$$\overline{EFlux_{X_T}} = \overline{p_T u_T} = \frac{p_T u_T^*}{2} \qquad (* \text{ means conjugate}) \tag{A-1}$$

$$\overline{EFlux_{Y_T}} = \overline{p_T v_T} = \frac{p_T v_T^*}{2} \qquad (* \text{ means conjugate}) \tag{A-2}$$

where p is the pressure and u and v are the velocities in the cross-shore and longshore directions, respectively:

$$p_T = -\rho \frac{\partial \phi_T}{\partial t} \tag{A-3}$$

$$u_T = vel_{r_T} \cos(\theta) - vel_{\theta_T} \sin(\theta) \tag{A-4}$$

$$v_T = vel_{r_T} \sin(\theta) + vel_{\theta_T} \cos(\theta) \tag{A-5}$$

where $vel_{r_T} = \frac{\partial \phi_T}{\partial r}$ and $vel_{\theta_T} = \frac{1}{r} \frac{\partial \phi_T}{\partial \theta}$.

The total potential outside of the anomaly is defined as the sum of the incident potential and the scattered potential due to the change in depth:

$$\phi_T = \phi_I + \phi_S \tag{A-6}$$

Therefore the equation to determine the time averaged energy flux, in the x direction, at a single point due to the incident potential and the reflected potential is

$$\overline{EFlux_{X\,T}} = p_T u_T^* = (p_I + p_S)(u_I + u_S)^* = p_I u_I^* + p_I u_S^* + p_S u_I^* + p_S u_S^* \qquad \text{(A-7)}$$

The wave angle at each point is then solved employing

$$\alpha = \tan^{-1}\left(\frac{real\left(\overline{EFlux_{Y\,T}}\right)}{real\left(\overline{EFlux_{X\,T}}\right)}\right) + \alpha_I \qquad \text{(A-8)}$$

where α_I is the incident wave direction.

APPENDIX B
ANALYTIC FAR-FIELD APPROXIMATION OF ENERGY REFLECTION

The far-field approximation for the energy reflection starts by constructing a half circle of large radius in the upwave region of the anomaly that captures all the reflected energy flux. The depth integrated, time-averaged energy flux is calculated where total reflected energy flux at any location is

$$\overline{EFlux}_S = p_I vel^*_{rS} + p_S vel^*_{rI} + p_S vel^*_{rS} \tag{B-1}$$

where p is the pressure and vel_r is the velocity in the radial direction:

$$p = -\rho \frac{\partial \phi}{\partial t} \tag{B-2}$$

$$vel_r = \frac{\partial \phi}{\partial r} \tag{B-3}$$

Large value approximations are taken for the appropriate Bessel functions (Abramowitz and Stegun, 1964) and the operation $\int_{\pi/2}^{3\pi/2} \left(p\, vel^*_r\right) d\theta$ is performed to quantify the energy flux around the entire arc. After simplifying the resulting equations, the forms for the components of Eq. B.1 are

$$\int_{\pi/2}^{3\pi/2} \left(p_s\, vel^*_{rS}\right) d\theta = \frac{\rho\omega}{2\pi} \sum_{M=1}^{\infty} \left[\sum_{N=1}^{\infty} \left[A_M A^*_N \{Q_{MN}\} e^{i(N-M)\pi/2} \right] \right] \tag{B-4}$$

$$\int_{\pi/2}^{3\pi/2}\left(p_I\, vel_{rS}^*\right)d\theta = \frac{-ipgH}{4\pi}\sum_{M=1}^{\infty}\left[\sum_{N=1}^{\infty}\left[\gamma_M A_N^*\{Q_{MN}\}\cos\left(kr - M\frac{\pi}{2} - \frac{\pi}{4}\right)e^{-i\left(kr - N\frac{\pi}{2} - \frac{\pi}{4}\right)}\right]\right] \quad \text{(B-5)}$$

$$\int_{\pi/2}^{3\pi/2}\left(p_S^*\, vel_{rI}\right)d\theta = \frac{-ipgH}{4\pi}\sum_{M=1}^{\infty}\left[\sum_{N=1}^{\infty}\left[A_N^*\gamma_M\{Q_{MN}\}i\sin\left(kr - M\frac{\pi}{2} - \frac{\pi}{4}\right)e^{-i\left(kr - N\frac{\pi}{2} - \frac{\pi}{4}\right)}\right]\right] \quad \text{(B-6)}$$

where after the substitution

$$\cos\left(kr - M\frac{\pi}{2} - \frac{\pi}{4}\right) + i\sin\left(kr - M\frac{\pi}{2} - \frac{\pi}{4}\right) = e^{i\left(kr - M\frac{\pi}{2} - \frac{\pi}{4}\right)} \quad \text{(B-7)}$$

which allows Eqs. B-5 and B-6 to be combined

$$p_I\, vel_{rS}^* + p_S^*\, vel_{rI} = \frac{-ipgH}{4\pi}\sum_{M=1}^{\infty}\left[\sum_{N=1}^{\infty}\left[\gamma_M A_N^*\{Q_{MN}\}e^{i(N-M)\pi/2}\right]\right] \quad \text{(B-8)}$$

In Eqs. B.4 – B.8 A_N is the unknown reflected wave amplitude coefficient for each Bessel function mode, γ is defined in Eq. 4.17, and M and N are the Bessel function modes uses in the solution, where if M = N:

$$Q_{MN} = \pi \quad \text{(B-9)}$$

and if M ≠ N:

$$Q_{MN} = \frac{\sin(M+N)3\pi/2 - \sin(M+N)\pi/2}{(M+N)} + \frac{\sin(M-N)3\pi/2 - \sin(M-N)\pi/2}{(M-N)} \quad \text{(B-10)}$$

Using Eqs. B.4 – B.10 the energy reflected by a bathymetric anomaly can be approximated in the far-field using the amplitude coefficients determined using the 3-D Step Model. The reflection coefficient is calculated after dividing the reflected energy

flux in the far-field by the energy flux incident on the bathymetric anomaly and taking the square root.

APPENDIX C
ANALYTIC NEARSHORE SHOALING AND REFRACTION METHOD

The Analytic S/R Model was developed to remove the limitation of the 3-D Step Model that requires a uniform depth outside the bathymetric anomaly and therefore prohibits any nearshore shoaling and refraction. The Analytic S/R Model uses the wave height and direction values obtained from the 3-D Step Model for a transect that represents the start of the nearshore region and the shoreward end of the uniform depth region. In the nearshore region the assumption of no wave transformation due to the bathymetric anomaly is made. Figure C-1 shows a schematic of the nearshore region.

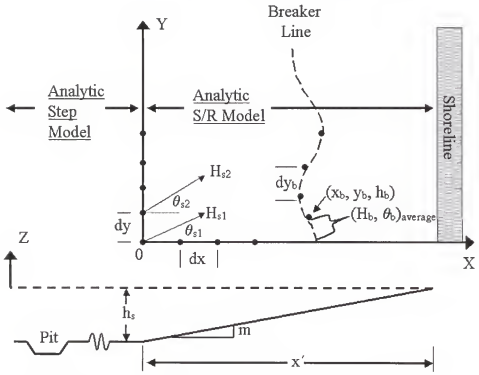

Figure C-1: Setup for analytic nearshore shoaling and refraction method

The Analytic S/R Model will first be formulated for the simplest case of a uniform nearshore slope, with appropriate changes for the case of a non-uniform slope defined by an equilibrium beach profile form.

The initial values of the wave height (Hs_j) and wave angle (θs_j) at the start of the nearshore region are determined using the analytic step method for a uniform depth, h_s. The nearshore refraction is computed using Snell's Law:

$$\frac{Sin\theta_{s,j}}{C_{s,j}} = \frac{Sin\theta_{i,j}}{C_{i,j}} \tag{C-1}$$

where the subscript i and j indicate the cross-shore and longshore location, respectively, and C is the celerity, which is taken to be the shallow water relationship:

$$C = \sqrt{g * h} \tag{C-2}$$

where for a linear slope, m, the water depth, h, is equal to $m*(x' - x_i)$ with x' defined in Figure C-1.

Next the approximation

$$Sin\theta = \frac{dy}{dx} \tag{C-3}$$

is made. Using Eqs. C-1 through C-3 allows

$$\frac{dy}{dx}_{i,j} = Sin\theta_{s,j}\frac{C_{i,j}}{C_{s,j}} = Sin\theta_{s,j}\frac{\sqrt{gh_{i,j}}}{\sqrt{gh_{s,j}}} = Sin\theta_{s,j}\frac{\sqrt{(x' - x_{i,j})}}{\sqrt{x'}} \tag{C-4}$$

A coefficient is defined, which varies only in the longshore:

$$B(y_j) = \frac{Sin\theta_{s,j}}{\sqrt{x'}} \tag{C-5}$$

Next the integral of Eq. C-4 is taken to relate the change in Y location to the change in X location:

$$\int_{y(s,j)}^{y(i,j)} dy = B(y_j) \int_{0}^{x(i,j)} \sqrt{x' - x_{i,j}}\, dx_{i,j} \tag{C-6}$$

Integration by parts yields

$$y_{i,j} = y_{s,j} + \frac{2}{3} B(y_j) \left[x'^{3/2} - (x' - x_{i,j})^{3/2} \right] \tag{C-7}$$

To determine the change in Y location based on the change in wave angle, which is known form Snell's Law (Eq. 6-1) the following equations were used

$$\frac{dy}{d\theta_{s,j}} = \frac{dy}{dB(y_j)} \frac{dB(y_j)}{d\theta_{s,j}} = \frac{2}{3} \left[x'^{3/2} - (x' - x_{i,j})^{3/2} \right] \frac{\cos\theta_{s,j}}{\sqrt{x'}} \tag{C-8}$$

$$\Delta y = \frac{dy}{d\theta} \Delta\theta_{s,j} \;\rightarrow\; \Delta y = \frac{2}{3} \left[x'^{3/2} - (x' - x_{i,j})^{3/2} \right] \frac{\cos\theta_{s,j}}{\sqrt{x'}} \Delta\theta_{s,j} \tag{C-9}$$

where Δy is the distance between wave rays and $\Delta\theta = \theta_{s,j+1} - \theta_{s,j}$.

Using the Eq. C-9 Δy can be obtained for a selected X location in the nearshore zone.

The shoaled wave height at any location in the cross-shore can be calculated using

$$H_{i,j} = H_{s,j} \sqrt{\frac{Cg_{s,j}}{Cg_{i,j}}} \sqrt{\frac{b_{s,j}}{b_{i,j}}} \tag{C-10}$$

where b is the spacing between wave rays, which determines the refraction, and Cg is the group velocity, which reveals the shoaling. Taking $Havg_{i,j}$ to be the average wave height for $H_{i,j+1}$ and $H_{i,j}$, $\theta avg_{i,j}$ to be the average wave angle for $\theta_{s,j+1}$ and $\theta_{s,j}$, and with the group velocity in the shallow water limit $\left(Cg_{shallow} = C = \sqrt{g * h}\right)$ the final equation for the shoaled and refracted wave height becomes

$$Havg_{i,j} = Havg_{s,j} \sqrt{\frac{\sqrt{h_{s,j}}}{\sqrt{h_{i,j}}}} \sqrt{\frac{dy \cos(\theta avg_{s,j+1})}{(dy + \Delta y)\cos(\theta avg_{i,j+1})}} \tag{C-11}$$

When $Havg_{i,j} \geq \kappa h_{i,j}$ then breaking occurs where κ is the breaking criteria. The wave height shoreward of the initial break point is equal to the breaking criteria times the depth.

The preceding formulation has been for a nearshore region with a planar beach. The Analytic S/R Model can also be formulated for a nearshore region with the nonlinear slope of an Equilibrium Beach Profile where the depth is determined employing

$$h = A(x' - x)^{2/3} \tag{C-12}$$

where A is a coefficient based on the grain size with dimensions of $m^{1/3}$. The change in the depth equation leads to changes in Eqs. C-4 through C-9 with the new equations taking the form

$$\frac{dy}{dx_{i,j}} = Sin\theta_{s,j}\frac{C_{i,j}}{C_{s,j}} = Sin\theta_{s,j}\frac{\sqrt{gh_{i,j}}}{\sqrt{gh_{s,j}}} = Sin\theta_{s,j}\frac{(x' - x_{i,j})^{1/3}}{x'^{1/3}} \tag{C-13}$$

$$B(y_j) = \frac{Sin\theta_{s,j}}{x'^{1/3}} \tag{C-14}$$

$$\int_{y(s,j)}^{y(i,j)} dy = B(y_j)\int_{0}^{x(i,j)} (x' - x_{i,j})^{1/3}\, dx_{i,j} \tag{C-15}$$

$$y_{i,j} = y_{s,j} + \frac{2}{3}B(y_j)\left[x'^{3/2} - (x' - x_{i,j})^{3/2}\right] \tag{C-16}$$

$$\frac{dy}{d\theta_{s,j}} = \frac{dy}{dB(y_j)}\frac{dB(y_j)}{d\theta_{s,j}} = \frac{3}{4}\left[x'^{4/3} - (x' - x_{i,j})^{4/3}\right]\frac{\cos\theta_{s,j}}{x'^{1/3}} \tag{C-17}$$

$$\Delta y = \frac{dy}{d\theta}\Delta\theta_{s,j} \;\rightarrow\; \Delta y = \frac{3}{4}\left[x'^{4/3} - (x' - x_{i,j})^{4/3}\right]\frac{\cos\theta_{s,j}}{x'^{1/3}}\Delta\theta_{s,j} \tag{C-18}$$

APPENDIX D
ANALYTIC SHORELINE CHANGE THEORY AND CALCULATION

Knowledge of the breaking wave height and angle in the nearshore zone allows the calculation of the longshore sediment transport and resulting change in shoreline position for a simplified nearshore system using the Analytic Shoreline Change Model (Shoreline Change Model). A valid domain for the Shoreline Change Model consists of a uniform depth region containing a bathymetric anomaly that connects to a nearshore region with a sloping bottom. The Analytic S/R Model (Appendix C) is employed to calculate the breaking wave height, angle, and location using the results of Analytic Step Model as the initial wave values at the juncture of the two regions.

For normally incident waves with no longshore gradient in wave height the equilibrium shoreline planform will be oriented normal to the incident waves. However, due to the offshore bathymetric anomaly, a non-uniform alongshore wave height and angle distribution at the start of the nearshore region develops, and a uniform shoreline planform will not be in equilibrium with the incident waves. The non-uniform breaking wave height and angles will induce the shoreline to change form until an equilibrium planform is achieved.

A simple version of the shoreline change model was developed in Bender (2001) for use with the analytic wave transformation model developed that did not account for nearshore shoaling and refraction and was limited to abrupt transitions in depth and shallow water waves. The continuity equation is the basis for a relationship between the

shoreline position and the change in volume for the profile. The assumptions of initially straight and parallel bottom contours are made in the Analytic S/R Model with no wave transformation in the nearshore region due to the bathymetric anomaly. These concepts are used to determine the longshore transport and resulting shoreline change.

Figure D-1 is a schematic of the nearshore region used in the Shoreline Change Model, which indicates the conventions for the coordinate system and angle directions used in the model.

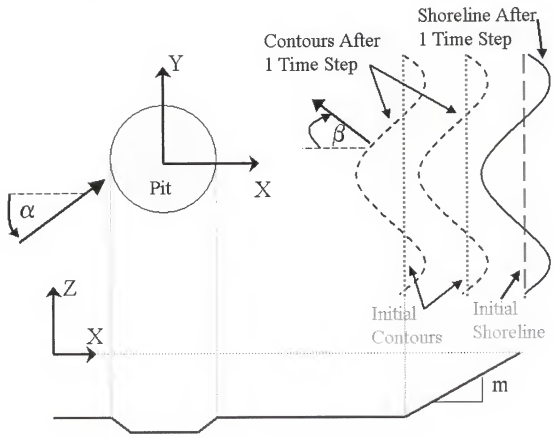

Figure D-1: Definition sketch for analytic shoreline change method showing shoreline and contours for initial location and after shoreline change.

The breaking wave height and angle at each point (i,j) of in the longshore direction of the nearshore zone are used to determine the longshore transport with a two-term transport equation:

$$Q_{total} = \frac{K_1 H_b^{2.5} \sqrt{g/\kappa} \sin(\beta + \alpha_b)\cos(\beta + \alpha_b)}{8(s-1)(1-p)} + \frac{-K_2 H_b^{2.5} \sqrt{g/\kappa} \cos(\beta + \alpha_b)}{8(s-1)(1-p)\tan(m)} \frac{dH_b}{dY_b}$$

$$Q_{total} = Q_1 + Q_2 \qquad \text{(D-1)}$$

where H_b is the breaking wave height, α_b is the breaking wave angle, β is the shoreline orientation, s is the ratio of sand to water densities, p is the porosity of the sediment, κ is the breaking criteria, K_1 and K_2 are the sediment transport coefficients, and tan(m) equals the slope of the nearshore zone. If an EBP form is used the nearshore slope (m) is equal to the average slope from the shoreline to the cross-shore breaking location averaged over the longshore. The first transport term is driven by the waves approaching the shore at an angle and is equivalent to the CERC transport equation (Shore Protection Manual, 1984) while the second term, which is sometimes not included, is due to the gradient in the wave heights or setup. Ozasa and Brampton (1979) and Gourlay (1982), among others, have studied the second transport term with the current formulation based on the form of Ozasa and Brampton.

Bakker (1971) developed a longshore current term based on the variation in longshore wave height; this method is outlined in Ozasa and Brampton (1979) and extended by Ozasa and Brampton to calculate the longshore transport for a variation in longshore wave height. Gourlay (1982) contains a thorough examination of the longshore transport caused by both the breaking wave angle and a longshore gradient in the wave height and provides an extensive review of various derivations of Eq. D-1.

Kraus (1983) states that K_1 and K_2 should be taken as site-specific parameters to be determined by calibration, with K_1 acting as a time-adjustment parameter and K_2 a function of the transport parameters of the individual beach. With Eq. D-1 it is possible to have either erosion or accretion at a particular location depending on the values of K_1 and K_2 selected and the breaking wave and shoreline conditions.

The shoreline change is calculated using the continuity equation:

$$\frac{\partial X}{\partial t} = \frac{\partial Q_{total}}{\partial Y}\frac{1}{h_* + B} \rightarrow \Delta X = \frac{\partial Q_{total}}{\partial Y}\frac{1}{h_* + B}\Delta t \tag{D-2}$$

where h_* is the closure depth, which is the depth of the uniform depth region, B is an assumed berm height and a positive change in X-direction indicates erosion. The maximum time step Δt_{max} for model stability is determined using

$$\Delta t_{\max} < \frac{\Delta Y^2}{2G} \tag{D-3}$$

where

$$G = \frac{K_1 H_b^{2.5}\sqrt{g/\kappa}}{8(s-1)(1-p)(h_* + B)} \tag{D-4}$$

This criterion dictated the time step used in the models.

The Analytic S/R Model determines the breaking wave height, angle and location. Due to the initial wave angles and wave refraction in the nearshore zone, the constant spacing between wave rays at the start of the nearshore slope is altered at the breaking location. The value of $\frac{dH_b}{dY_b}$ is determined by taking the gradient in the longshore direction and using a simple moving average procedure to smooth out some of the noise

created by the unequal longshore spacing of the wave rays with dY_b equal to the longshore spacing at breaking.

Using Eq. D-1, the total longshore transport (Q_{total}) is calculated and the change in the shoreline position at each longshore location is determined with Eq. D-2. The Y locations of the shoreline change values are the same as the Y locations of the initial wave height and angle values at the start of the nearshore region. The cross-shore slope is then translated in the cross-shore direction depending on the sign of ΔX, thus altering the bathymetric contours so they are no longer straight and parallel, just parallel. The new shoreline and bathymetric contour orientation (which is constant in the cross-shore direction) is determined using

$$\beta_{1,j} = \tan^{-1}\left(-\frac{X_{1,j+1} - X_{1,j}}{dy}\right) \tag{D-5}$$

The change in bathymetry from straight and parallel contours leads to a change in the nearshore refraction. Dean (2003) developed an analytic solution for the change in wave refraction, and consequential change in the breaking wave angle, caused by the change in shoreline orientation and contours:

$$\Delta\alpha_b = \beta_{1,j}\left(1 - \frac{C_b}{C_*}\right) \rightarrow \beta_{1,j}\left(1 - \frac{h_{b(i,j)}}{h_{(s)}}\right) \tag{D-6}$$

Eq. D-6 is used to modify the breaking wave angles determined from the Analytic S/R Model.

Small changes in the wave height and angle are assumed to result from the cross-shore translation of the nearshore zone as the planform evolves to a new equilibrium. The change in the refraction and shoaling caused by the new shoreline orientation are also assumed to be minimal. This allows the breaking wave height, angle, and location to

be determined once, for the initial shoreline position and orientation. These breaking wave values are then used to determine Q_{total} as the shoreline planform evolves.

REFERENCES

Abernethy, C.L., and Gilbert, G. 1975. Refraction of a wave spectrum. Report No. INT 117, Hydraulics Research Station. Wallingford, England.

Abramowitz, M., and Stegun, I. A. (Eds.). 1964. Handbook of Mathematical Functions. National Bureau of Standards, Applied Mathematics Series 55, U.S. Government Printing Office, Washington, D.C.

Applied Technology and Management. 1998. Martin County beach nourishment project: Project performance report. Gainesville, Florida.

Bakker, W.T. 1971. The influence of longshore variation of the wave height on the littoral current. Study Report WWK71-19. Ministry of Public Works (Rijkswaterstaat), The Hague, The Netherlands.

Bartholomeusz, E.F. 1958. The reflexion of long waves at a step. Proc. Camb. Phil. Soc., 54, pp. 106-118.

Battjes, J.A. and Janssen, J.P.F.M. 1978. Energy loss and set-up due to breaking of random waves. Proceedings of the 16th International Conference on Coastal Engineering, Hamburg, ASCE, New York, pp. 569-587.

Bender, C.J. 2001. Wave field modifications and shoreline response due to offshore borrow areas. Master's Thesis. Department of Civil and Coastal Engineering, University of Florida.

Bender, C.J. and Dean, R.G. 2001. Erosional hot spot prediction through wave analysis. Proceedings of the Fourth International Symposium on Ocean Wave Measurement and Analysis (WAVES 2001), ASCE, Reston, II, pp. 1306-1315.

Berkhoff, J.C.W., 1972. Computation of combined refraction-diffraction. Proceedings of the 13th International Conference on Coastal Engineering. Vancouver, ASCE, New York, pp. 471-490.

Berkhoff, J.C.W., Booij, N., and Radder, A.C. 1982. Verification of numerical wave propagation models for simple harmonic linear water waves. Coastal Engineering, 6: 255-279.

Black, J.L. and Mei, C.C. 1970. Scattering and radiation of water waves. Technical Report No. 121. Water Resources and Hydrodynamics Laboratory, Massachusetts Institute of Technology.

Black, J.L., Mei, C.C., and Bray, M.C.G. 1971. Radiation and scattering of water waves by rigid bodies. Journal of Fluid Mechanics, 46: 151-164.

Booij, N. 1983. A note on the accuracy of the mild-slope equation. Coastal Engineering, 7: 191-203.

Cavaleri, L. and Malanotte-Rizzoli, P. 1981. Wind wave prediction in shallow water: Theory and applications. Journal of Geophysical Research, 86, #C11: 10961-10973.

Chawla A., and Kirby J.,T. 1996. Wave transformation over a submerged shoal. Report No. CACR-96-03. Department of Civil Engineering, University of Delaware.

Collins, J.I., 1972. Prediction of shallow water spectra. Journal of Geophysical Research, 77, No 15: 2693-2707.

Combe, A.J., and Soileau, C.W. 1987. Behavior of man-made beach and dune: Grand Isle, Louisiana, Proceedings of Coastal Sediments 1987, New Orleans, Louisiana, ASCE, New York, pp. 1232-1242.

Copeland, G.J.M. 1985. A practical alternative to the "mild-slope" wave equation. Coastal Engineering, 9: 125-149.

Dally, W.R., Dean, R.G., and Dalrymple, R.A. 1985. Wave height variations across beaches of arbitrary profile. Journal of Geophysical Research, 90: 11917-11927.

Dalrymple, R.A., Kirby, J.T., and Hwang, P.A. 1984. Wave diffraction due to areas of energy dissipation. Journal of Waterway, Port, Coastal and Ocean Engineering, 110: pp. 67-79.

Danish Hydraulic Institute (DHI). 1998. MIKE 21: Elliptic mild slope (EMS) wave module, Release 2.7. User Guide and Reference Manual. Hørsholm.

Dean, R.G. 1964. Long wave modification by linear transitions. Journal of the Waterways and Harbors Division, ASCE, 90 (1): 1-29.

Dean, R. G. 2003. Beach nourishment: Theory and practice. World Scientific, Singapore.

Dean, R.G., Liotta, R., and Simon, G. 1999. Erosional hot spots. UFL/COEL-99/021. Department of Coastal and Oceanographic Engineering, University of Florida.

Dingemans, M.W. 1983. Verification of numerical wave equation models with field measurements. CREDIZ verification Haringvliet. Report W488. Delft Hydraulics Laboratory, Delft, pp. 137.

Ebersole, B.A., Cialone, M.A., and Prater, M.D. 1986. Regional coastal processes numerical modeling system, Report 1, A linear wave propagation model for engineering use. Technical Report CERC-86-4. CERC, Department of the Army, WES, Corps of Engineers.

Gourlay, M.R. 1982. Nonuniform alongshore currents and sediment transport- A one-dimensional approach. Civil Engineering Research Report No. CD31. Department of Civil Engineering, University of Queensland, St Lucia, Queensland.

Grassa, J.M., and Flores, J. 2001. Discussion of: Maa, J.P.-Y., Hsu, T.-W., Tsai, C.-H., and Juang, W.J. 2000. Comparison of wave refraction and diffraction models. Journal of Coastal Research, 16 (4): 1073-1082. Journal of Coastal Research, 17 (3): 762-764.

Gravens, M.B., and Rosati, J.D. 1994. Numerical study of breakwaters at Grand Isle, Louisiana, Miscellaneous Paper CERC-94-16. U.S.Army Corps of Engineers, Vicksburg, Mississippi.

Hanson, H. 1987. GENESIS- A generalized shoreline change model for engineering use. Report 1007. Department of Water Resources Engineering, University of Lund, Lund, Sweden.

Hanson, H. 1989. Genesis – A generalized shoreline change numerical model. Journal of Coastal Research, 5 (1): 1-27.

Hasselmann, K., Barnett, T.P., Bouws, E., Carlson, H., Cartwright, D.E., Enke, K., Ewing, J.A., Geinapp, H., Hasselmann, D.E., Kruseman, P., Meerburg, A., Müller, P., Olbers, D.J., Richter, K., Sell, W., and Walden, H. 1973. Measurements of wind-wave growth and swell decay during the Joint North Sea Wave Project (JONSWAP), Dtsch. Hydrogr. Z. Suppl. 12, A8.

Holthuijsen, L.H., Booij, N., Ris, R.C., Haagsma, IJ.G., Kieftenburg, A.T.M.M., and Kriezi, E.E. 2000. SWAN User Manual (not the short version), SWAN Cycle III, Version 40.11. Department of Civil Engineering, Delft University of Technology. GA Delft, the Netherlands.

Horikawa, K., Sasaki, T. and Sakuramoto, H. 1977. Mathematical and laboratory models of shoreline change due to dredged holes. Journal of the Faculty of Engineering, The University of Tokyo, XXXIV, No. 1: 49-57.

Hsu, T.W. and Wen, C.C. in review. On the radiation boundary conditions and energy dissipation for wave calculation. Journal of Waterway, Port, Coastal and Ocean Engineering.

Inman, D.L. and Rusnak, G.S. 1956. Changes in sand level on the beach and shelf at La Jolla, California. Technical Memorandum No 82. US Army Corps of Engineers, Beach Erosion Board.

Jachec, S.M. and Bosma, K.F. 2001. Erosional hot spot prediction through wave analysis. Proceedings of the Fourth International Symposium on Ocean Wave Measurement and Analysis (WAVES 2001), ASCE, Reston, II, pp. 1326-1335.

Janssen, P.A.E.M. 1989. Wave induced stress and the drag of air flow over sea waves. Journal of Physical Oceanography. 19: 745-754.

Janssen, P.A.E.M. 1991. Quasi-linear theory of wind-wave generation applied to wave forecasting. Journal of Physical Oceanography, 21: 1631-1642.

Jolas, P. 1960. Passage de la houle sur un seuil. Houle Blanche, 15, pp. 148.

Kennedy, A. B., Kirby, J. T., Chen, Q., and Dalrymple, R. A. 2000. Boussinesq-type equations with improved non-linear performance. Wave Motion, 33: 225-243.

Kirby, J.T. 1986. Higher-order approximations in the parabolic equation method for water waves. Journal of Geophysical Research, 91: 933-952.

Kirby, J.T. and Dalrymple, R.A. 1983a. Propagation of obliquely incident waves over a trench. Journal of Fluid Mechanics, 133: 47-63.

Kirby, J.T. and Dalrymple, R.A. 1983b. The propagation of weakly nonlinear waves in the presence of varying depth and currents. Proceedings 20th Congress I.A.H.R. Moscow.

Kirby, J.T. and Dalrymple, R.A. 1986. An approximate model for nonlinear dispersion in monochromatic wave propagation models. Coastal Engineering, 9: 545-561.

Kirby, J.T. and Dalrymple, R.A. 1994. User's manual, combined refraction / diffraction model, REF/DIF-1, Version 2.5. Center for Applied Coastal Research, Department of Civil Engineering, University of Delaware. Newark, Delaware.

Kirby, J.T., Dalrymple, R.A. and Seo, S.N. 1987. Propagation of obliquely incident waves over a trench. Part 2. Current flowing along trench. Journal of Fluid Mechanics, 176: 95-116.

Kirby, J. T., Wei, G., Chen, Q., Kennedy, A. B. and Dalrymple, R. A. 1998. FUNWAVE 1.0, Fully nonlinear Boussinesq wave model. Documentation and user's manual. Report CACR-98-06. Center for Applied Coastal Research, Department of Civil and Environmental Engineering, University of Delaware.

Kojima, H., Ijima, T. and Nakamuta, T. 1986. Impact of offshore dredging on beaches along the Genkai Sea, Japan. Proceedings 20th International Conference on Coastal Engineering, Taipai, II, ASCE, New York, pp. 1281-1295.

Komar, P.D. 1969. The longshore transport of sand on beaches. Ph. D thesis. University of California, San Diego.

Komen, G.J., Hasselmann, S., and Hasselmann, K. 1984. On the existence of a fully developed wind-sea spectrum. Journal of Physical Oceanography, 14: 1271-1285.

Komen, G.J., Cavaleri, L., Donelan, M., Hasselmann, K., Hasselmann, S., and Janssen, P.A.E.M. 1994. Dynamics and Modeling of Ocean Waves. Cambridge University Press.

Kraus, N.C. 1983. Application of a shoreline prediction model. Proceedings of Coastal Structures '83, Arlington, Virginia, ASCE, New York, pp. 632-645.

Kraus, N.C., and Harikai, S. 1983. Numerical model of the shoreline change at Oarai Beach. Coastal Engineering, 7: 1-28.

Kreisel, G. 1949. Surface Waves. Q. Appl Maths, 7: 21-44.

Lamb, H. 1924. Hydrodynamics: 5th Edition. University Press, Cambridge. Section 176.

Lassiter, J.B. 1972. The propagation of water waves over sediment pockets. PhD. Thesis, Massachusetts Institute of Technology.

Lee, J J. and Ayer, R.M. 1981. Wave propagation over a rectangular trench. Journal of Fluid Mechanics,110: 335-347.

Lee, J.J., Ayer, R.M., and Chiang, W.-L. 1981. Interaction of waves with submarine trenches. Proceedings 17th International Conference on Coastal Engineering, Sydney, ASCE, New York, pp. 812-822.

Liotta, R. 1999. Erosional hot spots: Causes and case studies at Dade and Manatee Counties. Master's Thesis, Department of Coastal Engineering, University of Florida.

Louisiana Oil Spill Coordinator's Office (LOSCO). 1999. Color Infrared Orthophoto. Date of source image aerial photography, 24-Jan-1998.

Maa, J.P.-Y., and Hwung, H.-H. 1997. A wave transformation model for harbor planning. Proceedings of the Third International Symposium on Ocean Wave Measurement and Analysis (WAVES 97), Virginia Beach, Virginia, ASCE, New York, I, pp. 256-270.

Maa, J.P.-Y., and Hobbs, C.H. III. 1998. Physical impacts of waves on adjacent coasts resulting from dredging at Sandbridge Shoal, Virginia. Journal of Coastal Research, 14 (2): 525-536.

Maa, J.P.-Y., Hsu, T.-W., and . Hwung, H.-H. 1998a. RDE Model: A program for simulating water wave transformation for harbor planning. Special Scientific Report No. 136. Virginia Institute of Marine Science, Gloucester Point, Virginia.

Maa, J.P.-Y., Hwung, H.-H., and Hsu, T.-W. 1998b. A simple wave transformation model, PBCG, for harbor planning. Proceedings of the 3rd International Conference on Hydrodynamics, I, pp. 407-412.

Maa, J.P.-Y., Hsu, T.-W., Tsai, C.-H., and Juang, W.J. 2000. Comparison of wave refraction and diffraction models. Journal of Coastal Research, 16 (4): 1073-1082.

Maa, J.P.-Y., Hobbs, C.H. III.,and Hardaway, C.S. 2001. A Criterion for determining the impact on shorelines caused by altering wave transformation. Journal of Coastal Research, 17 (1): 107-113.

Madsen, O.S., Poon, Y.-K., and Graber, H.C. 1988. Spectral wave attenuation by bottom friction: Theory. Proceedings 21st International Conference on Coastal Engineering, Costa del Sol-Malaga, Spain, ASCE, New York, pp. 492-504.

Madsen, P.A. and Larsen, J. 1987. An efficient finite-difference approach to the mild-slope equation. Coastal Engineering, 11: 329-351.

McDougal, W.G., Williams, A.N. and Furukawa, K. 1996. Multiple pit breakwaters. Journal of Waterway, Port, Coastal, and Ocean Engineering, 122: 27-33.

Mei C.C., and Black, J.L. 1969. Scattering of surface waves by rectangular obstacles in water of finite depth. Journal of Fluid Mechanics, 38: 499-511.

Miche, M. 1951. Le pouvoir reflechissant des ouvrages maritimes exposes a l' action de la houle. Annals des Ponts et Chaussess. 121e Annee, pp. 285-319 (translated by Lincoln and Chevron, University of California, Berkeley, Wave Research Laboratory, Series 3, Issue 363, June 1954).

Miles, J.W. 1967. Surface-wave scattering matrix for a shelf. Journal of Fluid Mechanics, 28: 755-767.

Miles, J.W. 1982. On surface-wave diffraction by a trench. Journal of Fluid Mechanics, 115: 315-325.

Minerals Management Service. 2003. Environmental Surveys of Potential Borrow Areas on the East Florida Shelf and the Environmental Implications of Sand Removal for Coastal and Beach Restoration (NT-00-01). MMS Environmental Studies Program: Ongoing Studies, http://www.mms.gov/eppd/sciences/esp/profiles/nt/NT-00-01.htm, Accessed 15 January, 2003.

Motyka, J.M., and Willis, D.H. 1974. The effect of refraction over dredged holes. Proceedings 14th International Conference on Coastal Engineering, Copenhagen, ASCE, New York, pp. 615-625.

Newman, J.N. 1965a. Propagation of water waves over an infinite step. Journal of Fluid Mechanics, 23: 23-29.

Newman, J.N. 1965b. Propagation of water waves past long two-dimensional objects. Journal of Fluid Mechanics, 23: 399-415.

Ozasa, H. and Brampton, A.H. 1979. Models for predicting the shoreline evolution of beaches backed by seawalls. Report No IT 191. Hydraulics Research Station, Wallingford, England.

Price, W.A., Motyka, J.M. and Jaffrey, L.J. 1978. The effect of offshore dredging on coastlines. Proceedings 16th International Conference on Coastal Engineering, Hamburg, ASCE, New York, II, pp. 1347-1358.

Radder, A.C. 1979. On the parabolic equation method for water-wave propagation. Journal of Fluid Mechanics, 95:159-176.

Resio, D.T. 1987. Shallow-water waves. I: Theory. Journal of Waterway, Port, Coastal, and Ocean Engineering, 113 (3): 264-281.

Resio, D.T. 1988. Shallow-water waves. II: Data Comparisons. Journal of Waterway, Port, Coastal, and Ocean Engineering, 114 (1): pp. 50-65.

Sasaki, T. 1975. Simulation on shoreline and nearshore current. Proceedings of the Specialty Conference on Civil Engineering in the Oceans, ASCE, San Francisco, III, pp. 179-196.

Schwinger, J. and Saxon, D.S. 1968. Discontinuities in waveguides. Gordon and Breach, New York.

Shore Protection Manual. 1984. U.S. Army Corps of Engineers, CERC, U.S. Government Printing Office, Washington D.C.

Smith, J.K., Sherlock, A.R., and Resio, D.T. 2001. STWAVE: Steady-state spectral wave model, User's manual for STWAVE, Version 3.0. Final Report ERDC/CHL SR-01-1. U. S. Army Engineer Research and Development Center, Vicksburg, Mississippi.

Snyder, R.L., Dobson, F.W., Elliot, J.A., and Long, R.B. 1981. Array measurements of atmospheric pressure fluctuations above surface gravity waves. Journal of Fluid Mechanics, 102: 1-59.

Sretenskii, L.N. 1950. Refraction and reflexion of plane waves in liquids at a transition from one depth to another. (In Russian). Izv. Akad. Nauk SSSR, Otd. Tekhn. Nauk, pp. 1601.

Sumerell, H.R. 2000. Martin County, Florida beach nourishment project: Evaluation of project performance and prediction capabilities. Master's Thesis. Department of Civil and Coastal Engineering, University of Florida.

Takano, K. 1960. Effets d'un obstacle paralléllépipédique sur la propagation de la houle. Houille Blanche, 15: 247.

Tang, Y. 2002. The effect of offshore dredge pits on adjacent shorelines. Masters Thesis. Department of Civil and Coastal Engineering, University of Florida.

Wang, Z. and Dean, R.G. 2001. Manatee county beach nourishment project performance and erosional hot spot analyses. UFL/COEL-2001/003. Department of Civil and Coastal Engineering, University of Florida.

Wehausen, J.V. and Laitone, E.V. 1960. Surface Waves. Handbuch der Physik. Vol. 9: pp 446-477.

Wei, G., Kirby, J. T., Grilli, S. T. and Subramanya, R., 1995. A fully nonlinear Boussinesq model for surface waves. I. Highly nonlinear, unsteady waves. Journal of Fluid Mechanics, 294: 71-92.

Williams, A.N. 1990. Diffraction of long waves by a rectangular pit. Journal of Waterway, Port, Coastal, and Ocean Engineering, 116: pp. 459-469.

Williams, A.N. and Vasquez, J.H. 1991. Wave interaction with a rectangular pit. Journal of Offshore Mechanics and Arctic Engineering, 113: 193-198.

Williams, B.P. 2002. Physical modeling of nearshore response to offshore borrow pits. Masters Thesis. Department of Civil and Coastal Engineering, University of Florida.

BIOGRAPHICAL SKETCH

The author was born in Binghamton, New York, on December 28, 1976. He was raised in nearby Endwell and grew up looking forward to the annual family vacation to the shore where his fascination with the coast developed. Mr. Bender graduated from the University of Rhode Island with an ocean engineering degree in May of 1999. While attending the university he lettered all four years as a member of the varsity tennis team and was captain his final two seasons.

A post-graduation cross-country trip with his future wife was the culmination of many dreams to see the country and his scattered extended family. The author was awarded an Alumni Fellowship from the University of Florida to complete his graduate work in the Civil and Coastal Engineering Department starting in the fall of 1999. He obtained his master's degree in coastal engineering in the spring of 2001. This work is the culmination of his doctoral studies, which he found very rewarding.

The author enjoys spending time with his high school sweetheart and wife of over 2 years, Kathryn, and their dog, Rhody. Having accepted a job in Jacksonville, Florida, with Taylor Engineering, the author and his wife will remain well south of the cold and snow that define where they grew up, and much closer to the ocean.

I certify that I have read this study and that in my opinion it conforms to acceptable standards of scholarly presentation and is fully adequate, in scope and quality, as a dissertation for the degree of Doctor of Philosophy.

Robert G. Dean, Chairman
Graduate Research Professor of Civil and Coastal Engineering

I certify that I have read this study and that in my opinion it conforms to acceptable standards of scholarly presentation and is fully adequate, in scope and quality, as a dissertation for the degree of Doctor of Philosophy.

Daniel M. Hanes
Professor of Civil and Coastal Engineering

I certify that I have read this study and that in my opinion it conforms to acceptable standards of scholarly presentation and is fully adequate, in scope and quality, as a dissertation for the degree of Doctor of Philosophy.

Andrew Kennedy
Assistant Professor of Civil and Coastal Engineering

I certify that I have read this study and that in my opinion it conforms to acceptable standards of scholarly presentation and is fully adequate, in scope and quality, as a dissertation for the degree of Doctor of Philosophy.

Robert J. Thieke
Assistant Professor of Civil and Coastal Engineering

I certify that I have read this study and that in my opinion it conforms to acceptable standards of scholarly presentation and is fully adequate, in scope and quality, as a dissertation for the degree of Doctor of Philosophy.

U. H. Kurzweg

Ulrich H. Kurzweg
Professor of Mechanical and Aerospace Engineering

This dissertation was submitted to the Graduate Faculty of the College of Engineering and to the Graduate School and was accepted as partial fulfillment of the requirements for the degree of Doctor of Philosophy.

May 2003

Pramod P. Khargonekar
Dean, College of Engineering

Winfred M. Phillips
Dean, Graduate School

LD
1780
20 C3
.B458

UNIVERSITY OF FLORIDA
3 1262 08555 0407